بسم الله الرحمن الرحيم

اللهُ لا الهَ الا هوَ الحيُّ القيومُ لا تأخُذُهُ سِنَةٌ ولا نومٌ لهُ ما
في السمواتِ وما في الارضِ من ذا الذي يشفعُ عندَهُ
الا بإذنِهِ يعلَمُ ما بينَ أيديهِم وما خَلْفَهُم ولا يُحيطُونَ
بشيءٍ مِنْ عِلمِهِ إلا بِما شاءَ وسِعَ كرسيُّهُ السمواتِ
والأرضَ ولا يَؤُدُهُ حِفظُهُما وهوَ العليُّ العَظِيمُ

صدق الله العظيم

Drug Carrier Study Of Some New Nanocomposite Polymers

Drug Delivery Systems

Drug delivery system built on nanostructured is one of the rapidly promising areas currently that has acquired many researcher interests because of the suitable means of both side specific and time controlled drug delivery.

Lately, merged of polymeric system with drug delivery system built on nanostructured provides prolonged drug release. Among different kind of polymeric system, hydrogel regard as a suitable drug carrier for controlled drug release.

Hydrogel is crosslinked with a three dimensional network that able to absorb huge quantity of water because of contain to hydrophilic group in the network such as carboxylic, hydroxyl group and others.

Hydrogel can considerably use in drug delivery system. Hydrogel can be a suitable carrier for drug delivery system owing drug release from its matrix based on swelling/ or deswelling, the solubility of the drug in the release media, and the interaction between drug with the polymers. Hydrogel have capability to defend drugs from aggressive environment such as presence of enzymes and extreme pH in the inner organs like stomach. In addition, hydrogels physical characteristic make them as good selector for drug carrier. For example, hydrogels porosity permit drug loading into gel network and accordingly drug release at desired site. Hydrogel has able to appearing significant volume changes in response to small changes in pH, temperature and other environmental stimuli

Nanocomposite Hydrogels

Nanocomposite hydrogels, also famous as hybrid hydrogels, may be defined as hydrated polymeric networks, either chemically or physically crosslinked with each other and/ or with nanostructures or nanoparticles. Although there are numerous appropriateness for nanocomposite biomaterials, such as carbon-based nanomaterials (carbon nanotubes, graphene, nano diamonds), inorganic/ceramic nanoparticles (silica, silicates, calcium phosphate, hydroxyapatite), polymeric nanoparticles (dendrimers, polymer nanoparticles, hyperbranched polyesters), and metal/metal-oxide nanoparticles (iron oxide, gold, silver) are shared with the polymeric network to get nanocomposite hydrogels.

Smart Hydrogels

These are defined as hydrogels that suffer reversible large, physical or chemical changes in response to small external changes in the environmental circumstances, such as temperature, pH, light, electric field, magnetic field, ionic factors, biological molecules, etc.

Smart hydrogels have very promising applications in the biomedical field as delivery systems of therapeutic agents, tissue engineering scaffolds, cell culture supports, bio separation devices, actuators or sensors systems.

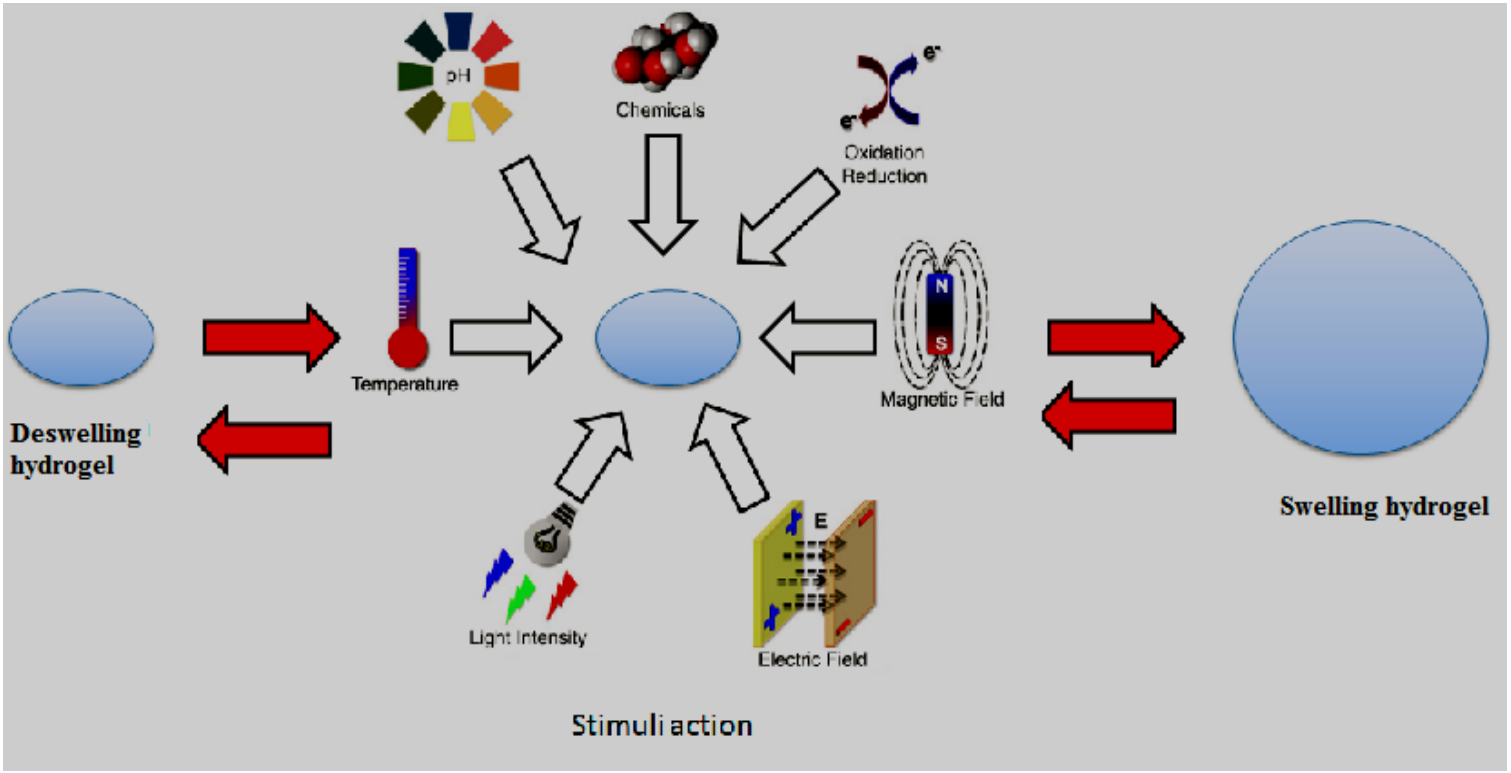

Figure (1): Stimuli responsive hydrogel

Synthesis of Nanomaterials

1. Synthesis of graphene oxide (GO)

Graphene oxide (GO) was synthesized from graphite powder using modified Hummer's method. In brief, graphite was oxidized by $KMnO_4$, $NaNO_3$ and H_2SO_4 in ice bath (at 0ºC).

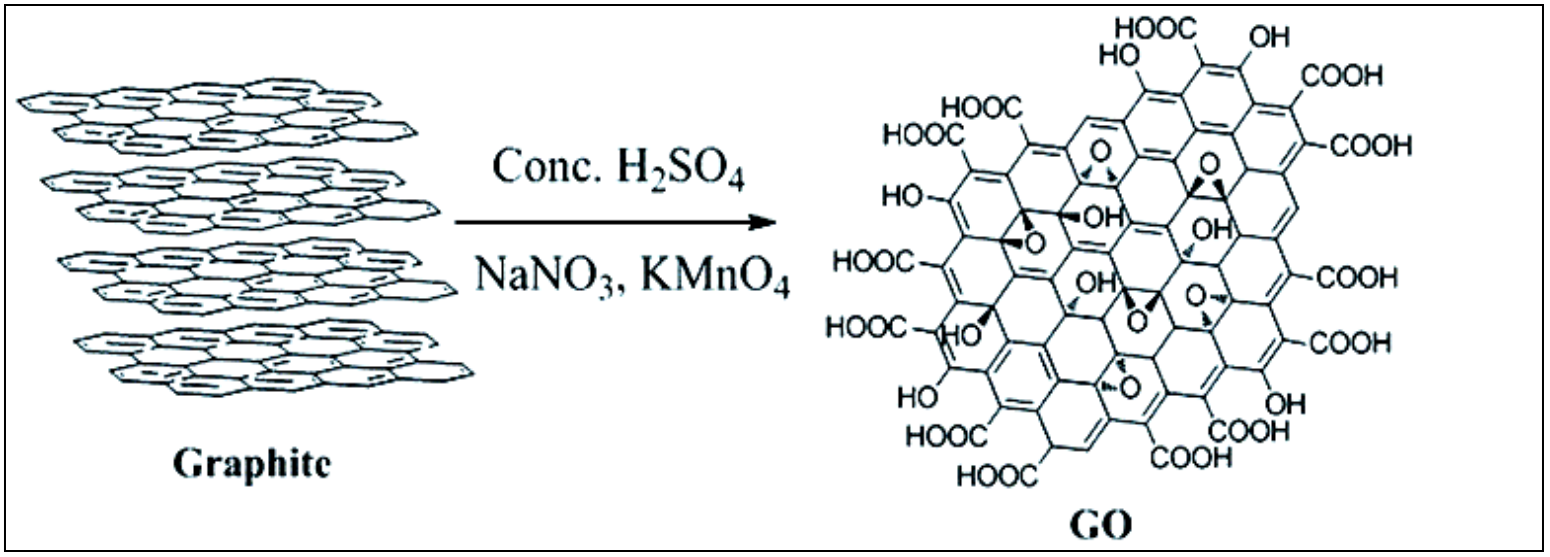

Scheme (1): Hummer's methods for synthesis GO

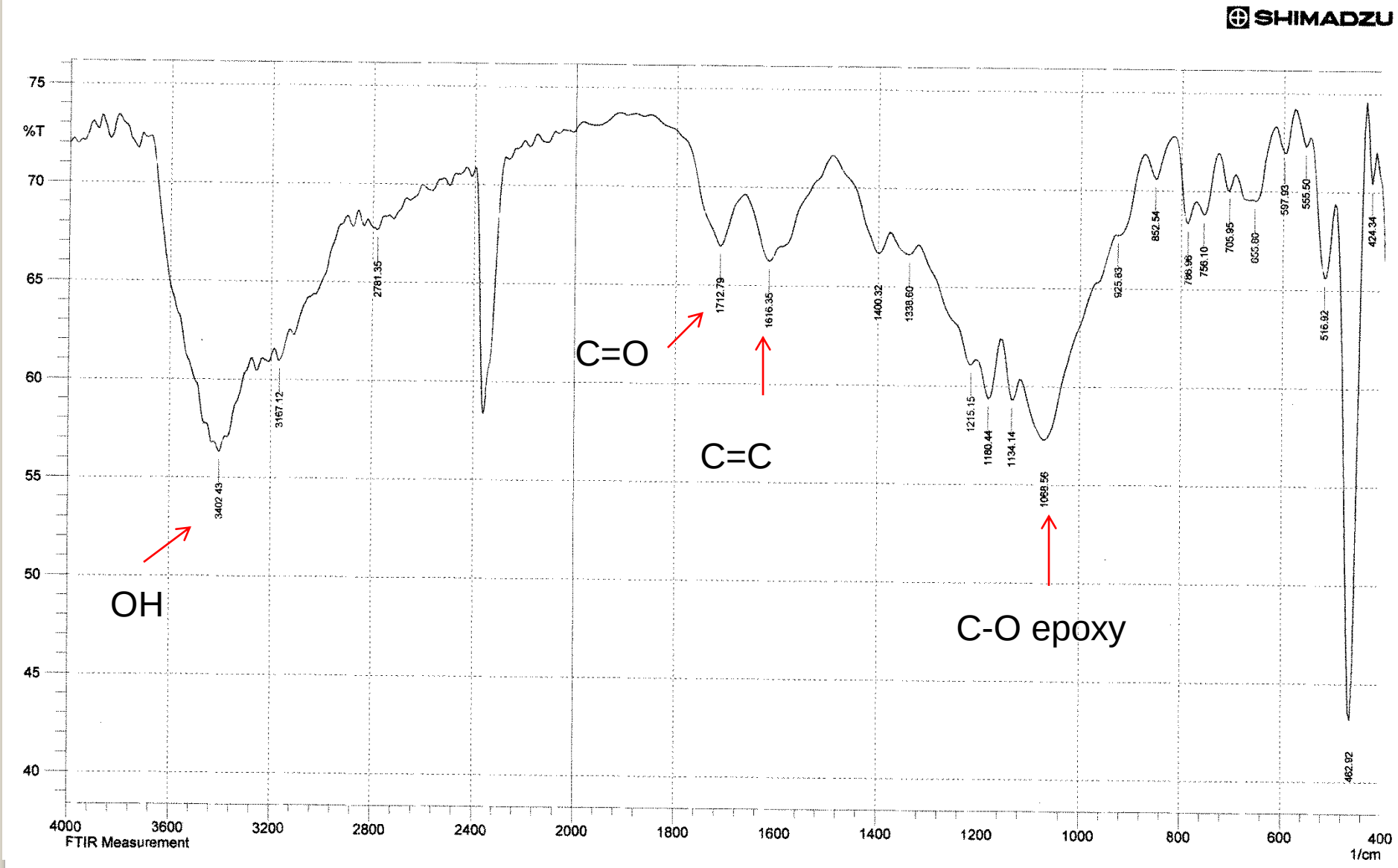

Figure (2): FT-IR spectrum of GO

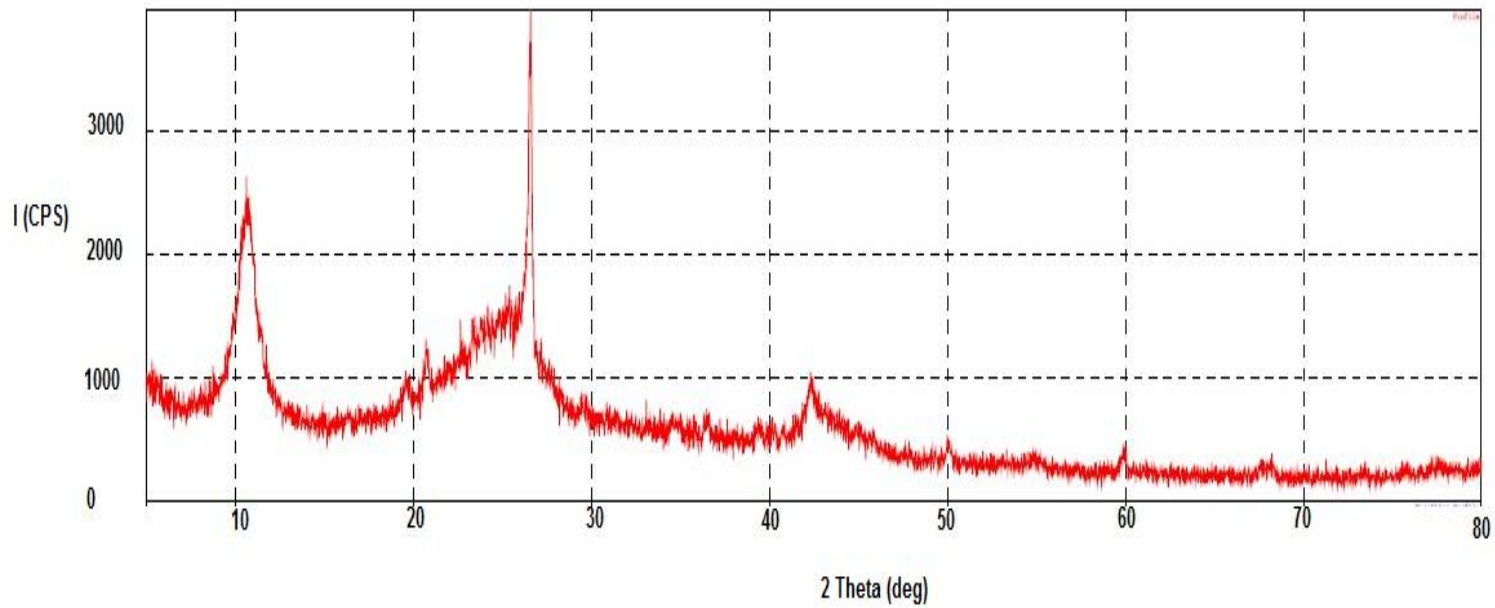

Figure (3): XRD for GO

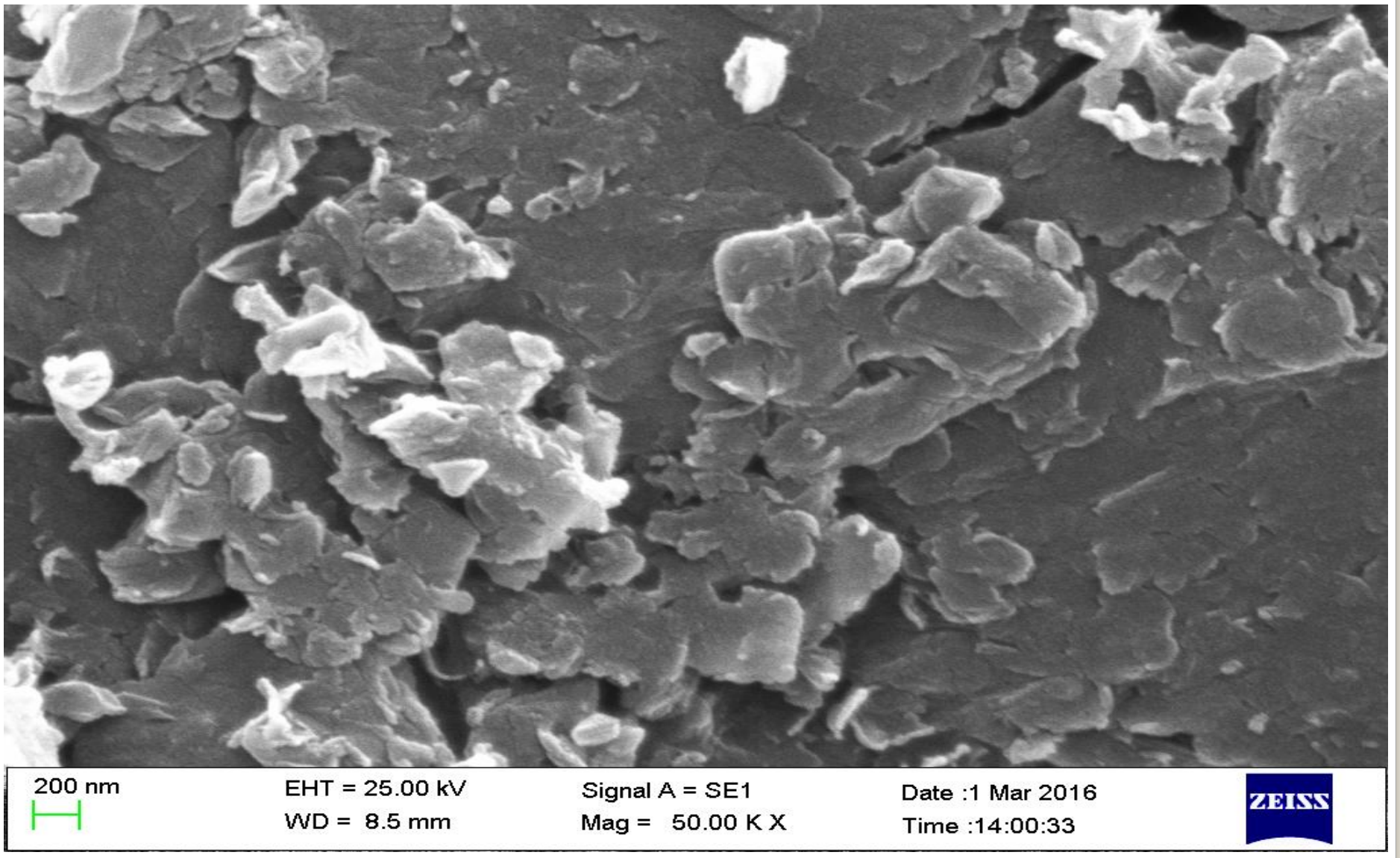

Figure (4): SEM photomicrograph of GO with magnification 50 KX

(a):

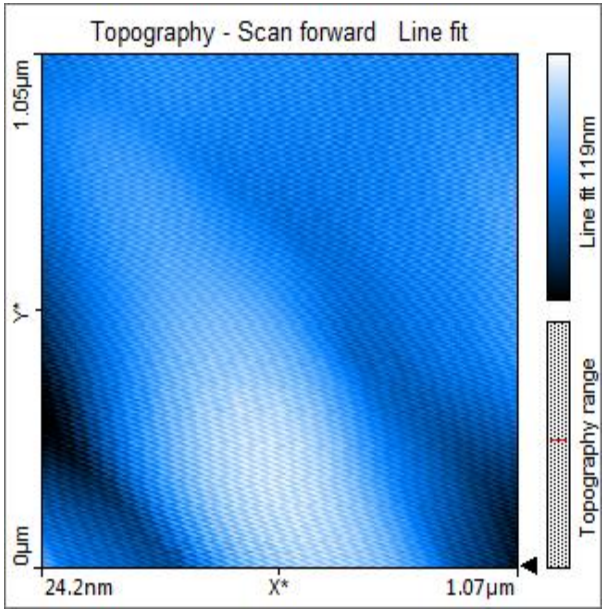

(b):

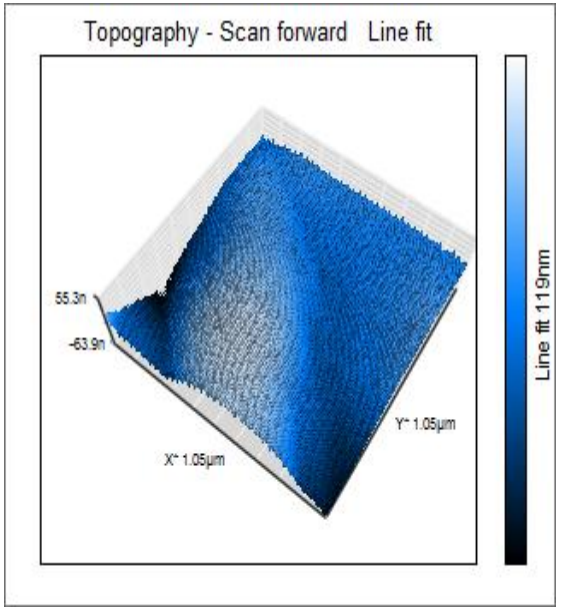

(c):

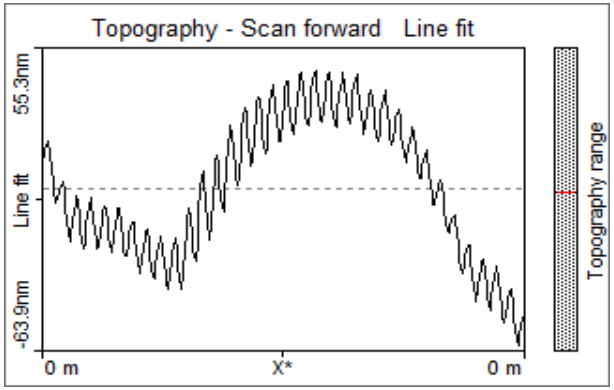

Figure (5): AFM photomicrograph of GO nanosheets, (a): scan topography, b: 3D topography, & (c): line graph topography

2. Synthesis of graphene (G)

In brief, GO dispersion was reduced by hydrazine monohydrate under reflux with stirring for (24 hrs).

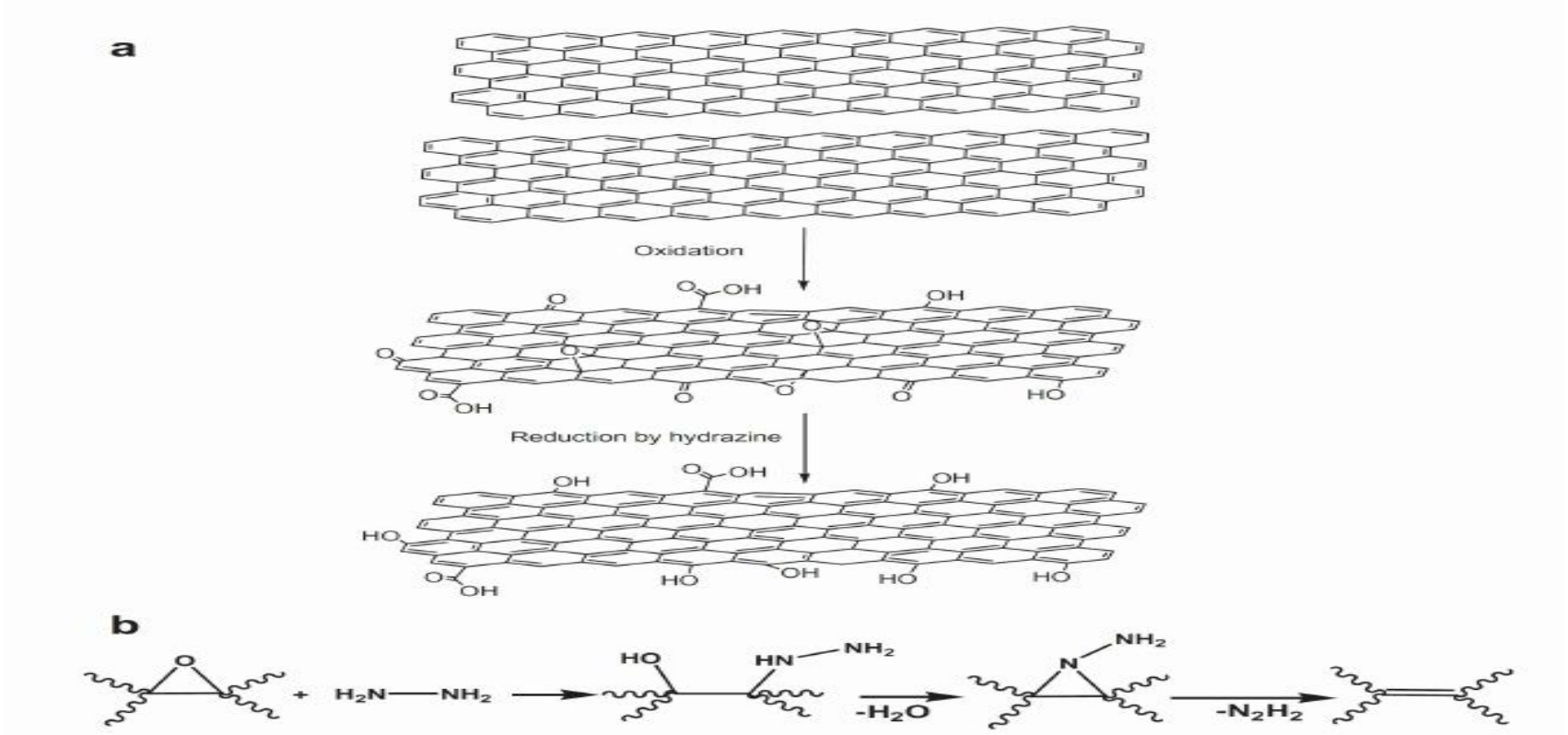

Scheme (2): Hummer's methods for synthesis G

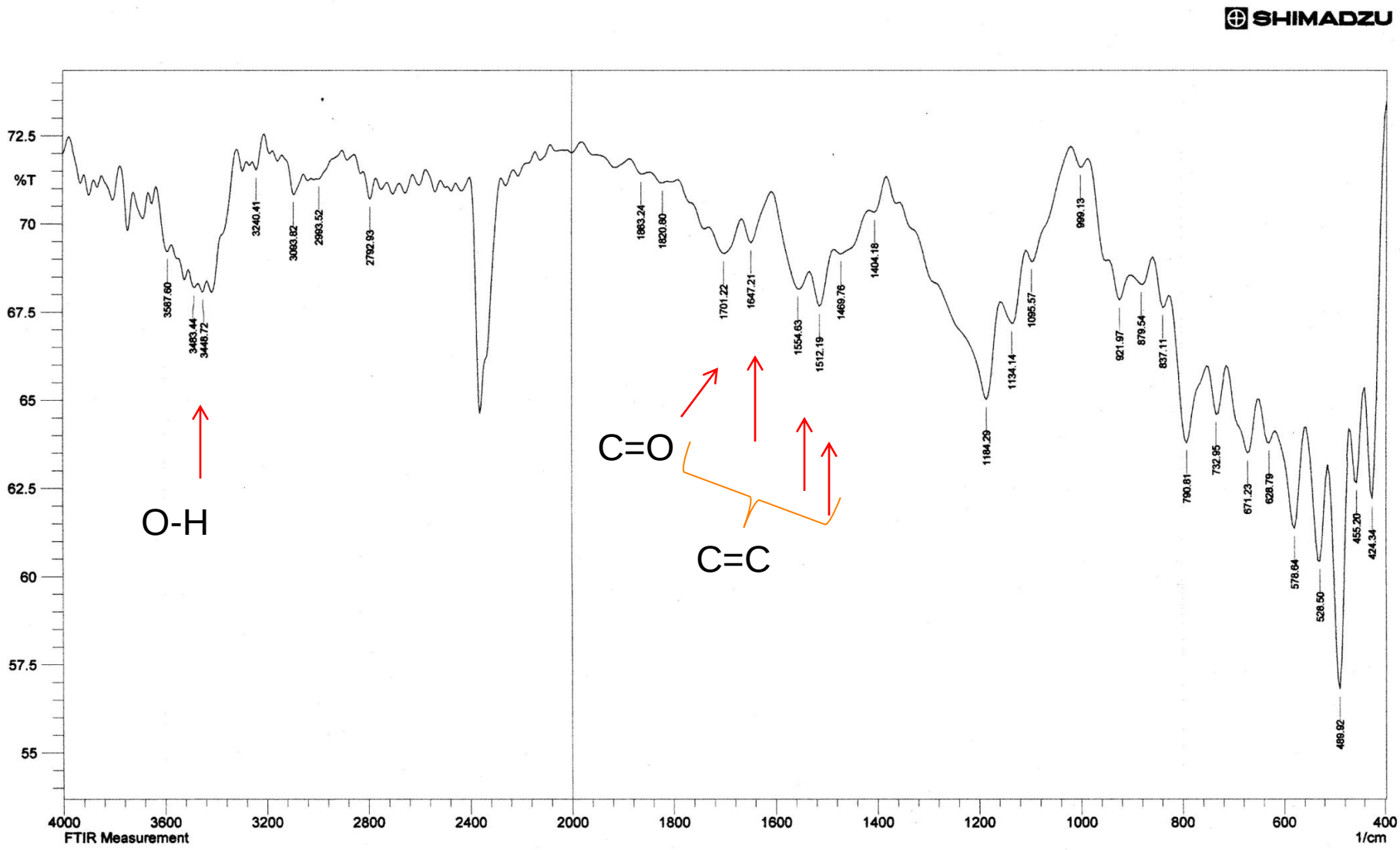

Figure (6): FT-IR spectrum of G

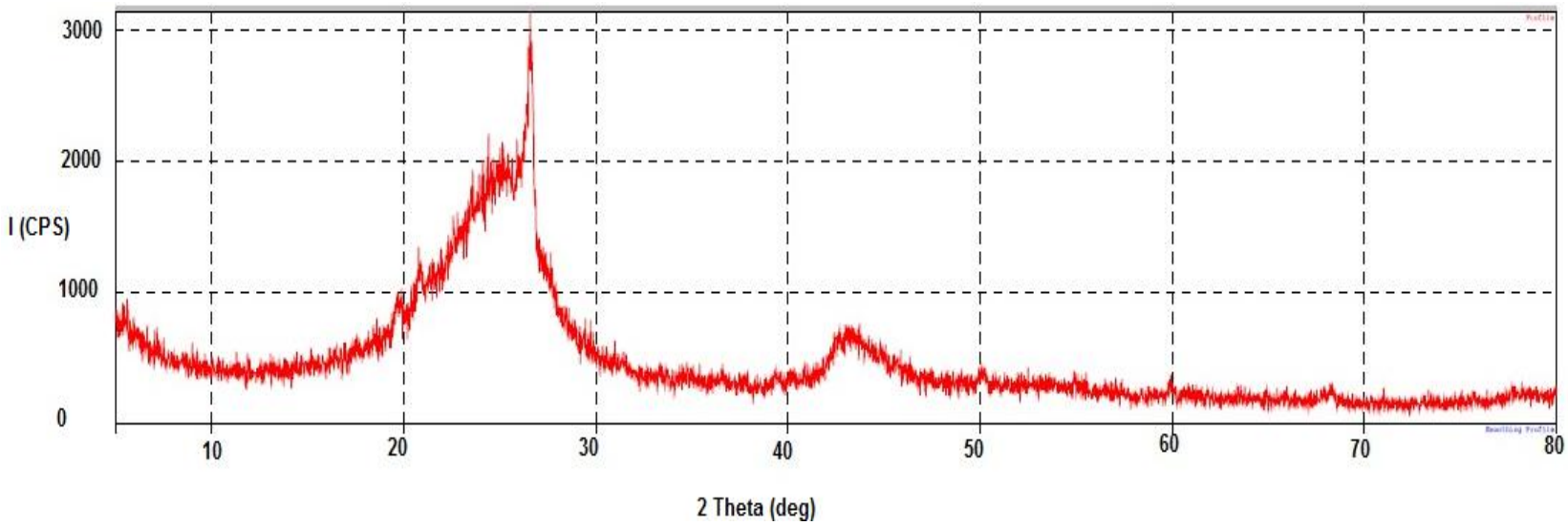

Figure (7): XRD for G

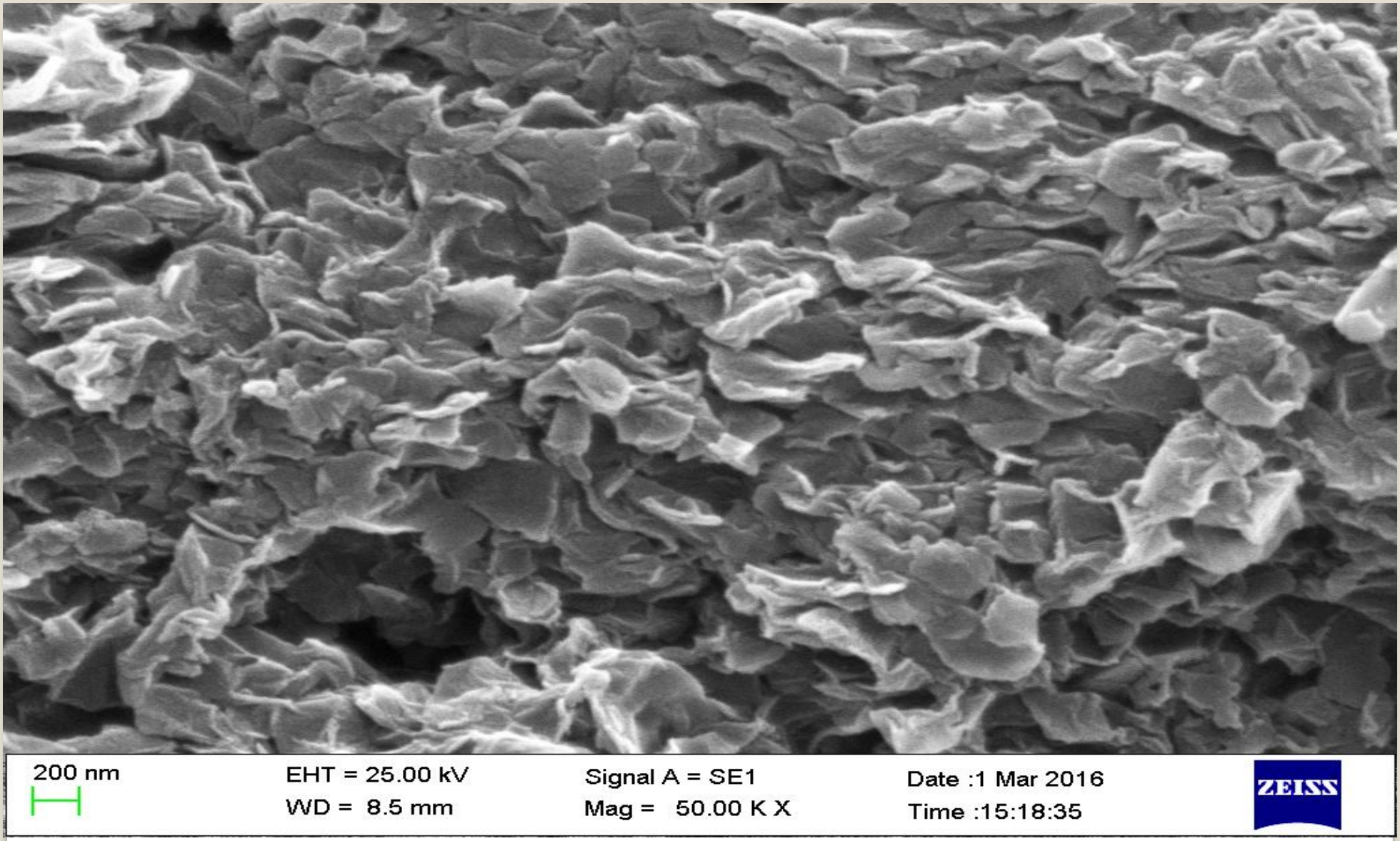

Figure (8): SEM photomicrograph of G with magnification 50 KX

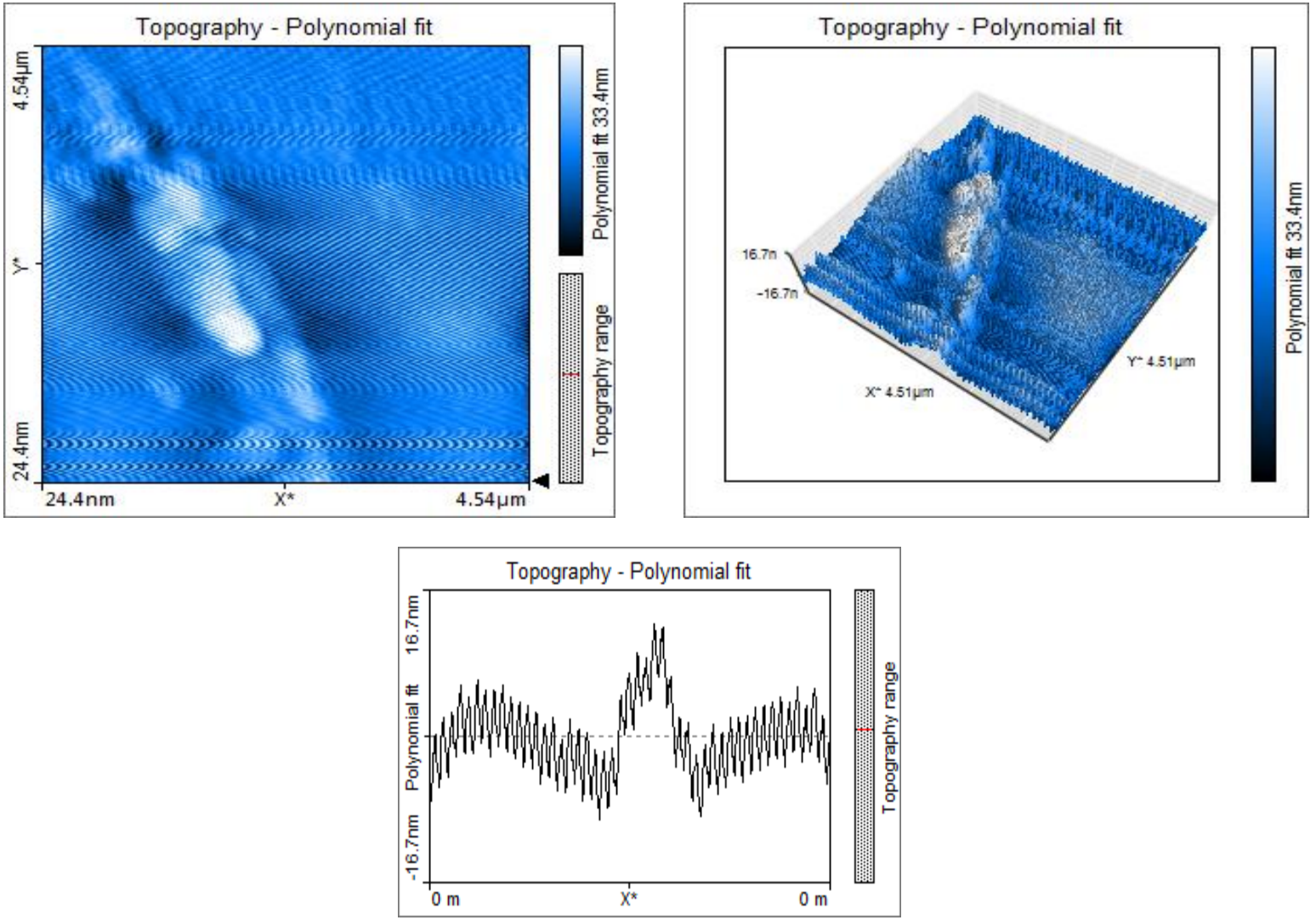

Figure (9): AFM photomicrograph of G nanosheets, (a): scan topography, b: 3D topography, & (c): line graph topography

3. Synthesis of magnetic nanoparticles of Fe_3O_4 (MNPs)

Magnetite nanoparticle was synthesized by chemical co- precipitation method. In brief, mixed solution of $FeCl_3$ and $FeSO_4.7H_2O$ (molar ratio 2:1) in water bath set at (60ºC) with stirring under nitrogen for(1 h) then added ammonium hydroxide as precipitant agent at (80ºC).

$$Fe^{+2} + 2Fe^{+3} + 8OH^- \rightarrow Fe_3O_4 + 4H_2O$$

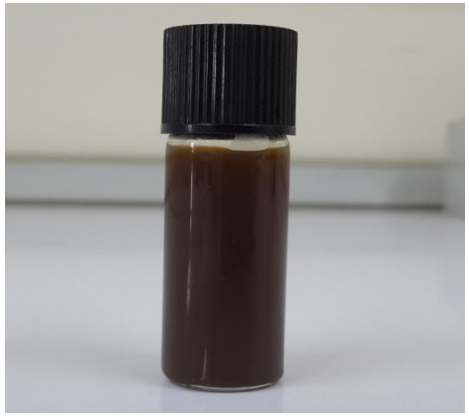

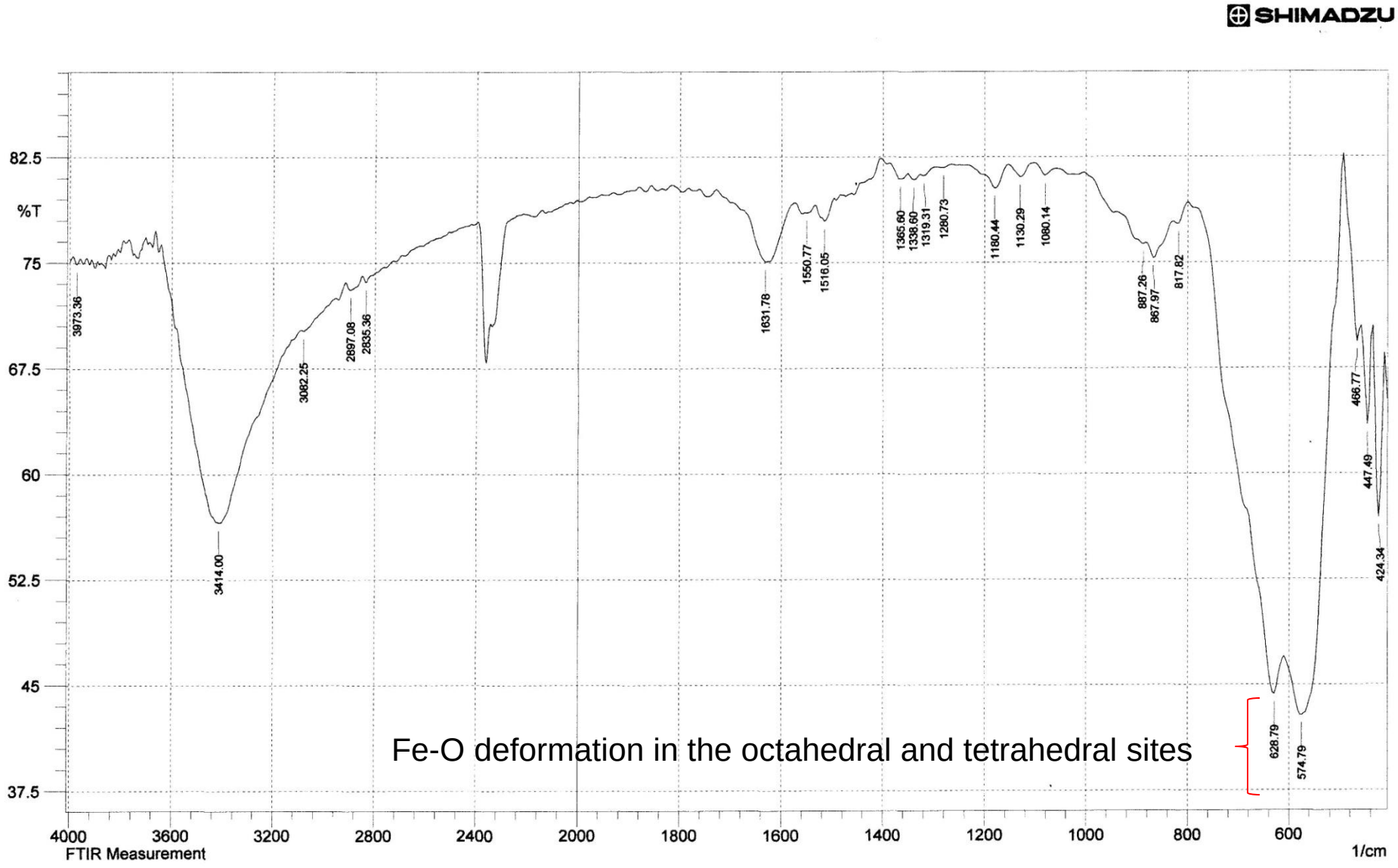

Figure (10): FT-IR spectrum of Fe_3O_4 MNPs

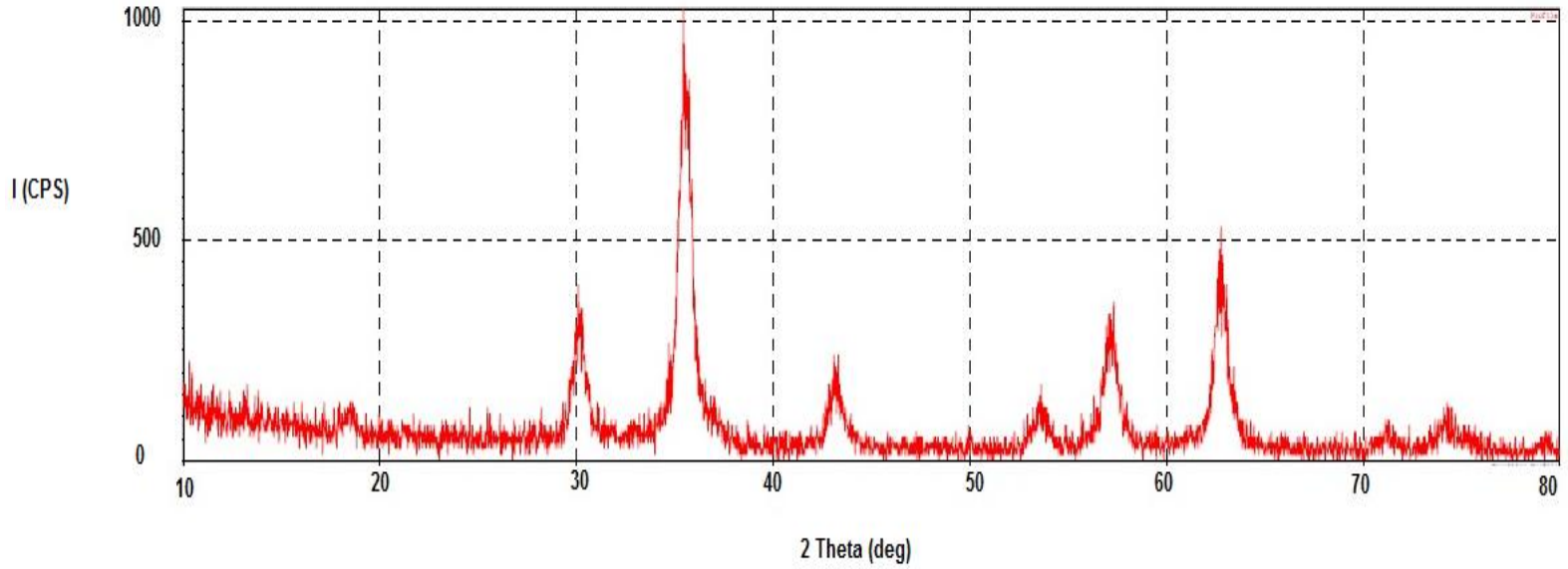

Figure (11): XRD for Fe_3O_4 MNPs

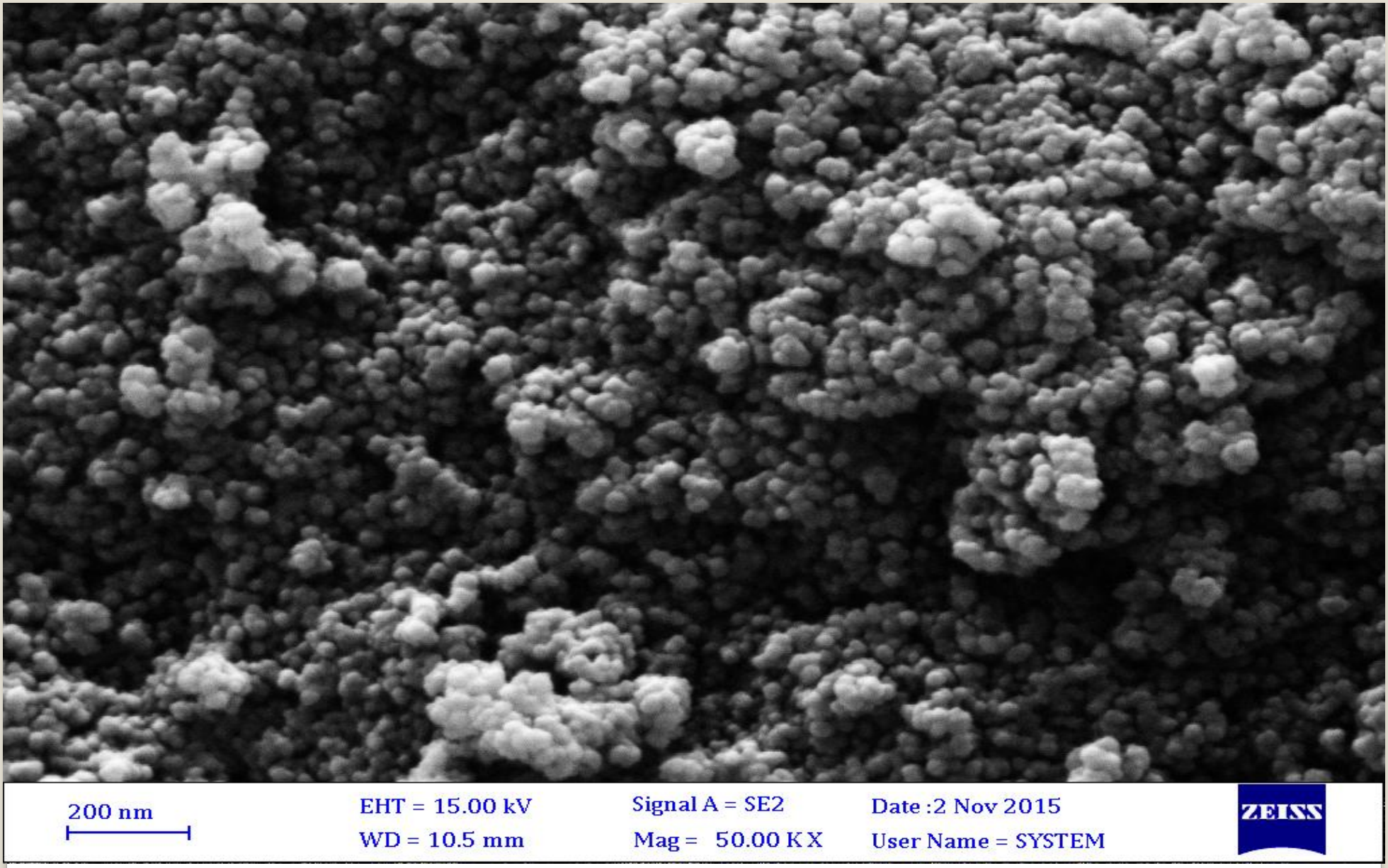

Figure (12): SEM photomicrograph of Fe_3O_4 with magnification 50 KX

The EDS analysis of uncoated sample was show the purity of Fe3O4 MNPs, and only the elements Fe and O appeared in the analysis in the selected area of the sample at SEM micrographs.

a)

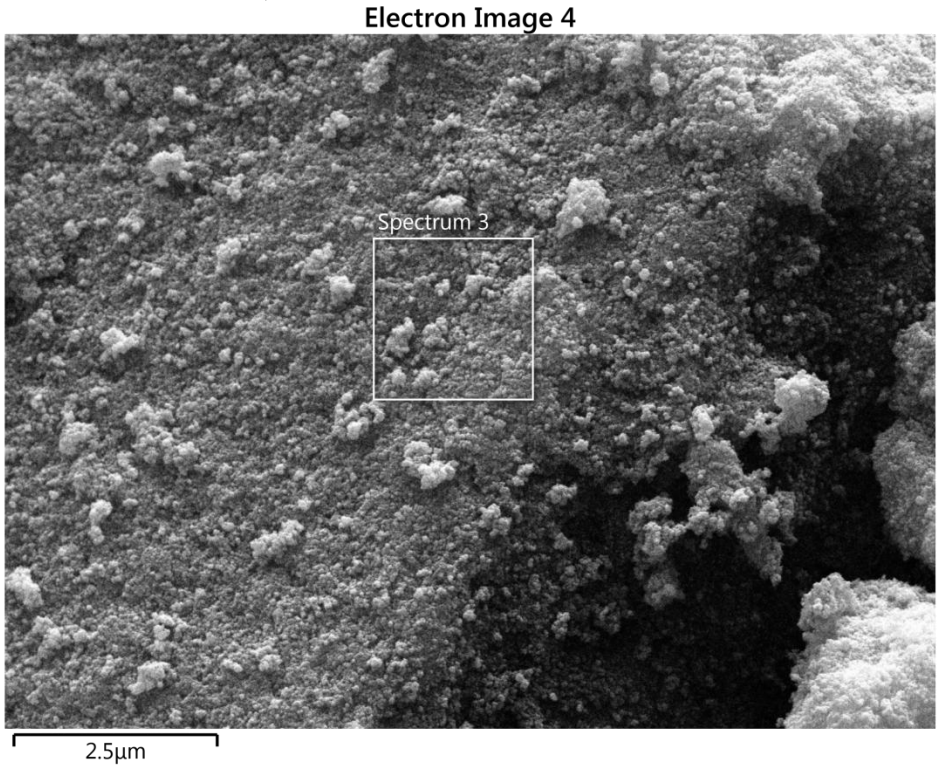

b)

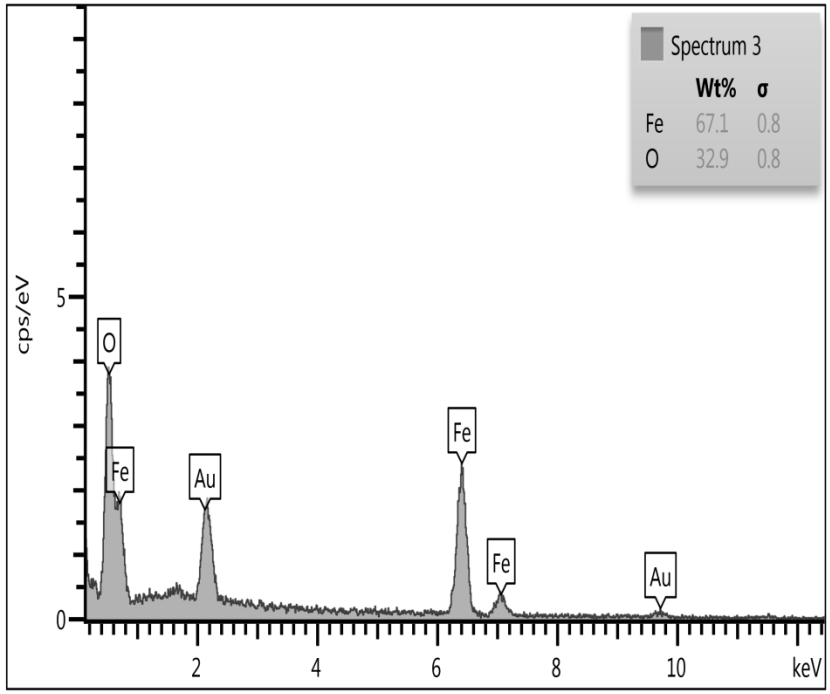

Figure (13): (a) SEM and (b) EDS for uncoated Fe_3O_4

TEM image of magnetite nanoparticles showed that the prepared nanoparticles was in a spherical form. The surface morphology of magnetite nanoparticles tends to aggregation due to its high surface energy, magnetization and large specific surface area effect

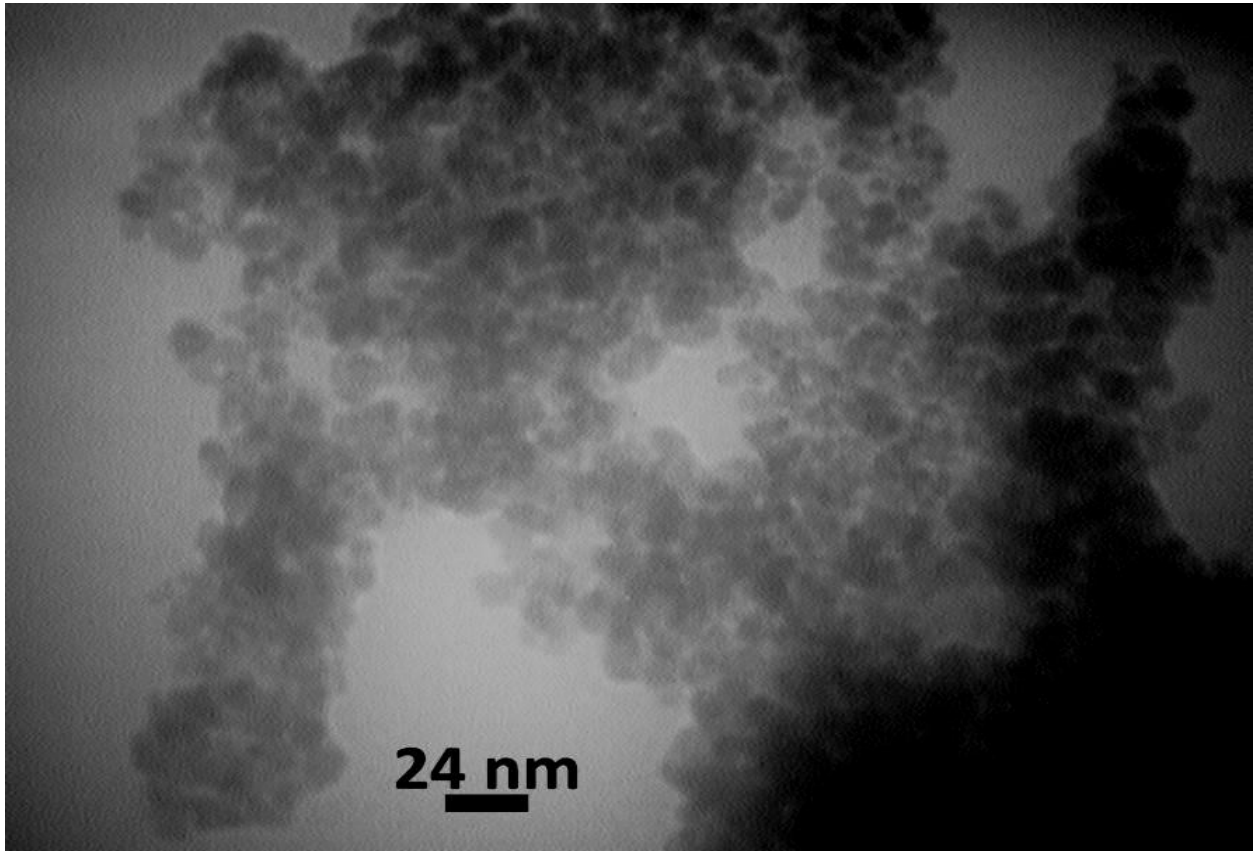

Figure (14): TEM photomicrograph of uncoated Fe_3O_4

(a)

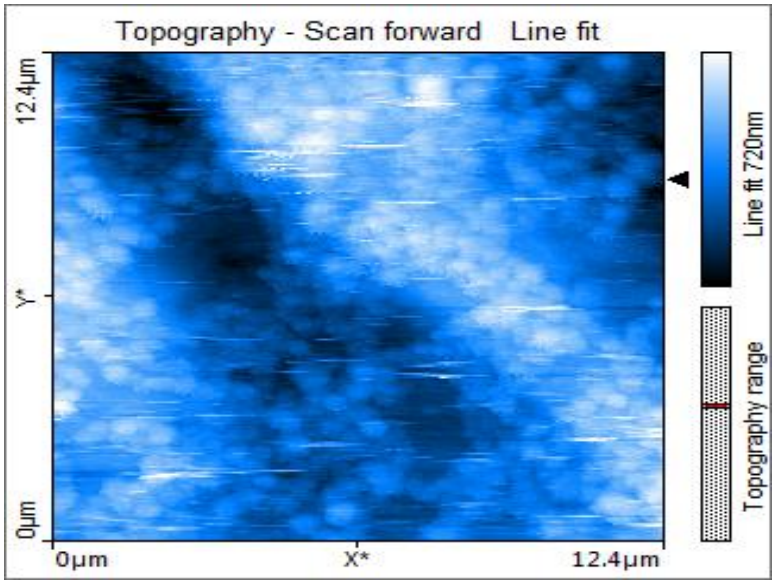

(b)

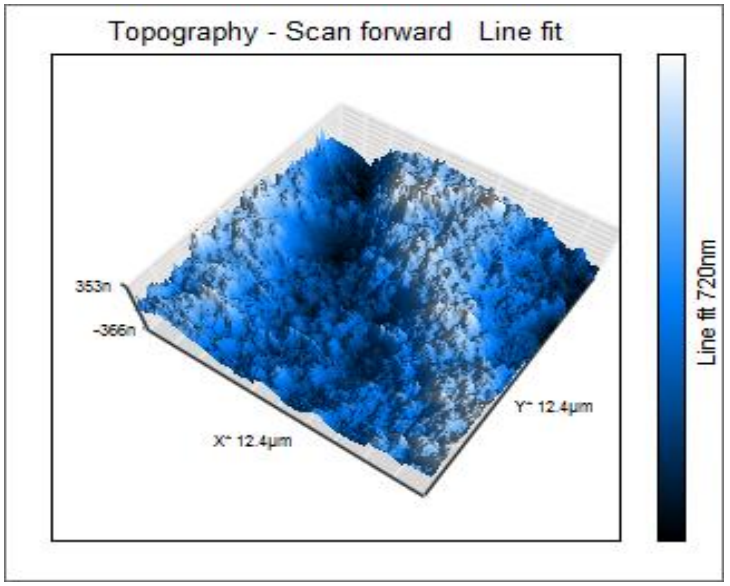

(c)

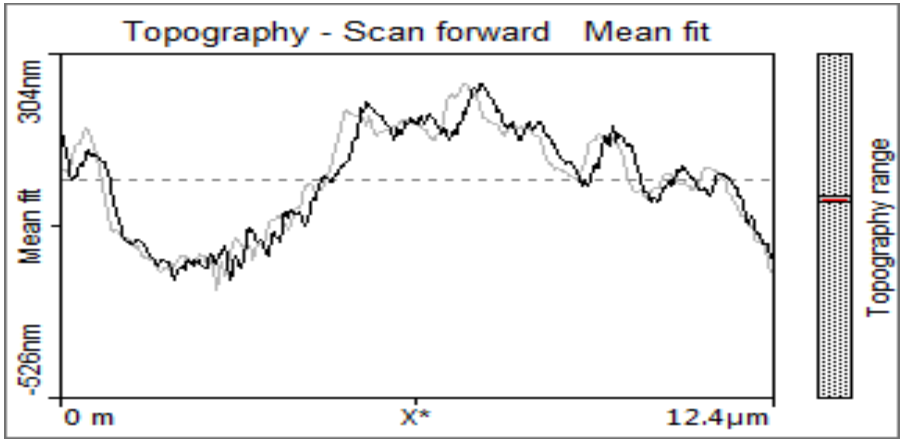

Figure (15): AFM photomicrograph of accumulation of Fe_3O_4 MNPs , (a): scan topography, b: 3D topography, & (c): line graph topography

(a)

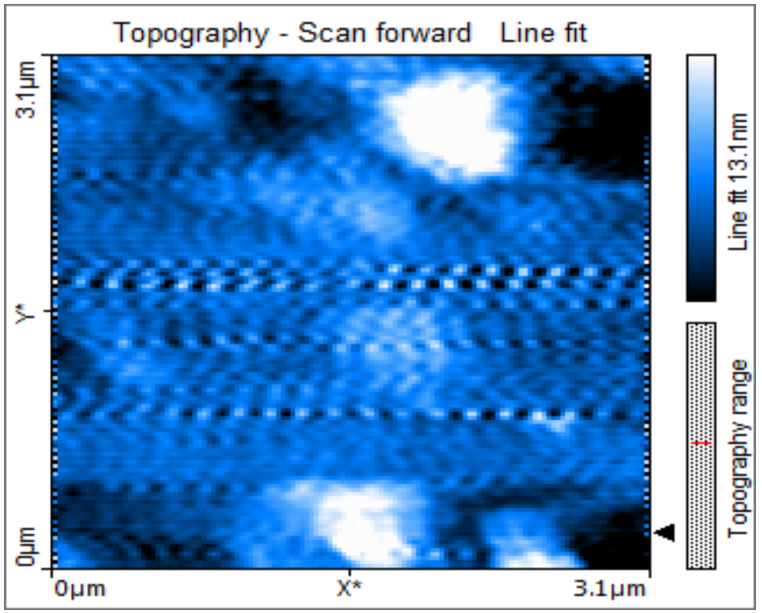

(b)

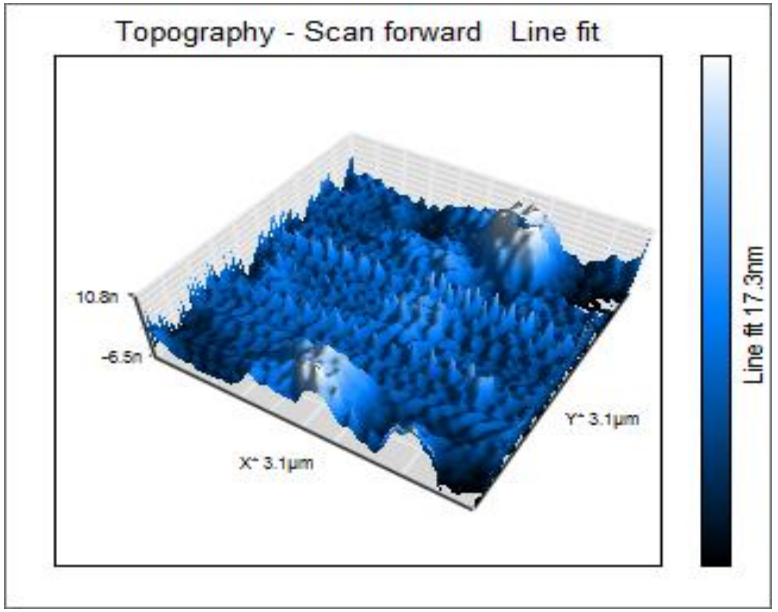

(c)

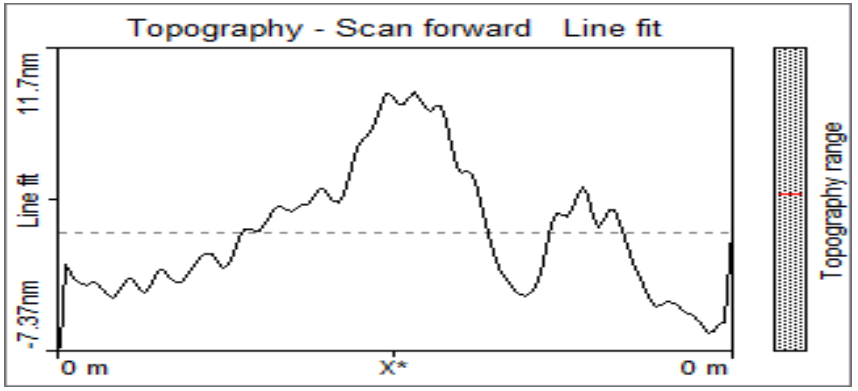

Figure (16): AFM photomicrograph of Fe_3O_4 MNPs , (a): scan topography, (b): 3D topography, & (c): line graph topography

Superparamagneticity of the uncoated magnetite was proved using vibrating sample magnetometry (VSM) with an applied magnetic field with the field range of -10000 to + 10000 Oersted at room temperature. As show in this figure, the hysteresis loop is completely reversible, the hysteresis has an "S" shape where both the descending and ascending loops coincide and yield zero coercivity, indicating that the magnetite nanoparticle is superparamagnetic.

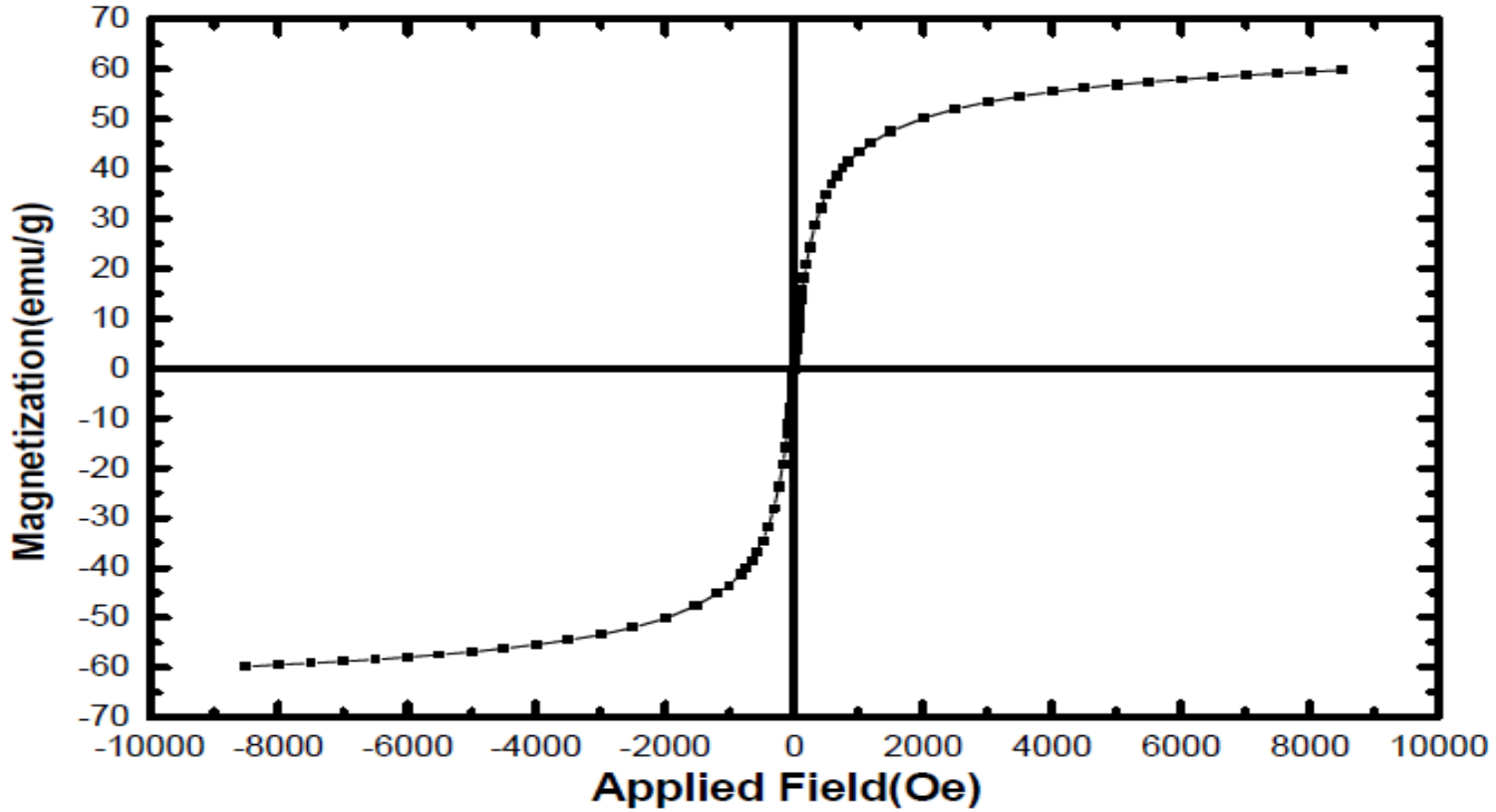

Figure (17): Hysteresis loop of uncoated Fe_3O_4

4. Synthesis of polyaniline (PANI)

In brief, aniline hydrochloride was oxidized by ammonium persulfate in ice bath.

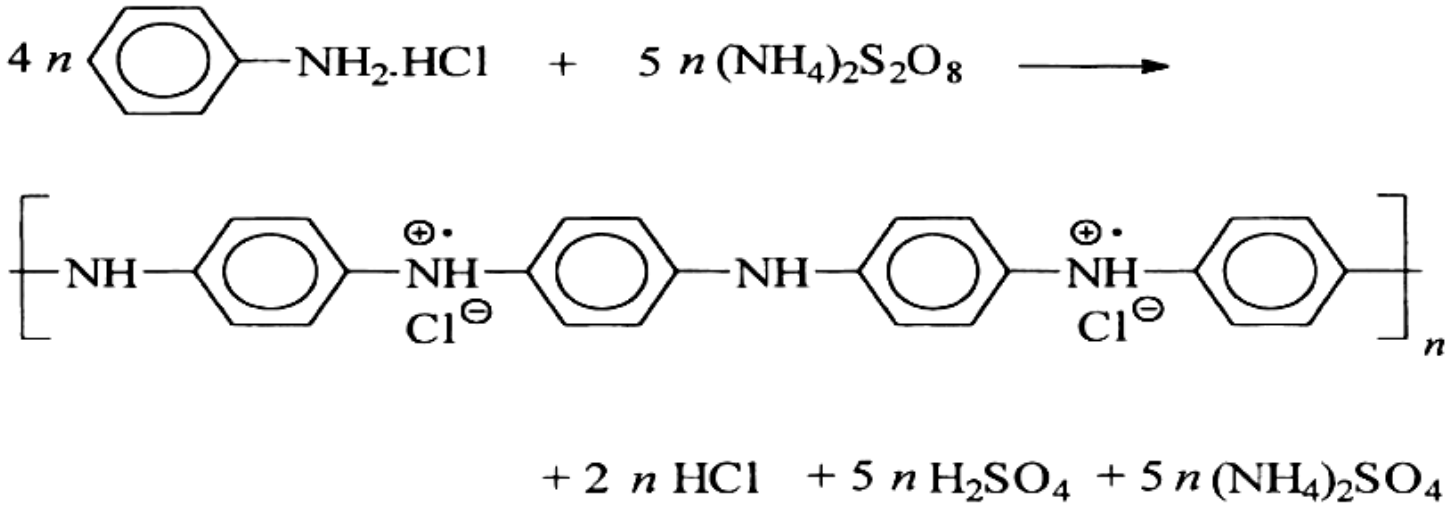

Scheme (3): Oxidation of aniline hydrochloride with ammonium persulfate yields polyaniline (emeraldine) hydrochloride

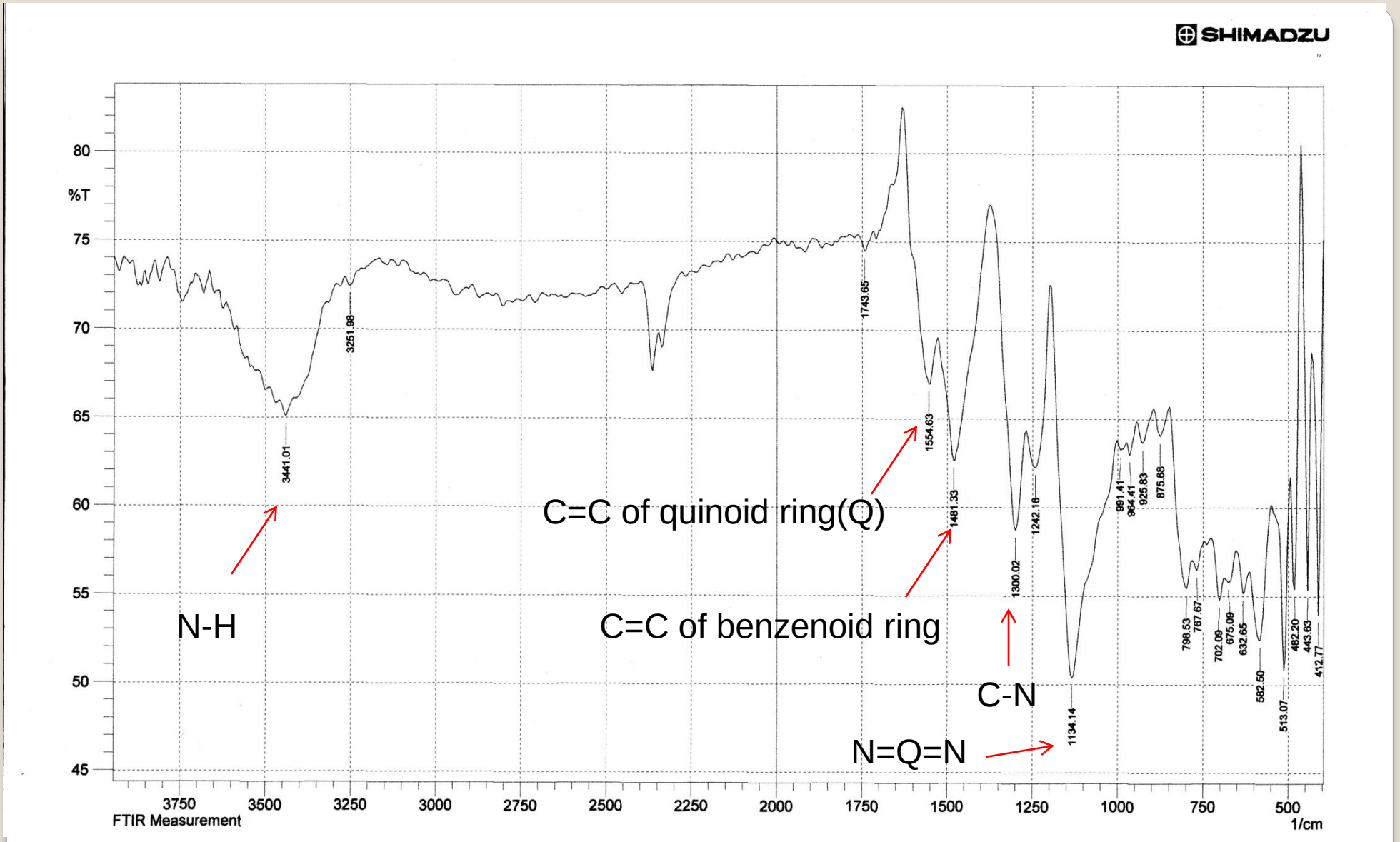

Figure (18): FT-IR spectrum of PANI

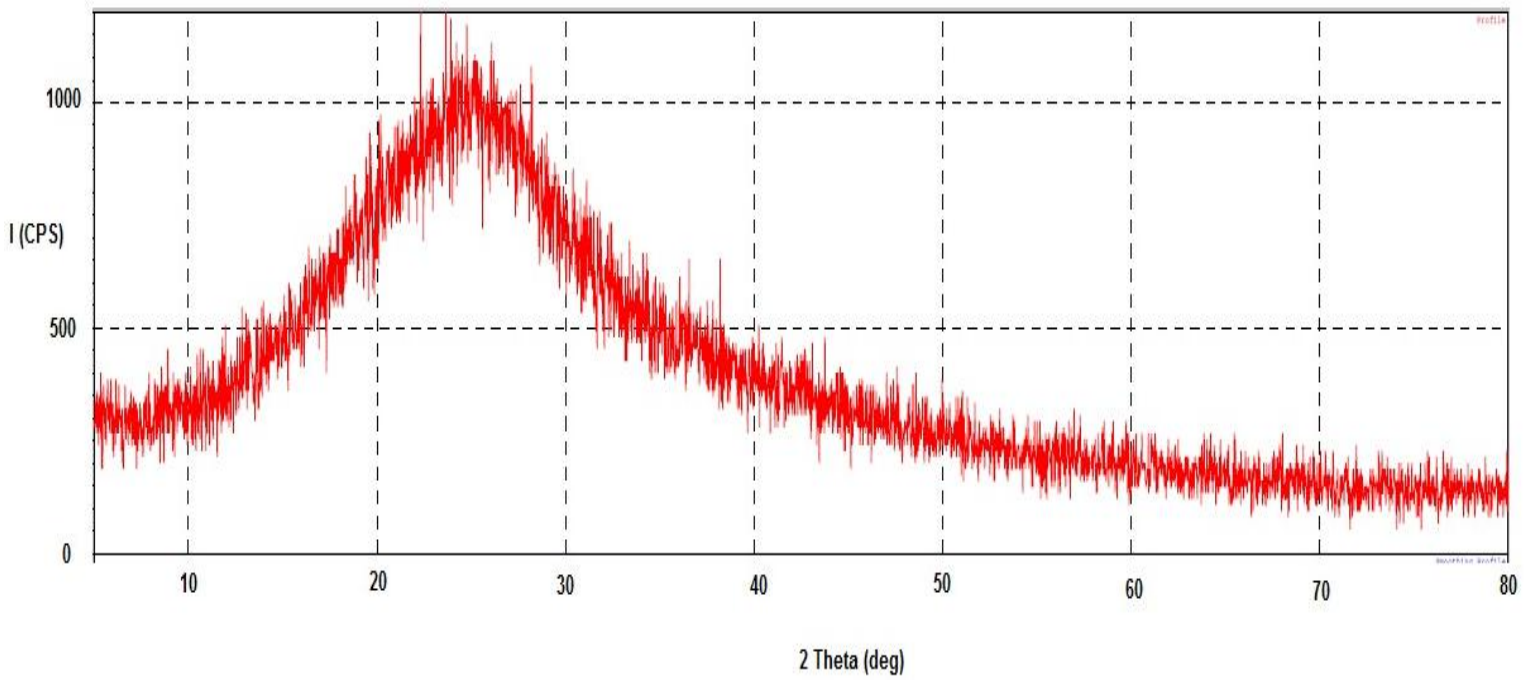

Figure (19): XRD for PANI

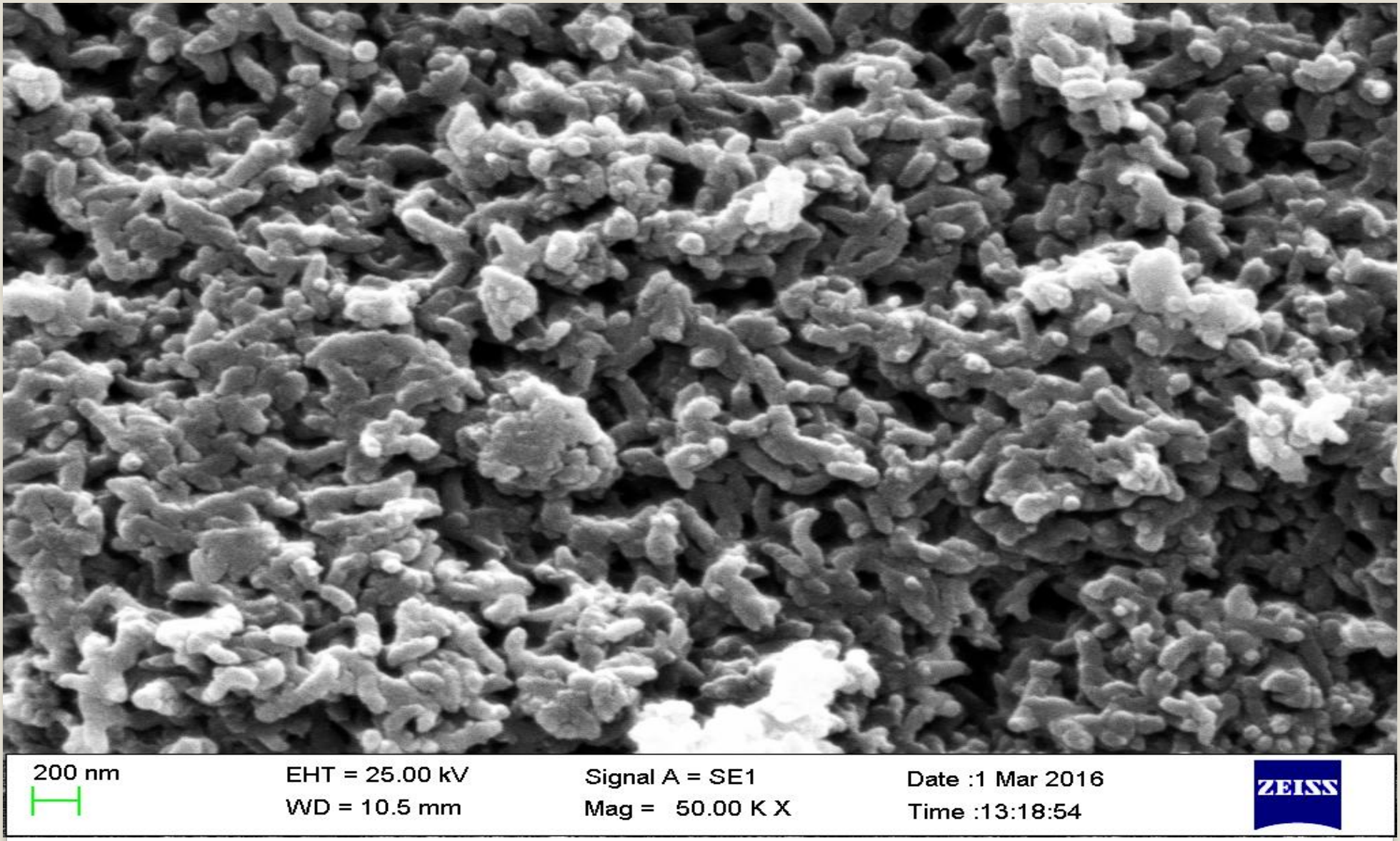

Figure (20): SEM photomicrograph of PANI with magnification 50 KX

Preparations of Hydrogels

PVA solution (10%w/v) was prepared by dissolving (10g) of PVA in (100ml) distilled water with stirring at 70ºC, chitosan solution (1%w/v) was prepared by dissolving (1g) of chitosan in acetic acid solution (1%) with stirring at 60ºC, and Pectin solution (2.5 %w/v) was prepared by dissolving(0.5g) of pectin in (20ml) distilled water with stirring at 50ºC.

1. Preparation of hydrogel (CPG) from crosslinking between chitosan and PVA by glutaraldehyde

CPG hydrogel was prepared by mixing equal volumes of PVA solution with chitosan solution. The mixture was stirred constantly until homogeneous at 60ºC and the appropriate amount of crosslinking agent (10 ml) of glutaraldehyde solution (1.25%) was added into the mixture under constant stirring with (2 drops) of concentrated H_2SO_4 concentration.

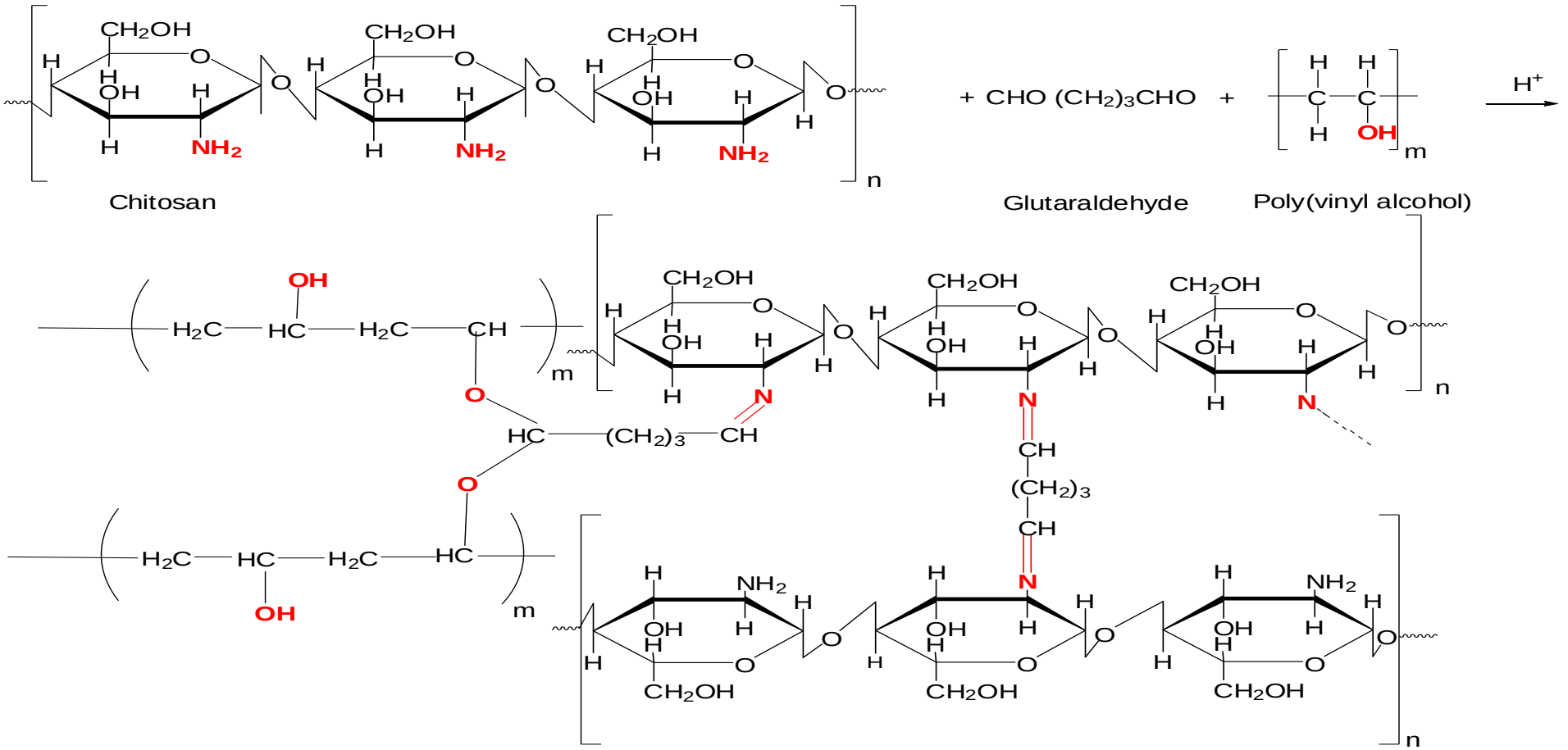

Scheme (4): Cross-linking of chitosan, PVA with glutaraldehyde

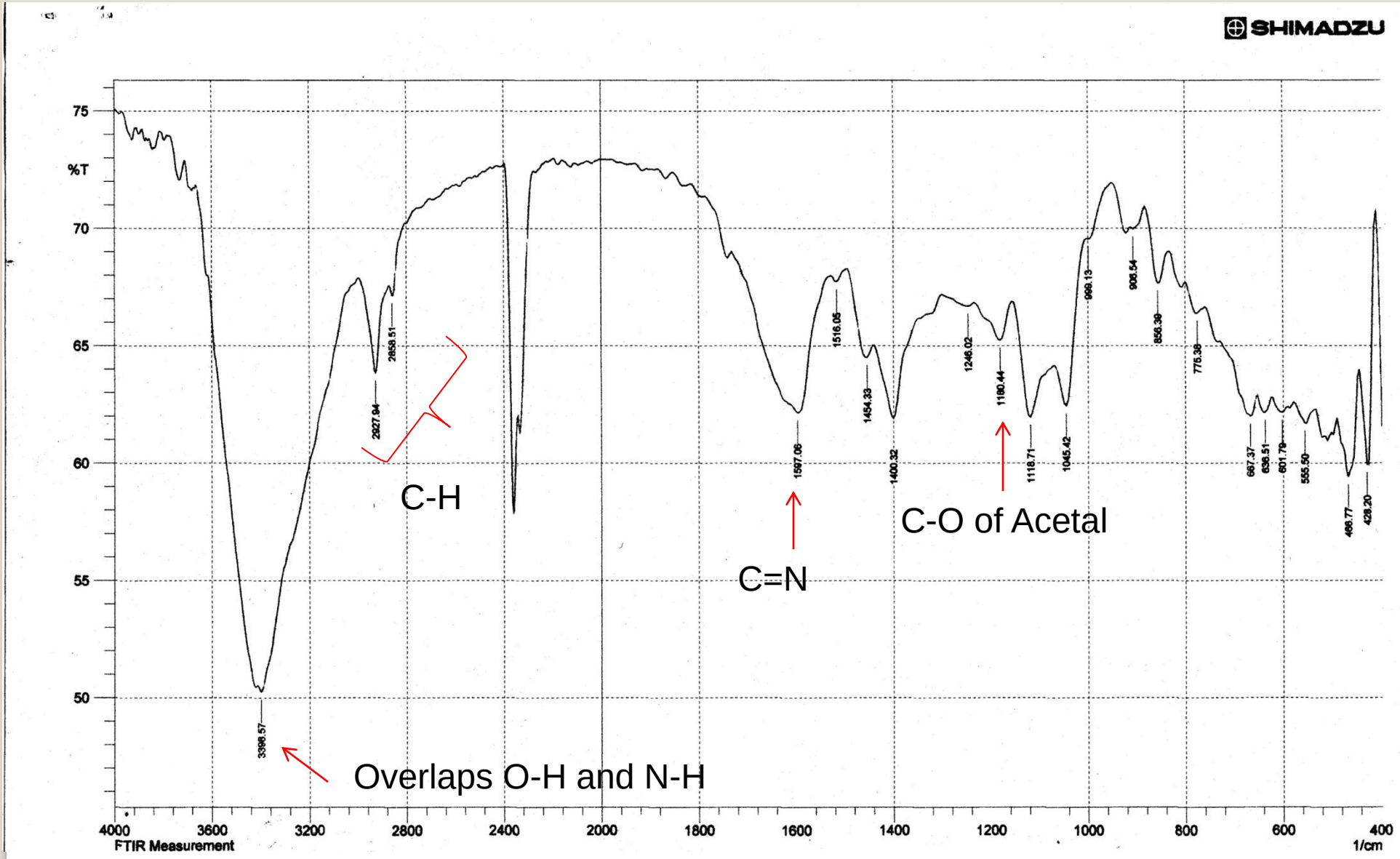

Figure (21): FT-IR spectrum of CPG hydrogel film

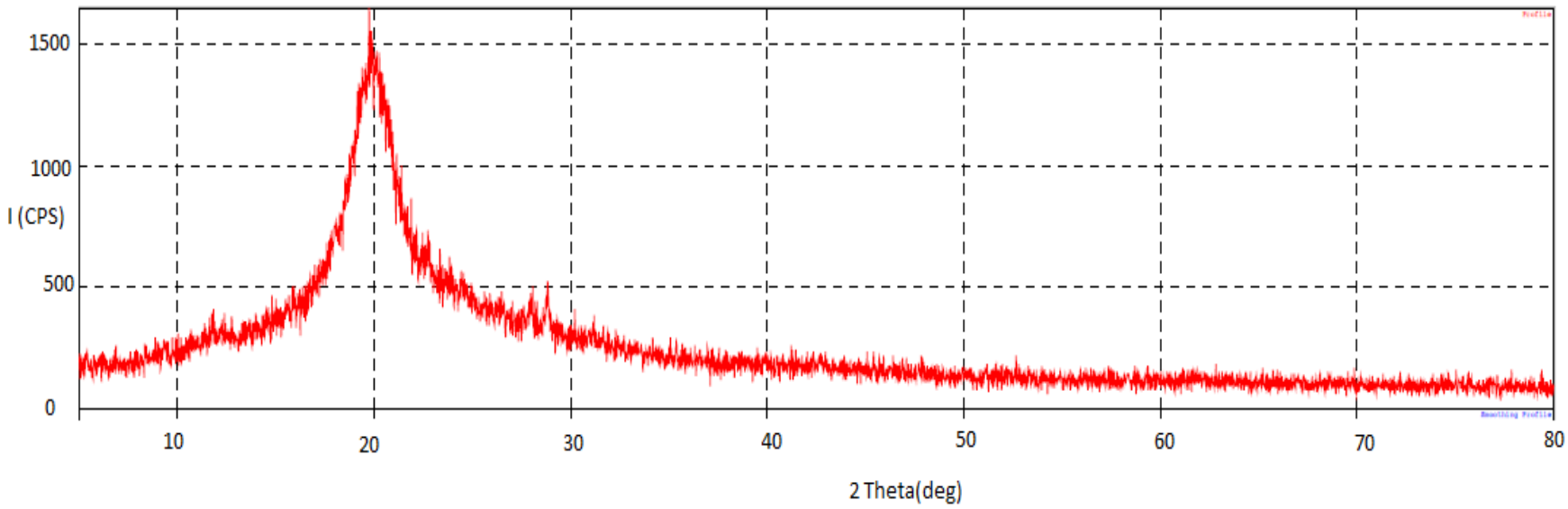

Figure (22): XRD for CPG hydrogel

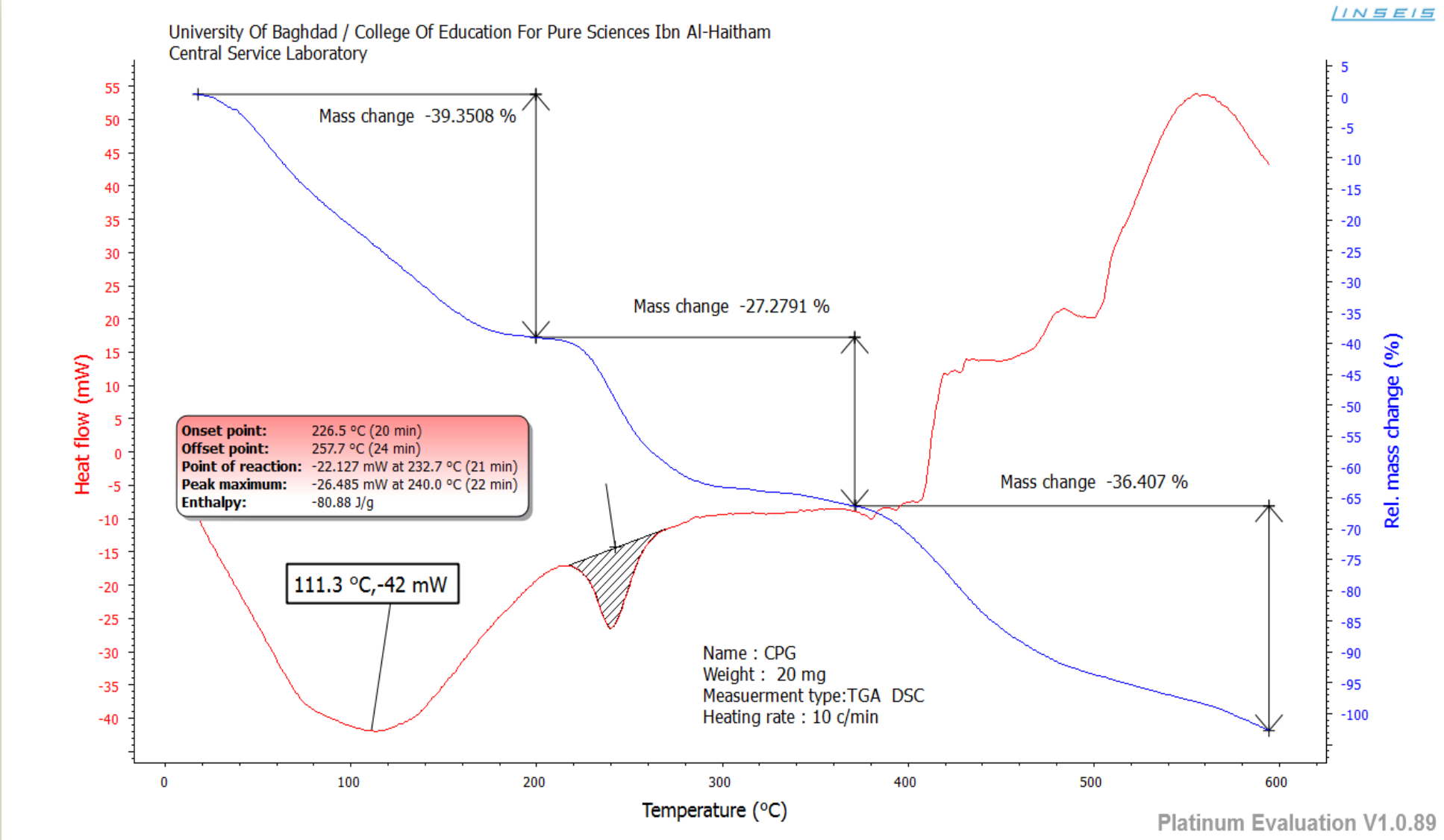

Figure (23): TGA and DSC of CPG hydrogel film

(a)

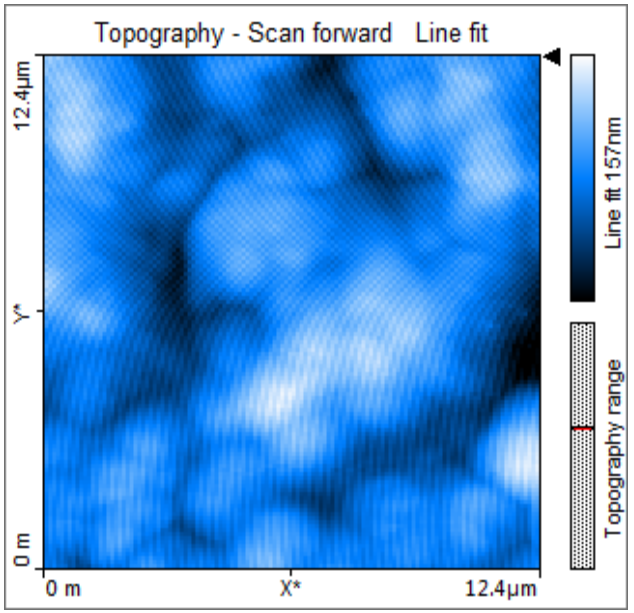

(b)

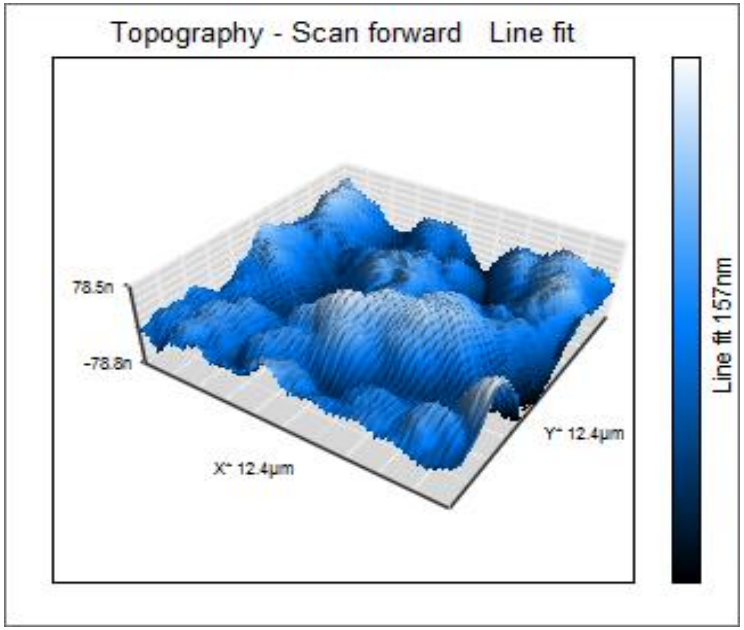

(c)

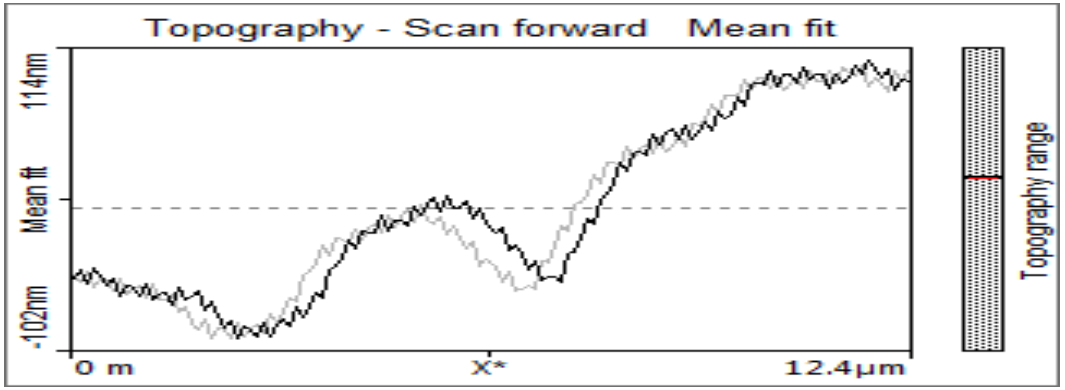

Figure (24): AFM photomicrograph of CPG , (a): scan topography, b: 3D topography, & (c): line graph topography

2. Preparation of hydrogel (CPM) from crosslinking between chitosan and PVA by maleic anhydride

CPM hydrogel was prepared with a similar method as above (preparation of CPG hydrogel) except added (0.3g) of maleic anhydride instead of glutaraldehyde as crosslinker agent.

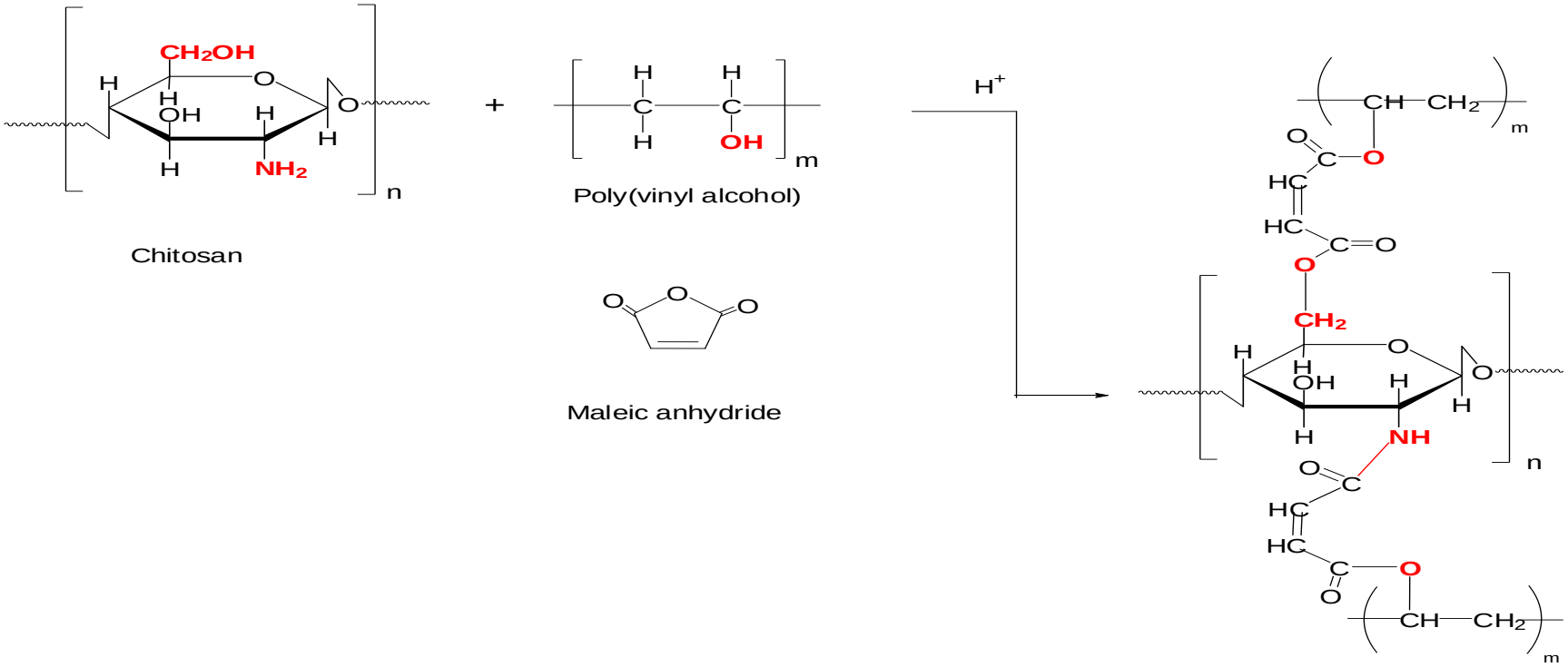

Scheme (5): Cross-linking of chitosan, PVA with maleic anhydride

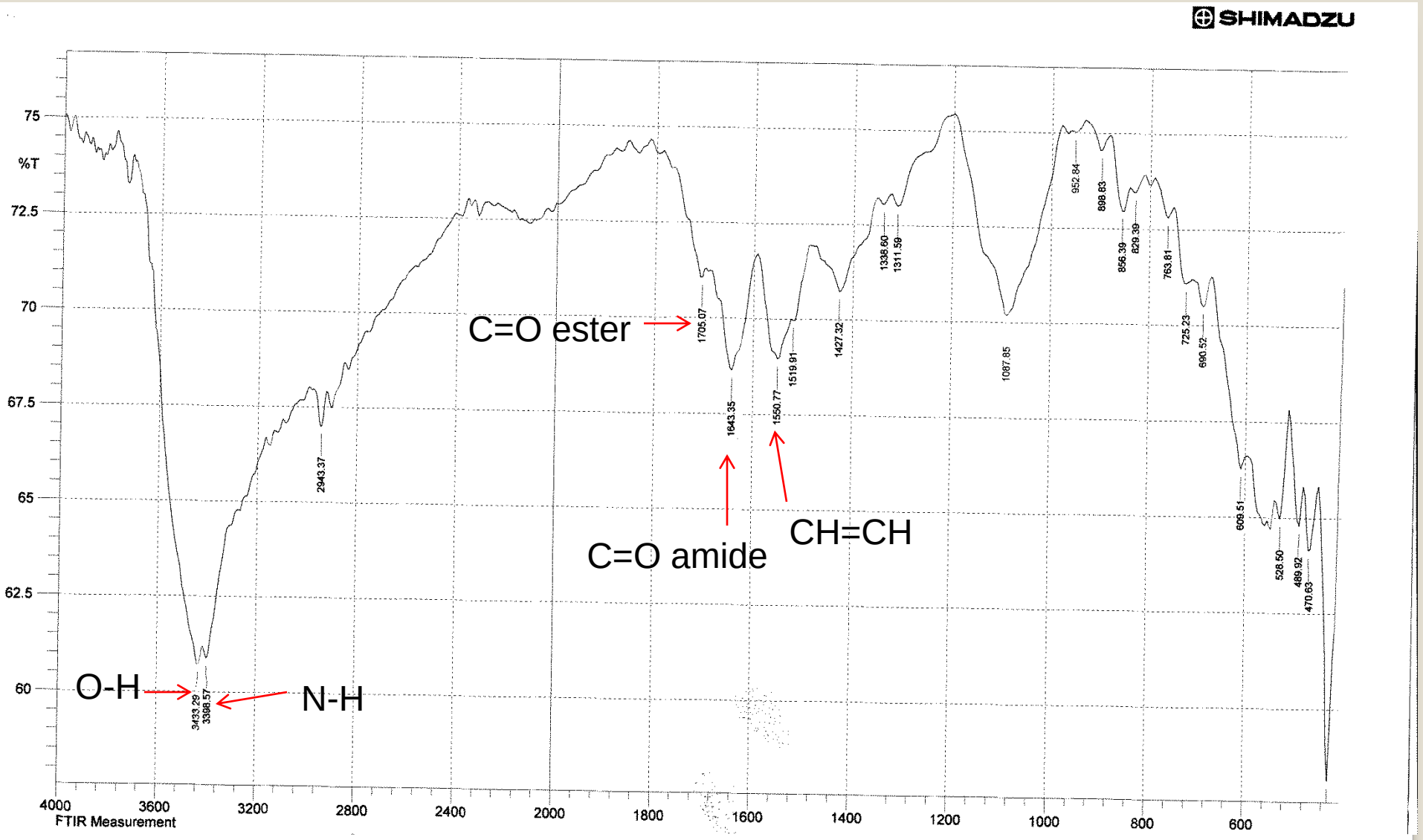

Figure (25): FT-IR spectrum of CPM hydrogel film

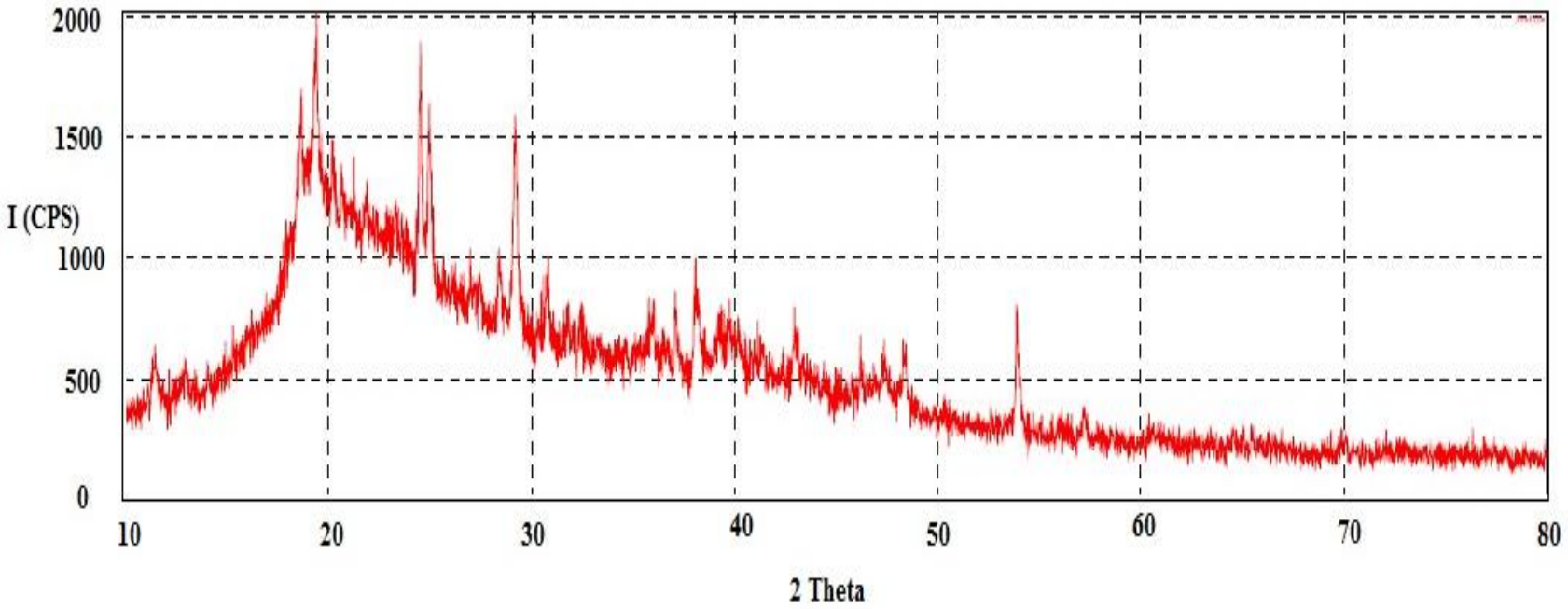

Figure (26): XRD for CPM hydrogel film

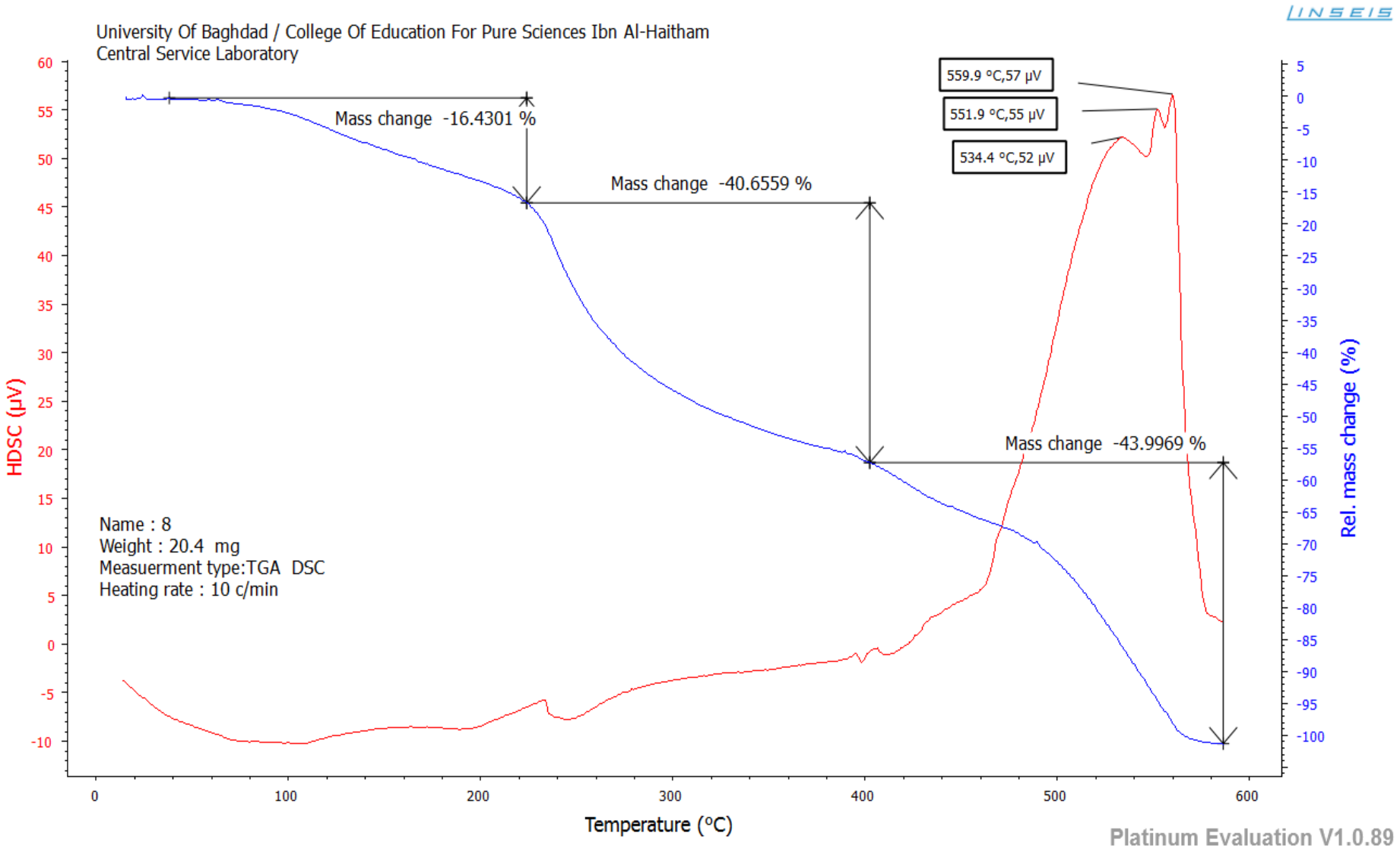

Figure (27): TGA and DSC of CPM hydrogel film

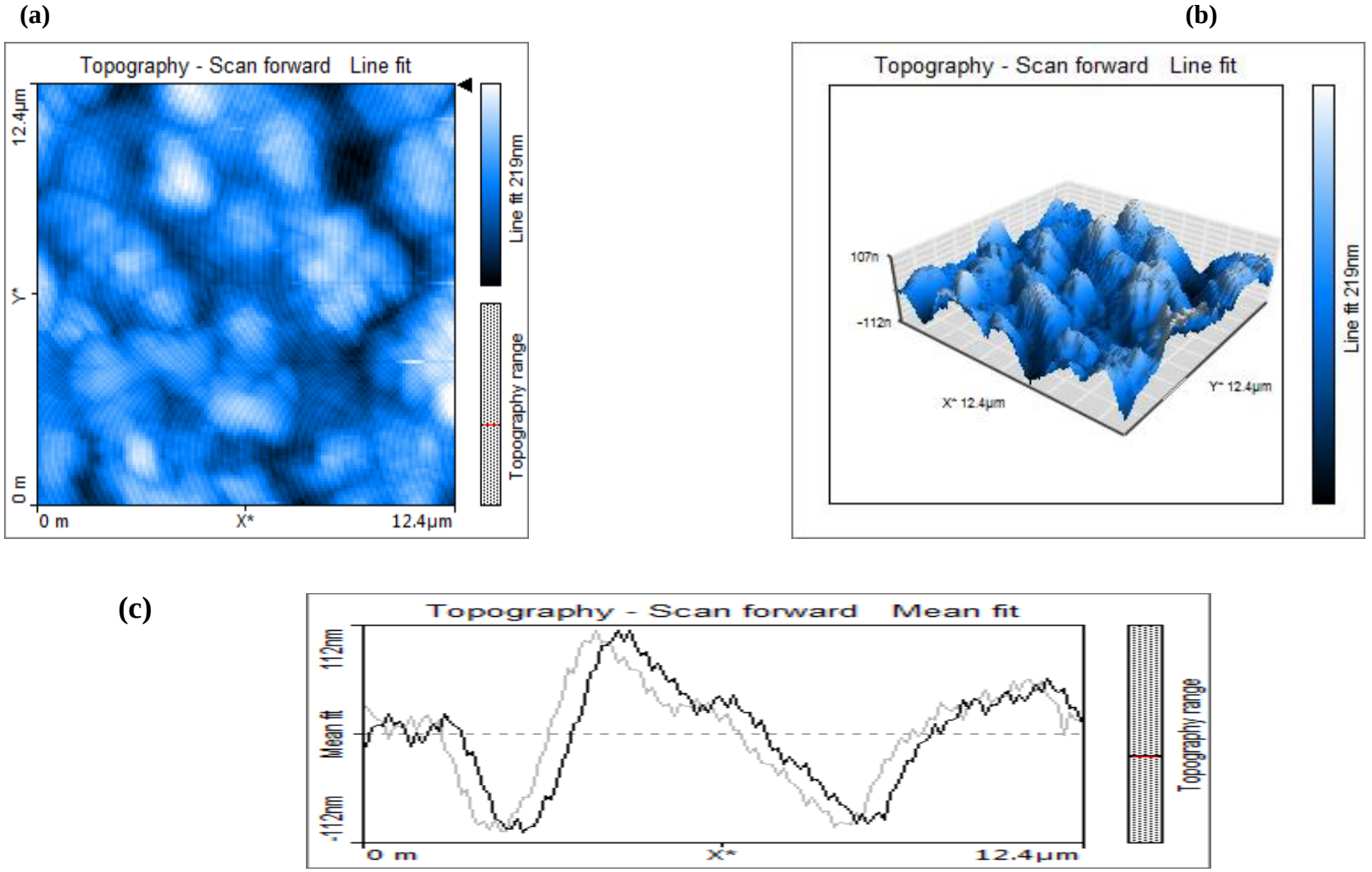

Figure (28): AFM photomicrograph of CPM , (a): scan topography, b: 3D topography, & (c): line graph topography

3. Preparation of hydrogel (PPM) from crosslinking between pectin and PVA by maleic anhydride

PPM hydrogel was prepared by mixing equal volumes of PVA solution with pectin solution. The mixture was stirred constantly until homogeneous at 60ºC and (0.3g) of maleic anhydride as crosslinker agent was added to the mixture under constant stirring with (2 drops) of glacial acetic acid.

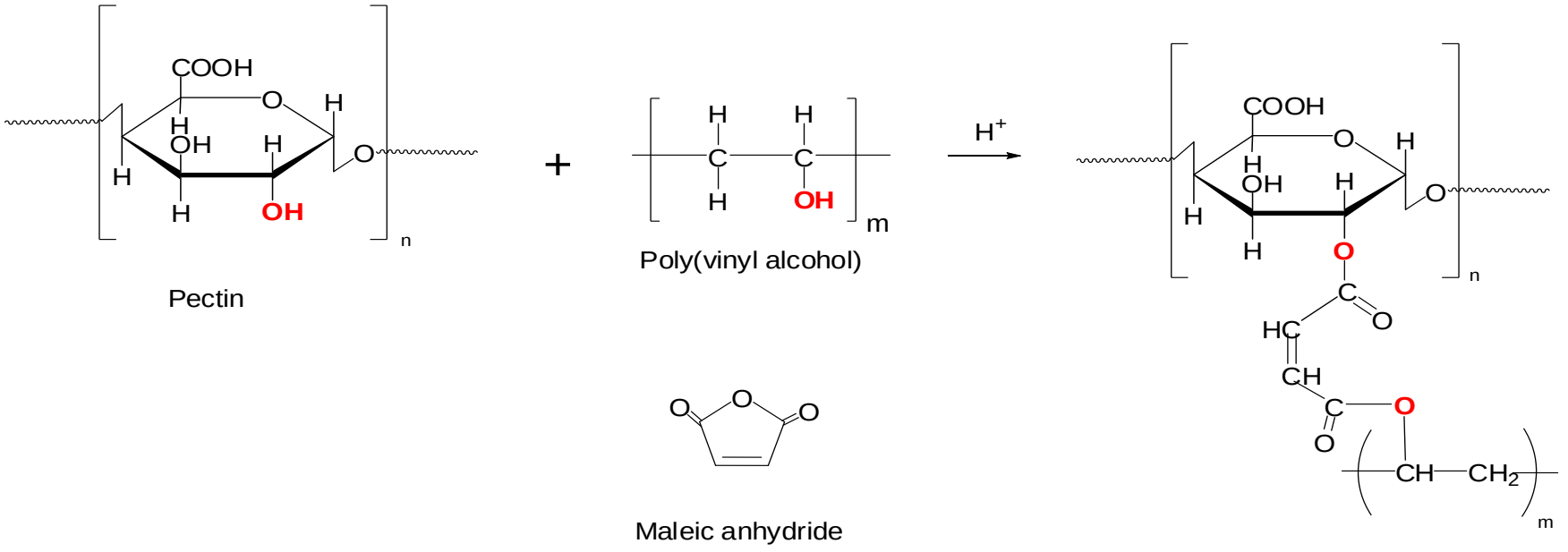

Scheme(6): Cross-linking of Pectin, PVA with maleic anhydride

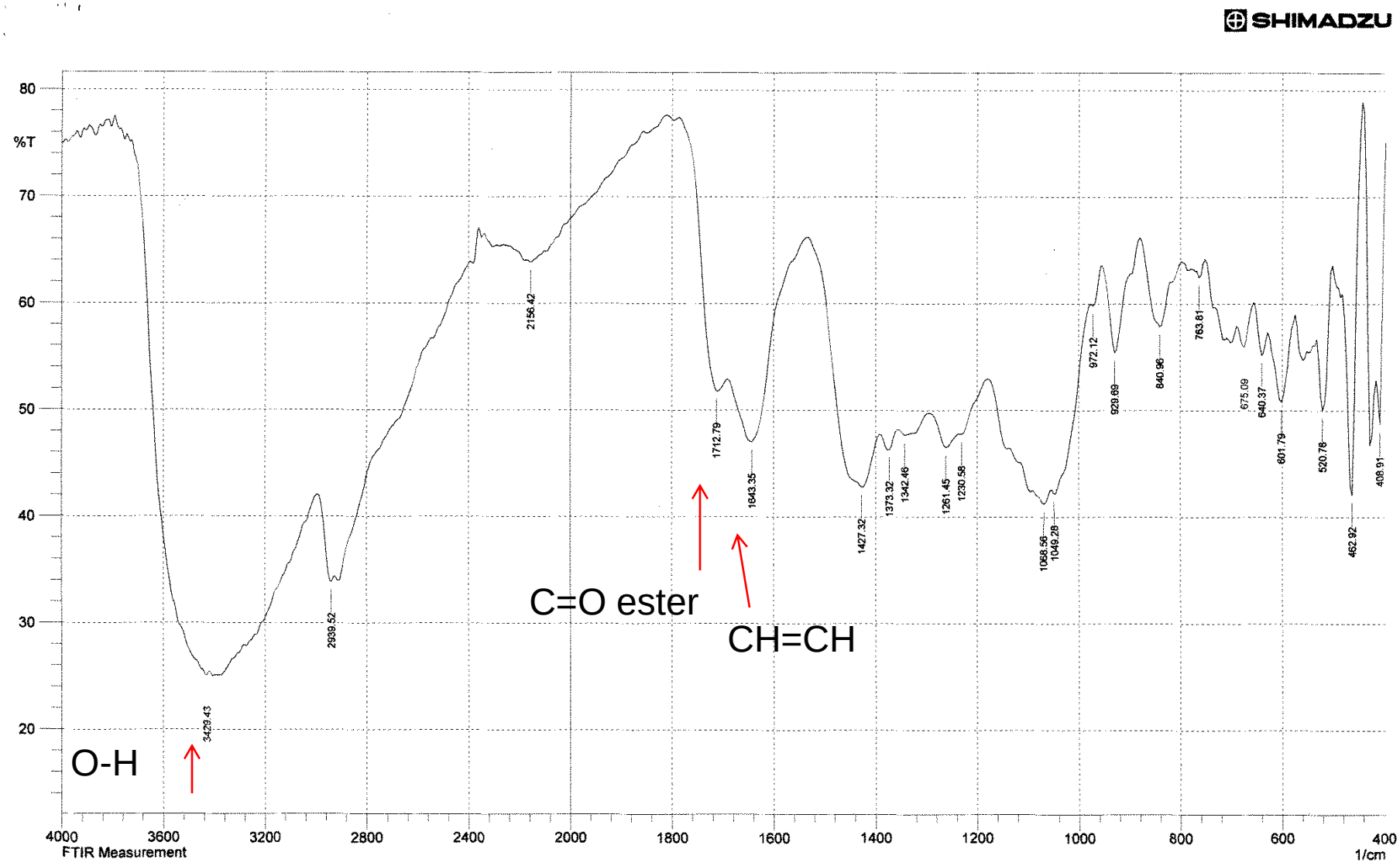

Figure (29): FT-IR spectrum of PPM hydrogel film

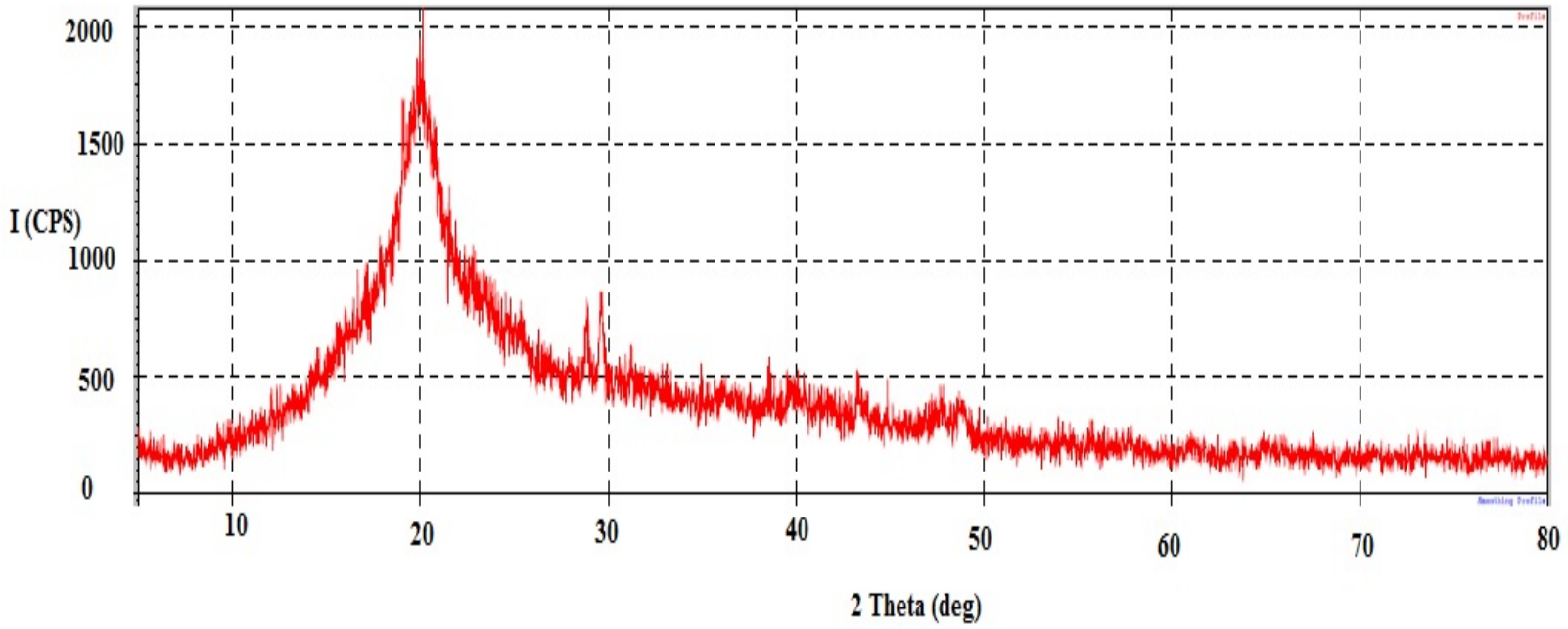

Figure (30): XRD for PPM hydrogel film

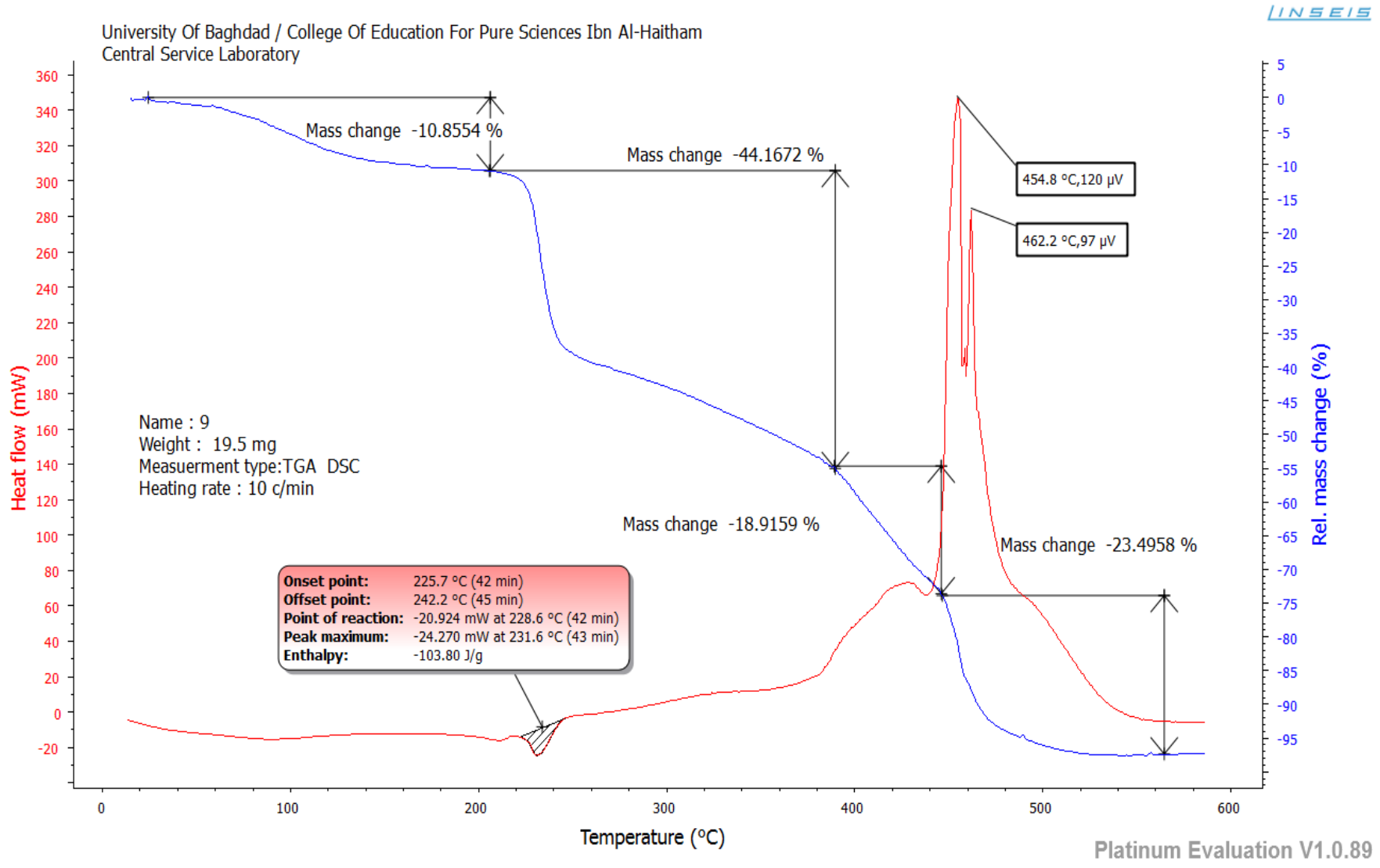

Figure (31): TGA and DSC of PPM hydrogel film

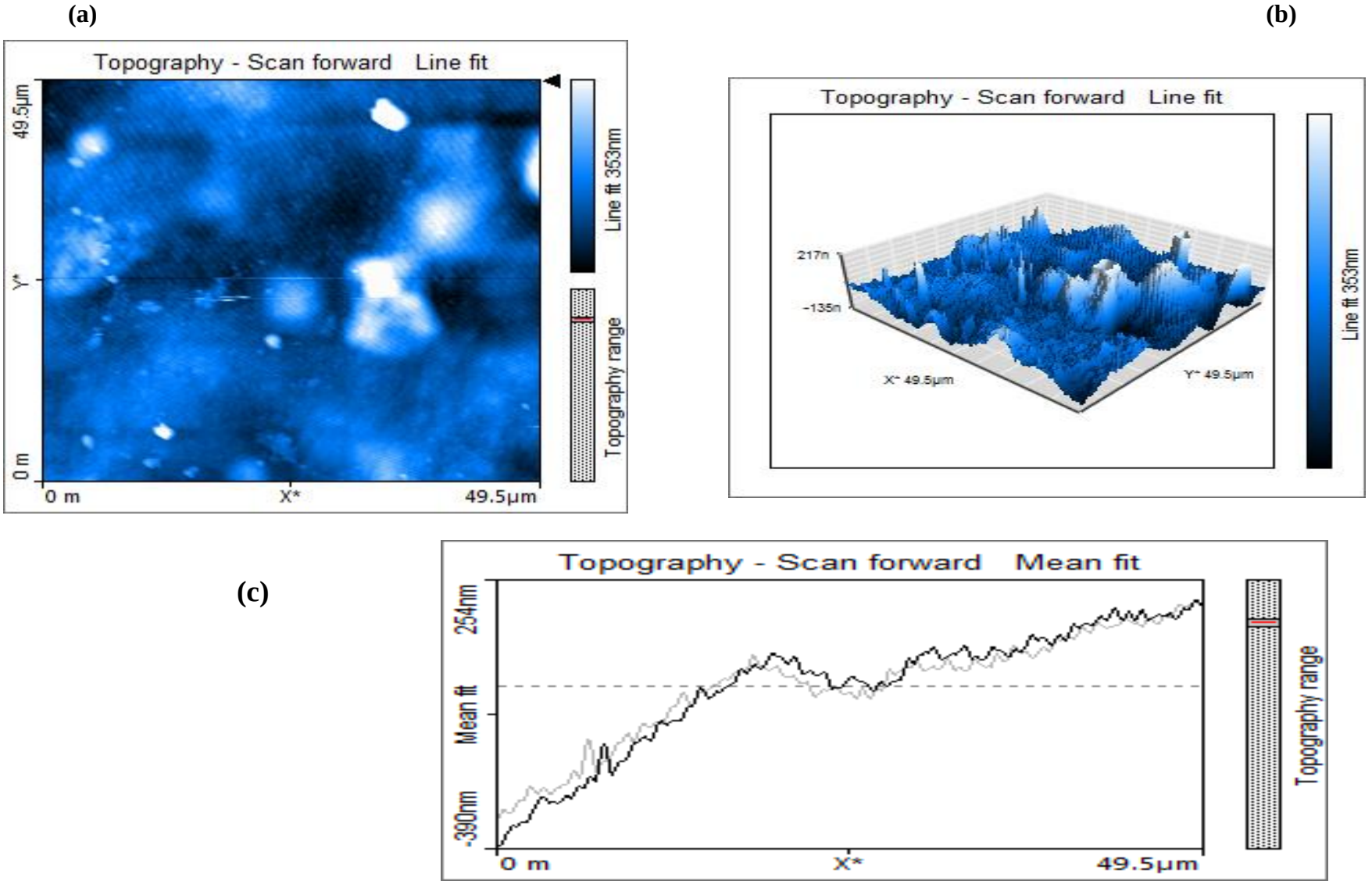

Figure (32): AFM photomicrograph of PPM , (a): scan topography, b: 3D topography, & (c): line graph topography

4. Preparation of hydrogel (PgA) from graft co-polymerization of acrylic acid on PVA

PgA hydrogel was prepared by mixing (20 ml) of PVA solution with (0.0375 g)of potassium persulphate (KPS) as initiator and (3.8ml)of acrylic acid under N_2 at 60ºC with (0.0375g) of (N,N´-methylenebisacrylamide(MBA)) as crosslinker at same temperature with stirring.

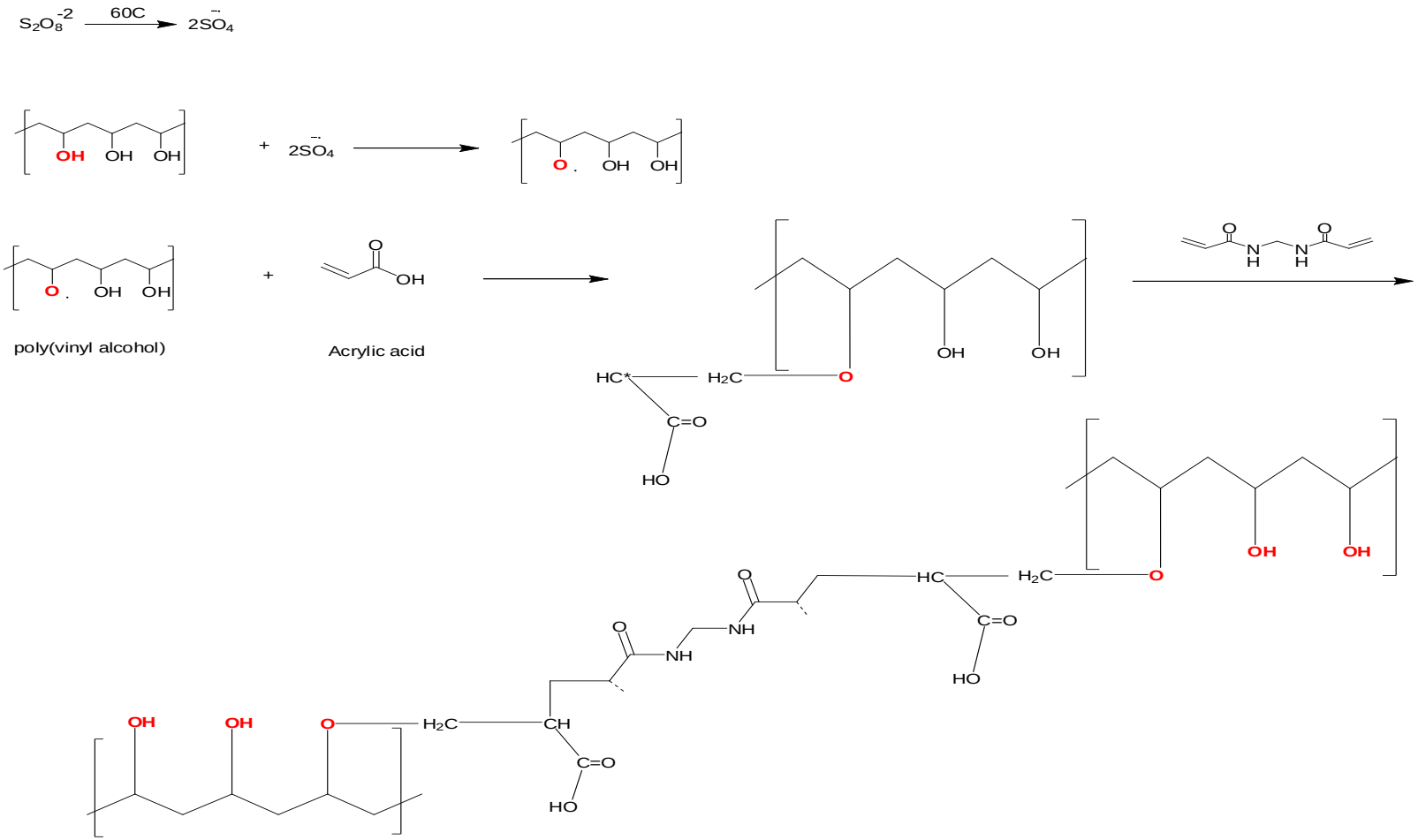

Scheme (7): grafted co-polymerization of Acrylic acid onto PVA

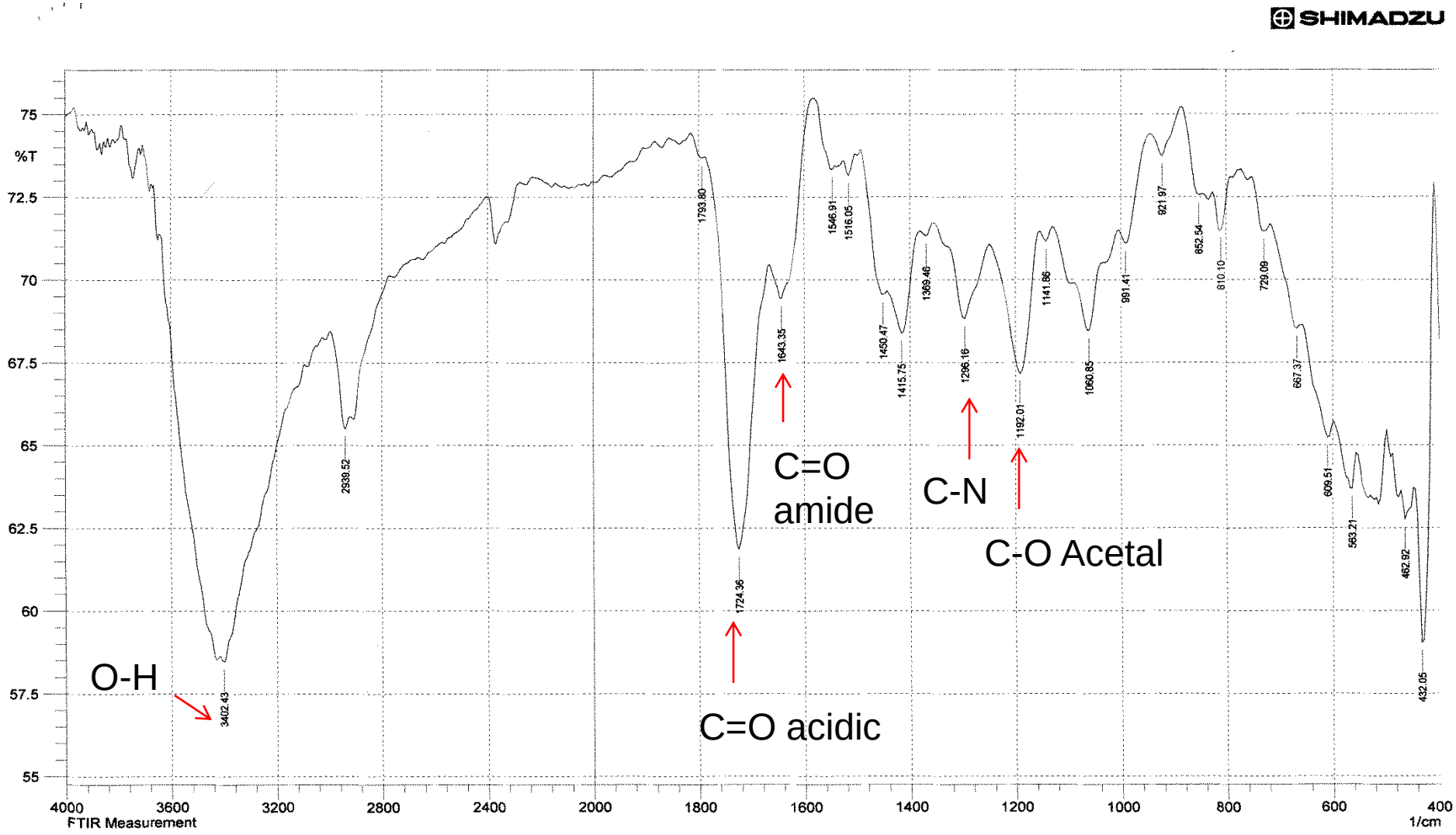

Figure (33): FT-IR spectrum of PgA hydrogel film

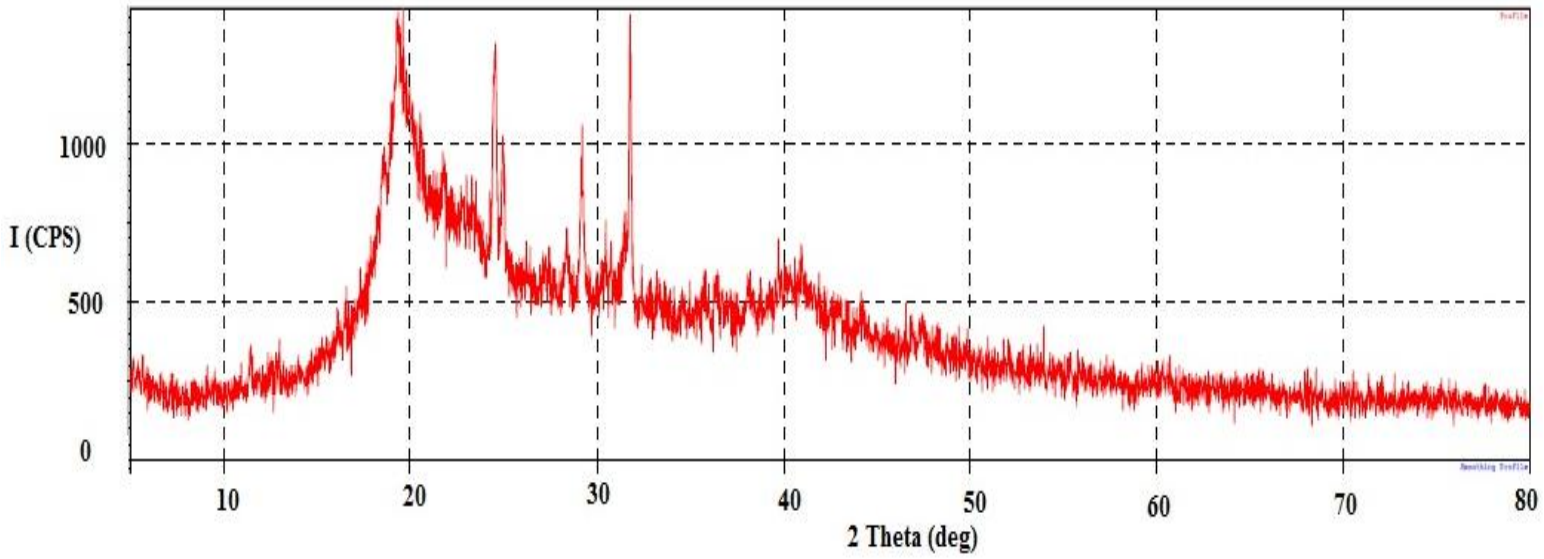

Figure (34): XRD for PgA hydrogel

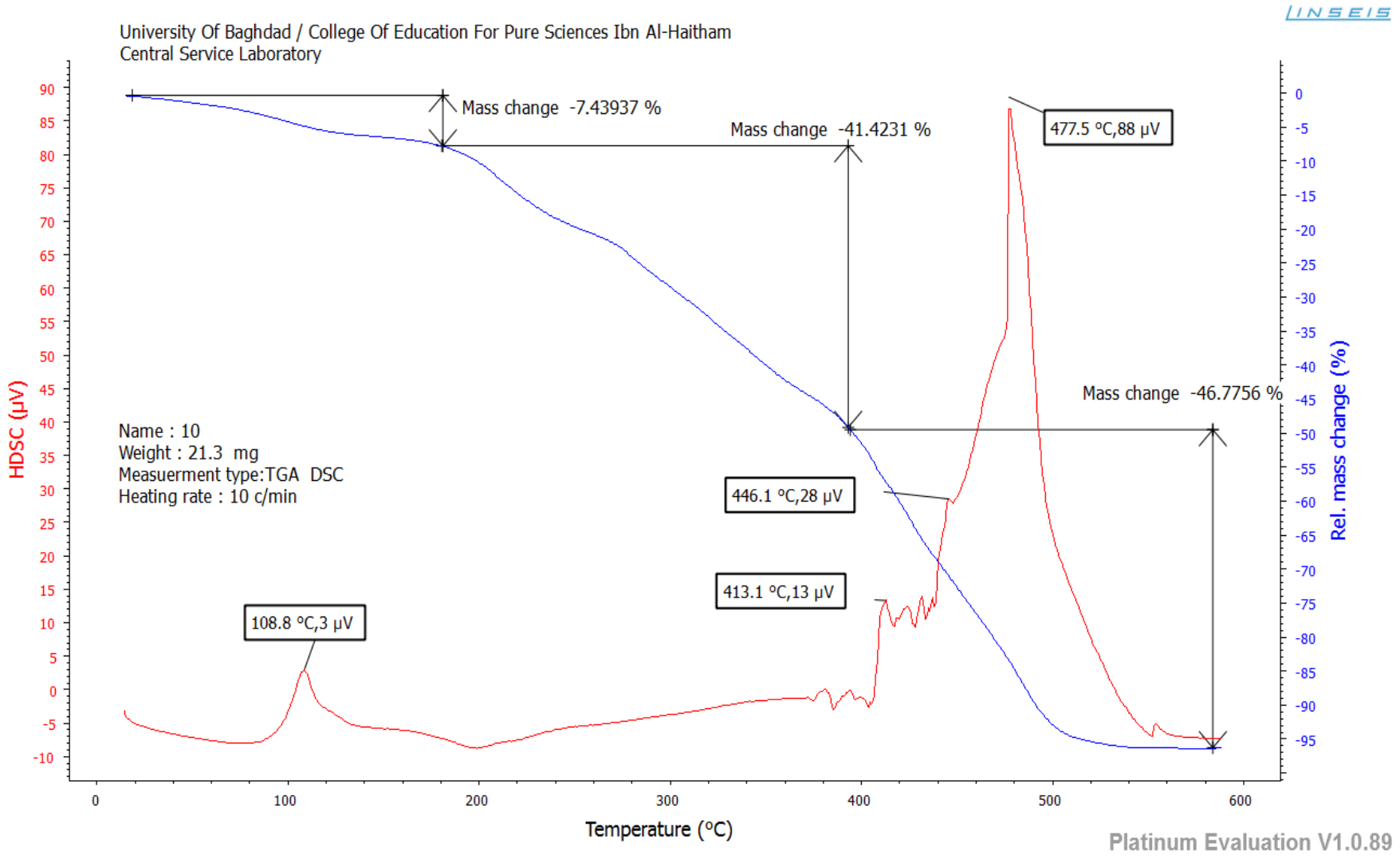

Figure (35): TGA and DSC of PgA hydrogel film

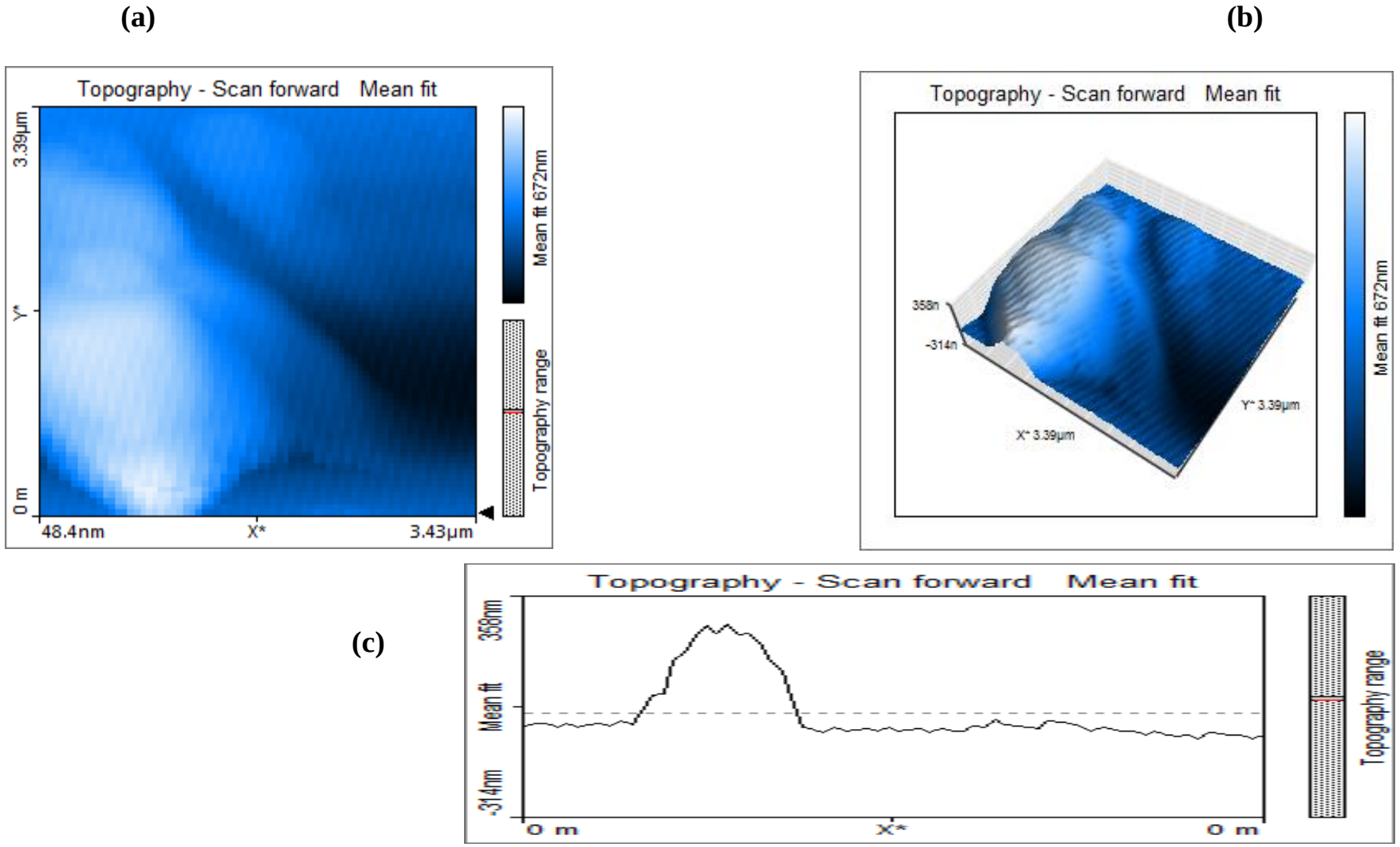

Figure (36): AFM photomicrograph of PgA , (a): scan topography, b: 3D topography, & (c): line graph topography

5. Preparation of hydrogel (CgA) from graft co-polymerization of acryl amide on chitosan

CgA hydrogel was prepared by mixing (20 ml) of chitosan solution with (0.07 g) of ammonium persulphate (APS) as initiator and (1g) of acrylamide under N_2 at 60ºC with (0.07g) of (N,N´-methylenebisacrylamide(MBA)) at same temperature with stirring[176].

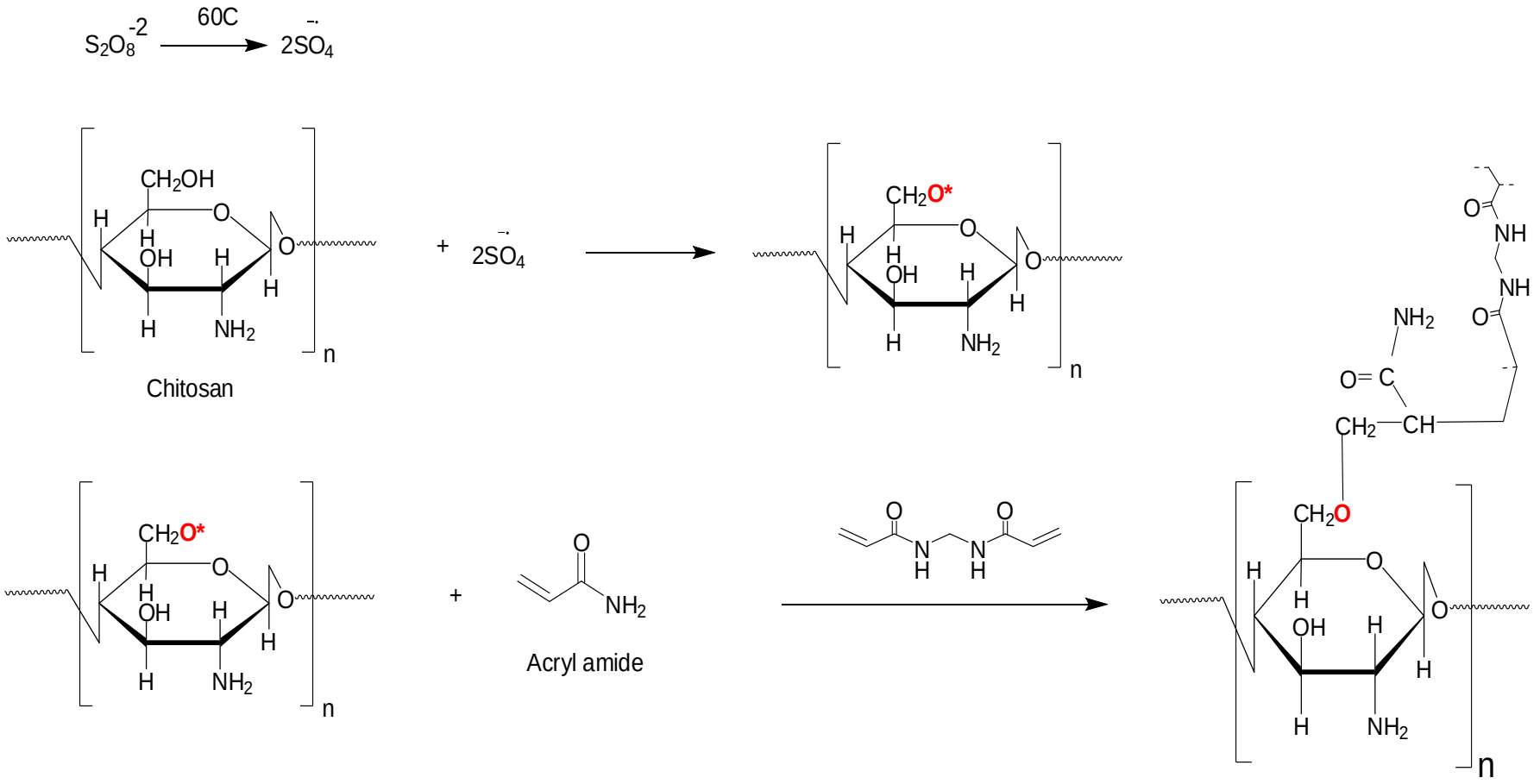

Scheme (8): APS-initiated graft copolymerization of acrylamide onto chitosan in the presence of MBA

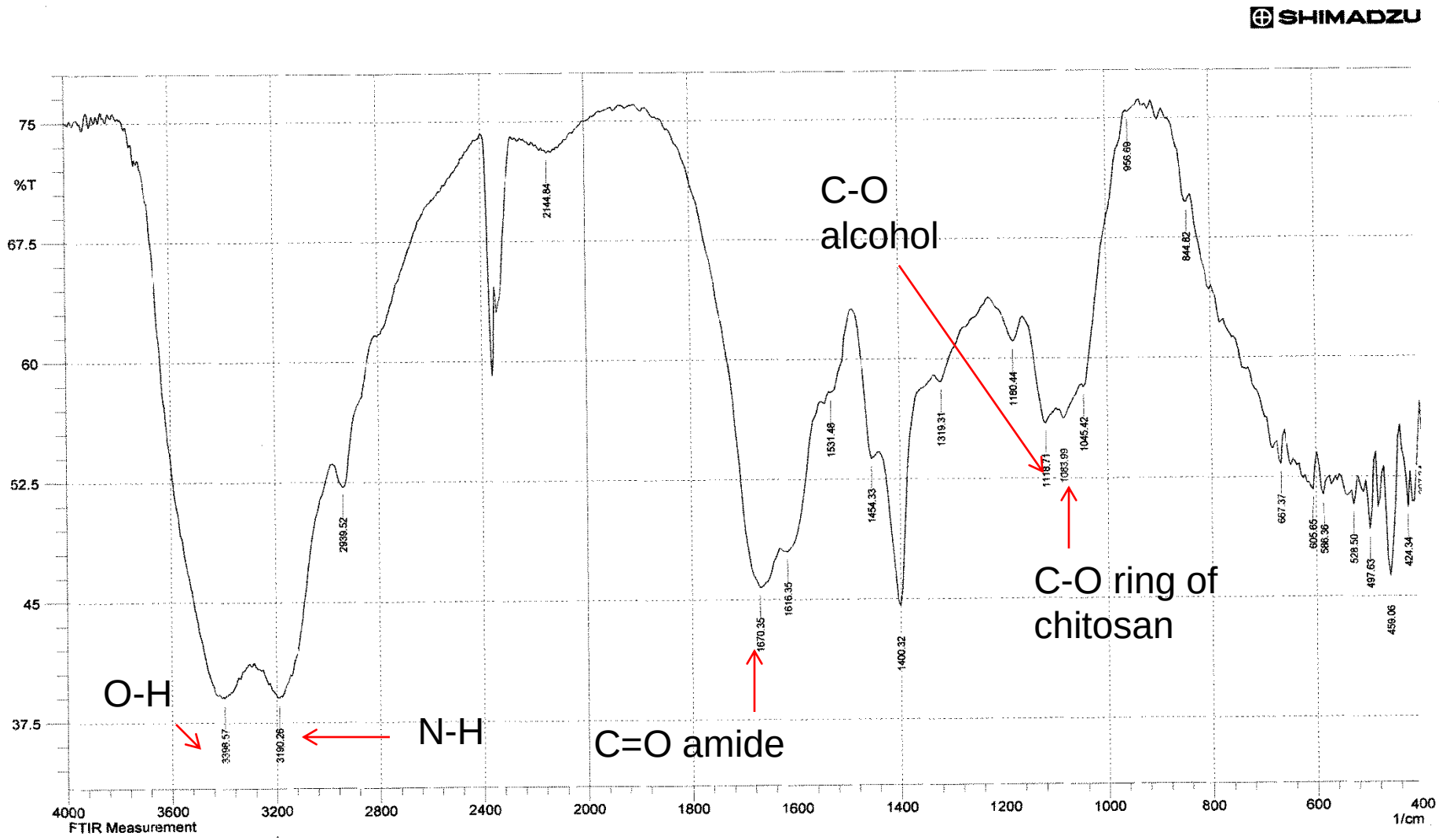

Figure (37): FT-IR spectrum of CgA hydrogel film

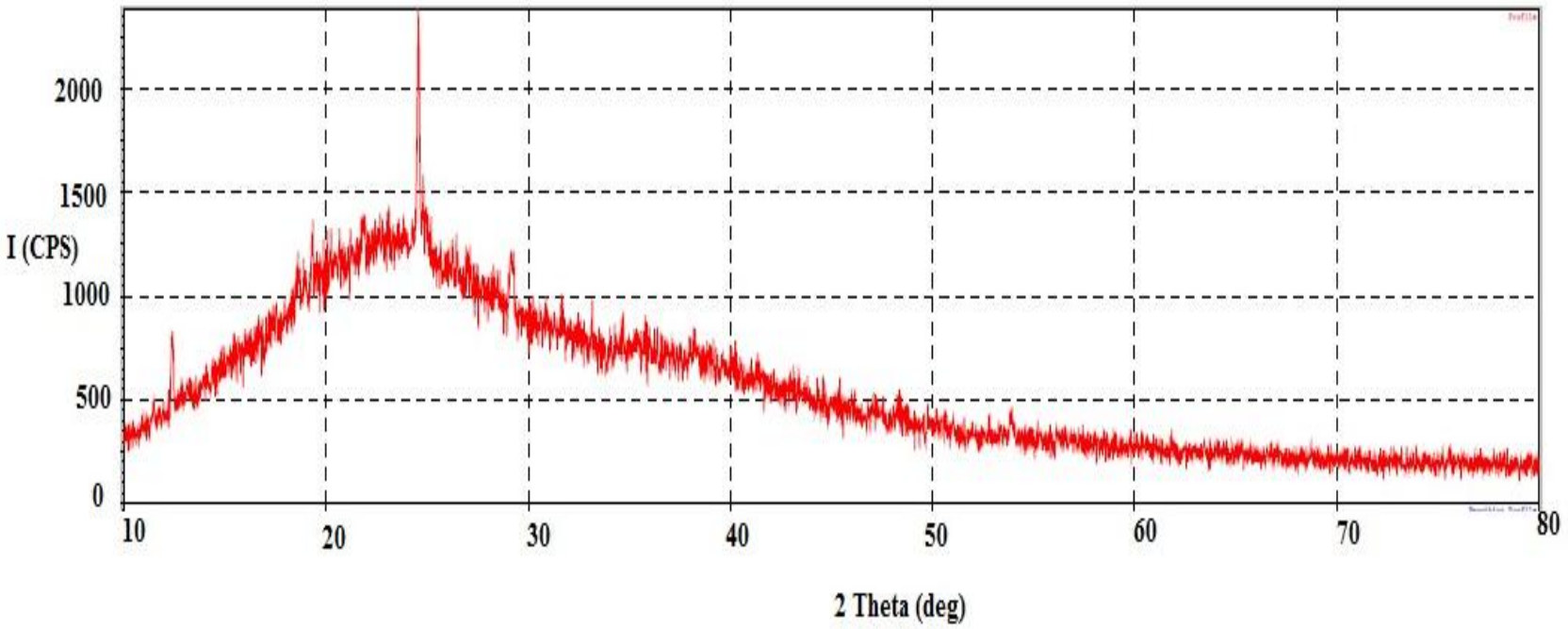

Figure (38): XRD for CgA hydrogel film

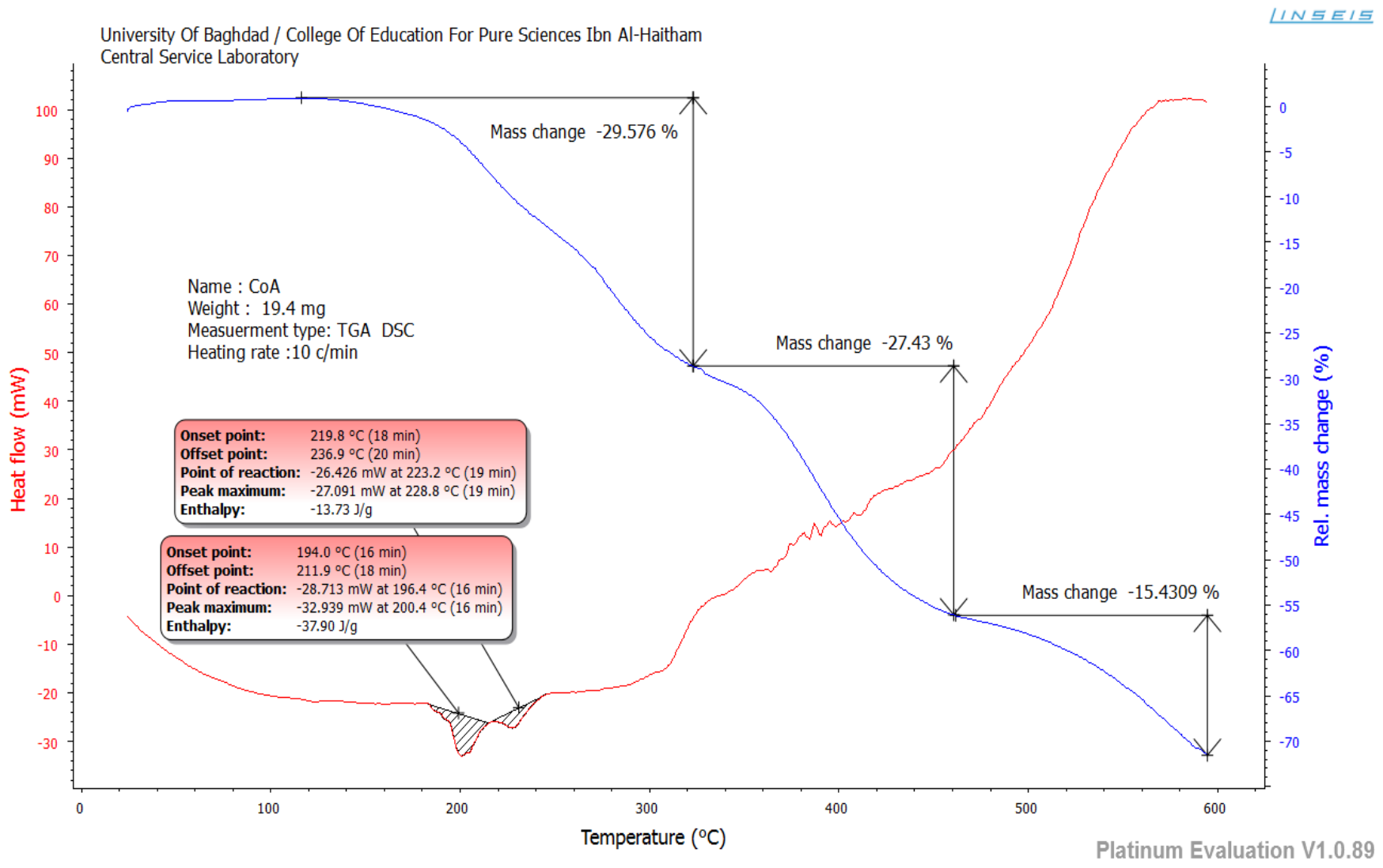

Figure (39): TGA and DSC of CgA hydrogel film

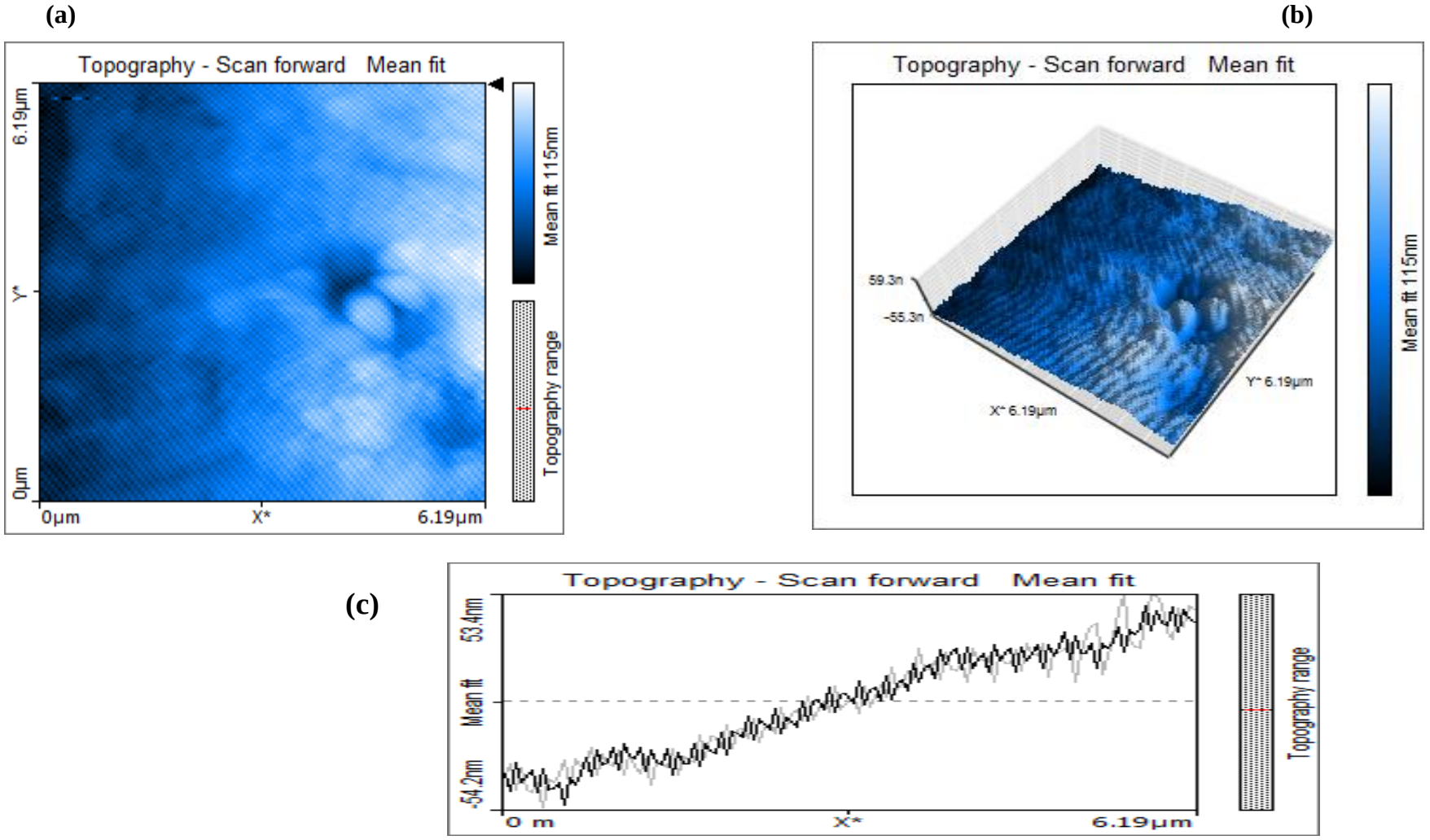

Figure (40): AFM photomicrograph of CgA , (a): scan topography, b: 3D topography, & (c): line graph topography

6. Preparation of hydrogel (IPN) from co-polymerization of acrylic acid and acryl amide in presence chitosan

IPN Hydrogel was synthesized by free radical polymerization of acrylamide (AM) and acrylic acid (AA) in presence of the chitosan (CHI). A determined mass of AM and AA with ratio (CHI/AA/AM) equal to (10/10/80 w%), together with APS (1.2×10^{-3} mol/L), MBA (3.3×10^{-2} mol/L), and TEMED in a (1:1) molar ratio with APS, were added to chitosan solution and stirred for ten minutes at room temperature under N_2. Finally it was placed in a water bath at 60°C for 6 h.

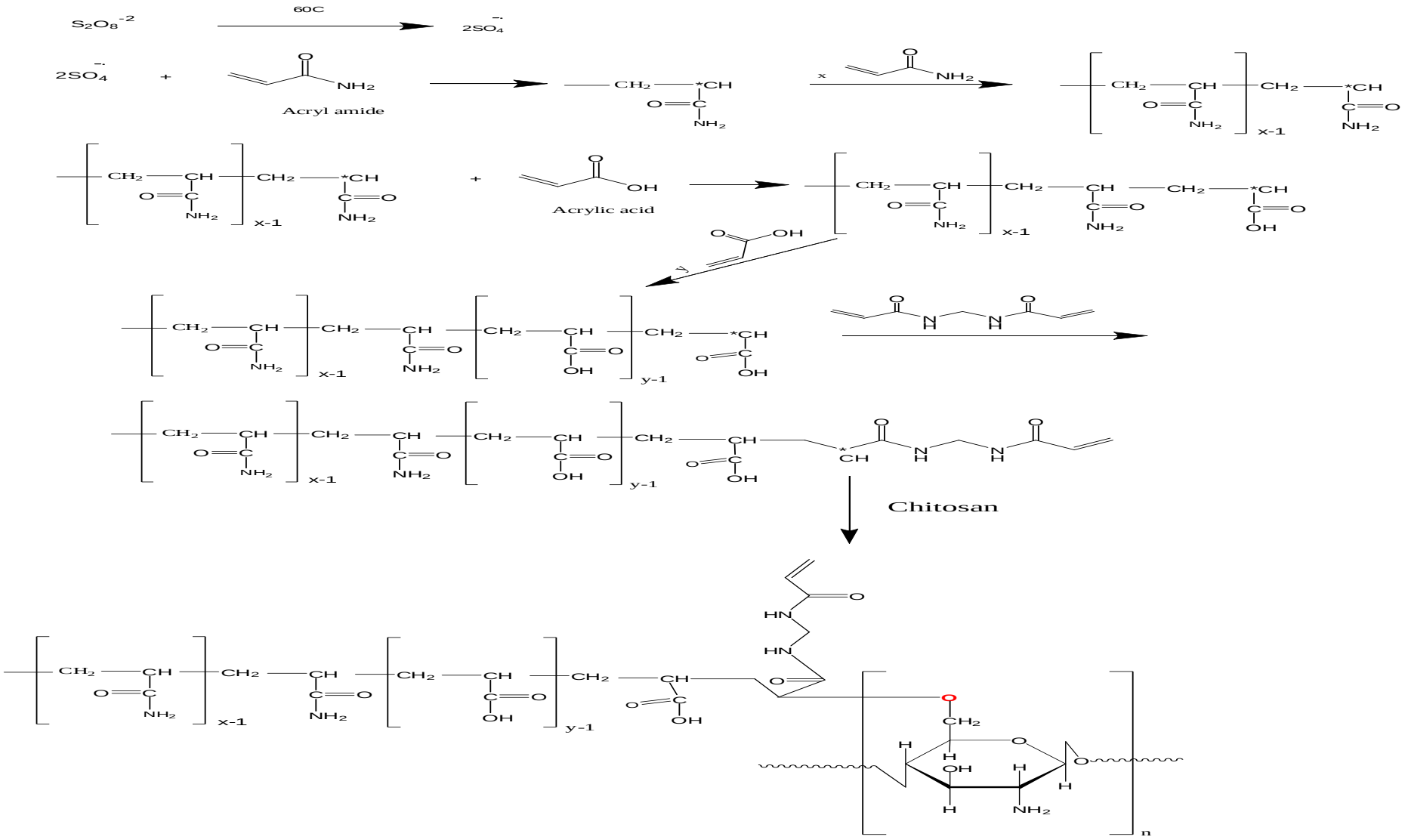

Scheme (9): Interpenetrating chitosan-poly (acrylic acid-co-acryl amide) hydrogel (IPN)

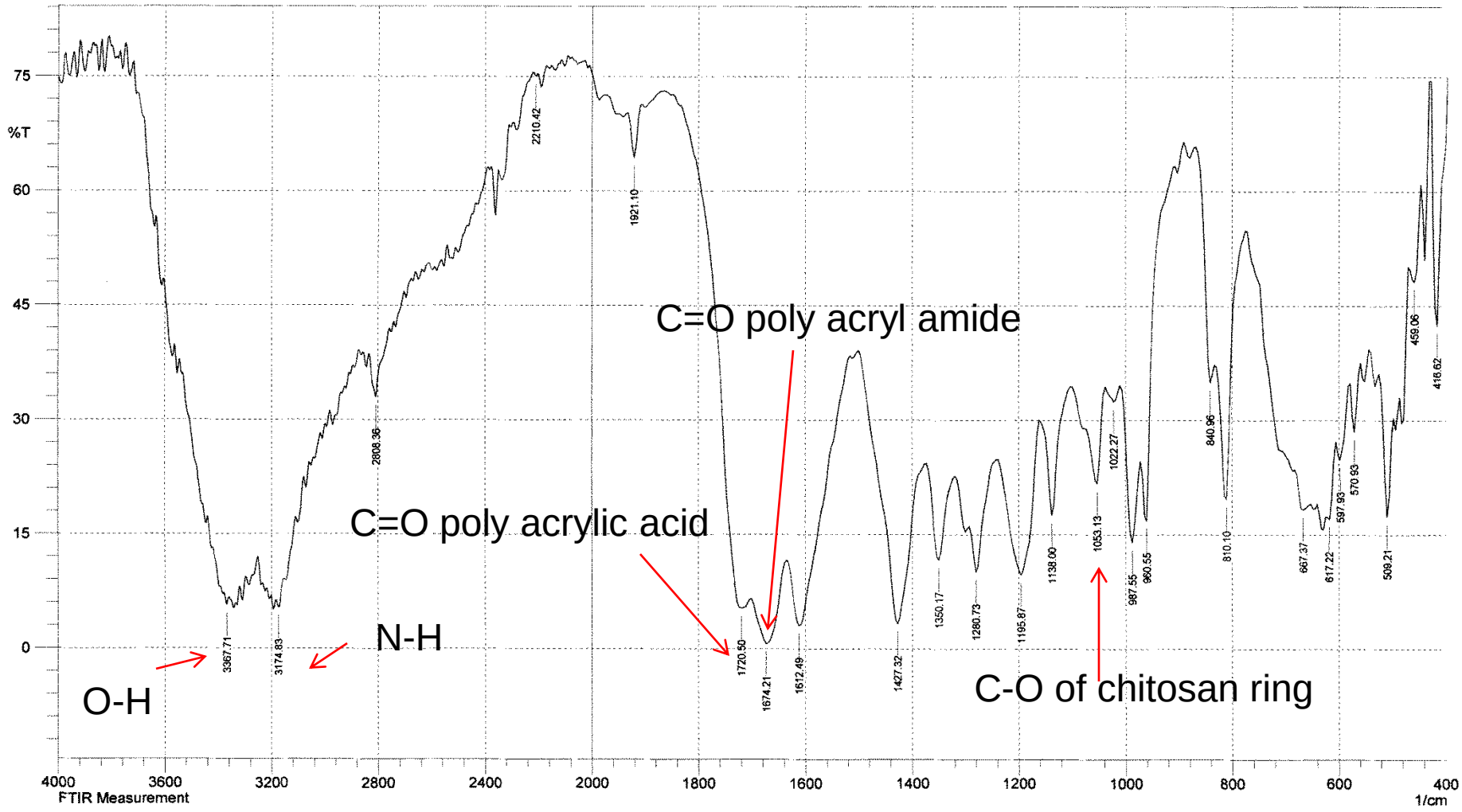

Figure (41): FT-IR spectrum of IPN film

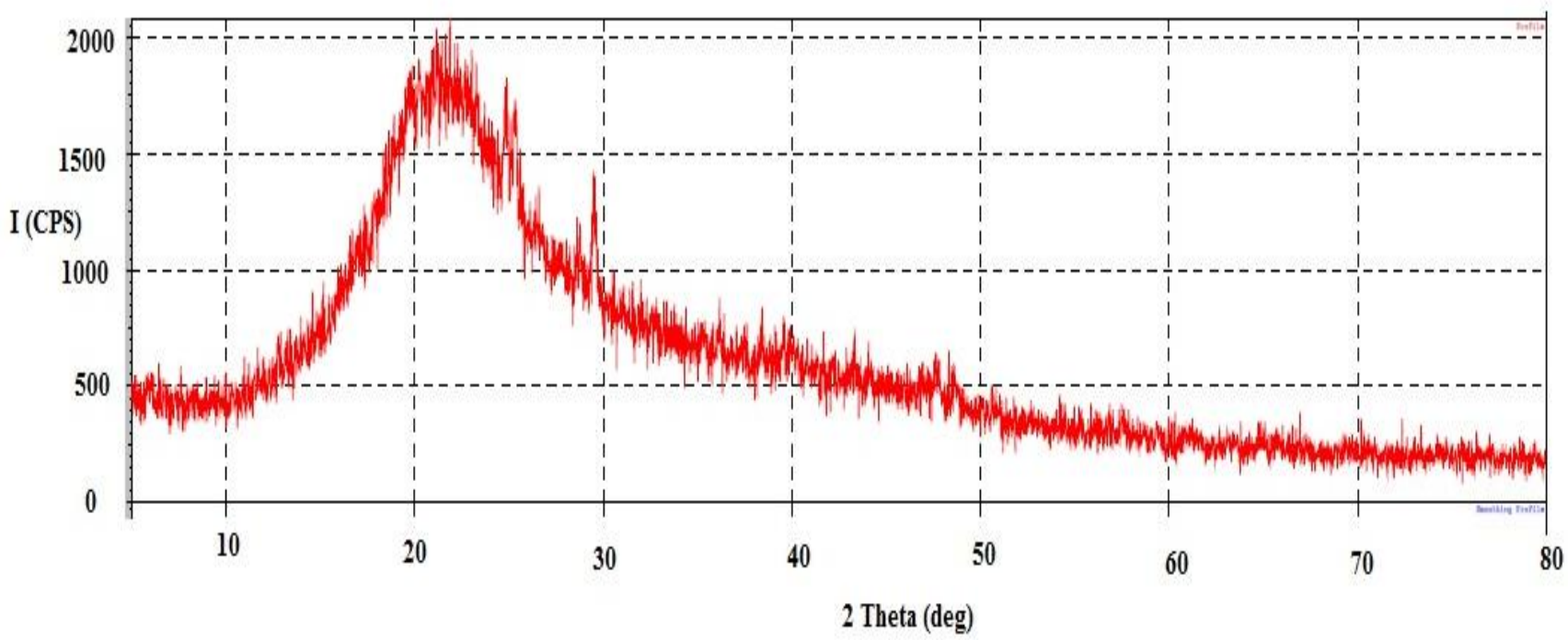

Figure (42): XRD for IPN hydrogel

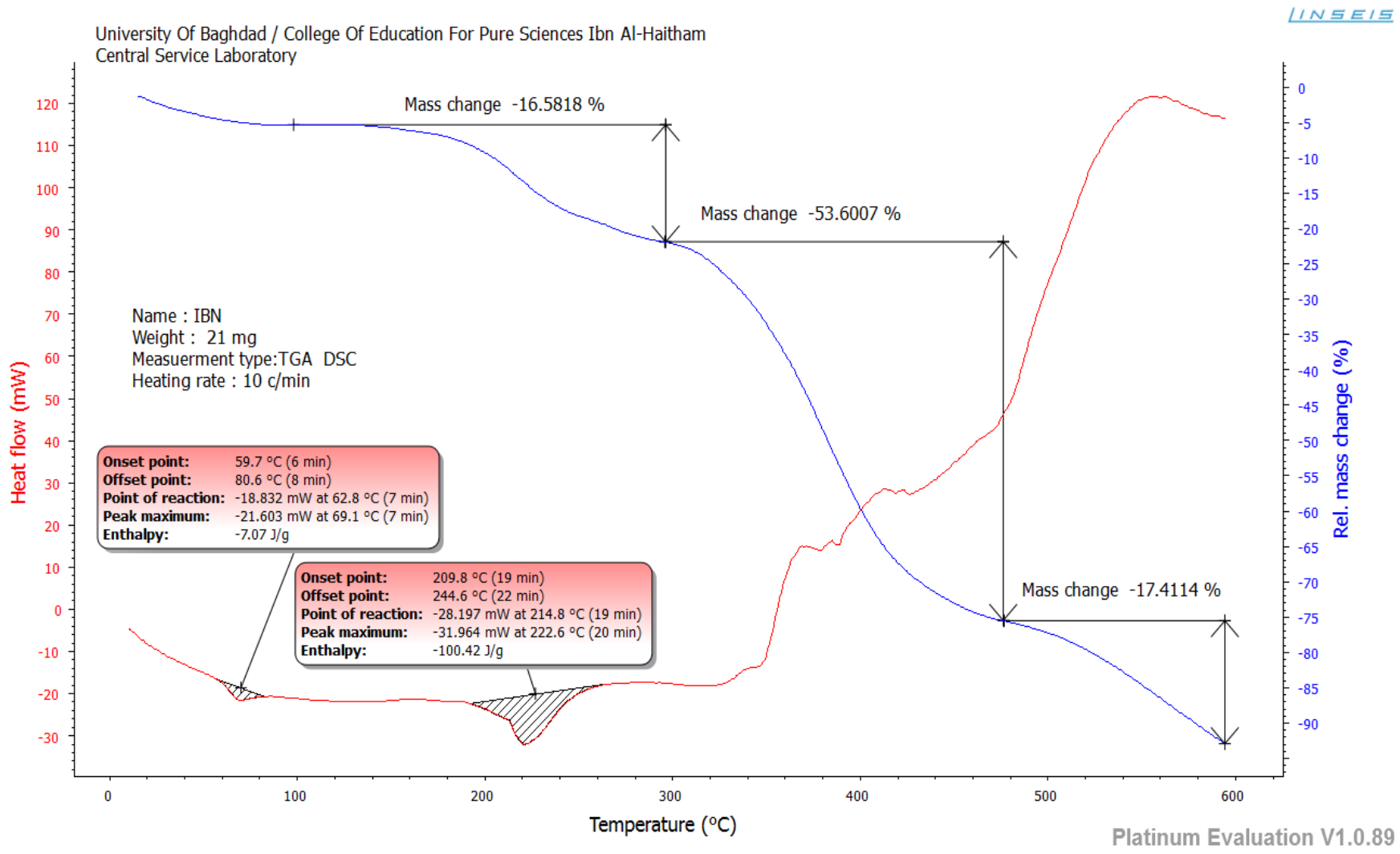

Figure (43): TGA and DSC of IPN hydrogel film

(a):

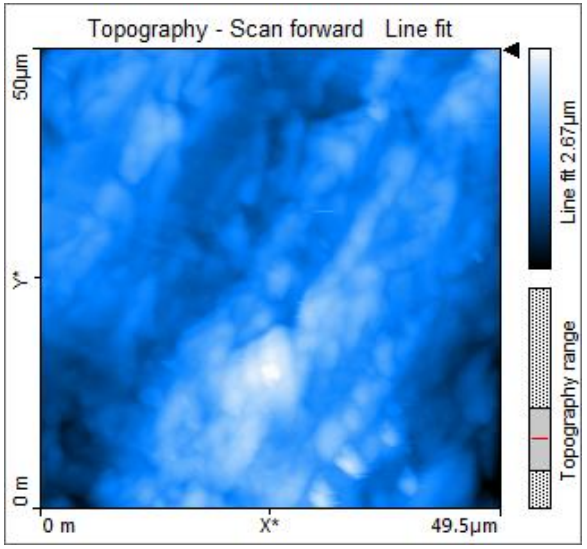

(b)

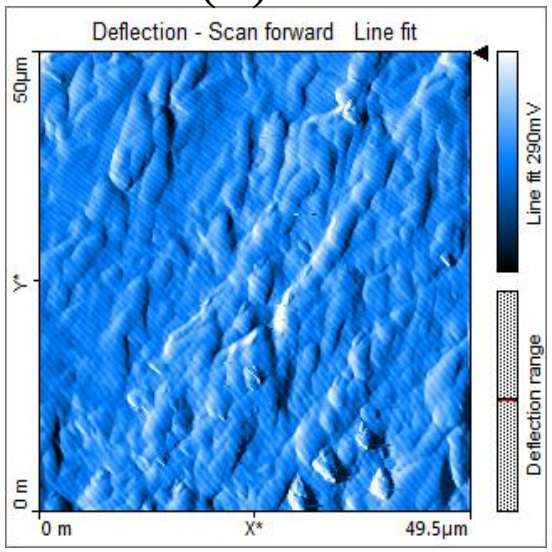

(c):

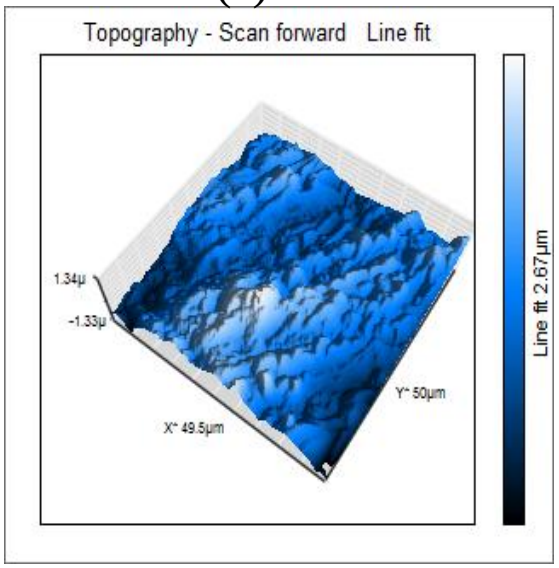

d

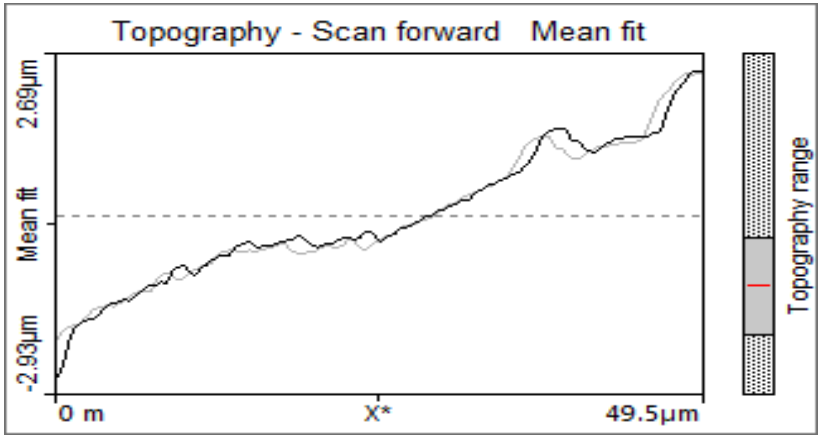

Figure (44): AFM photomicrograph of IPN , (a): scan topography, (b) : deflection scan, (c): 3D topography, & (d), line graph topography

The degree of swelling represent (S) changed with time in this figure, and it is obvious that the swelling increase with the time until it reaches the equilibrium state

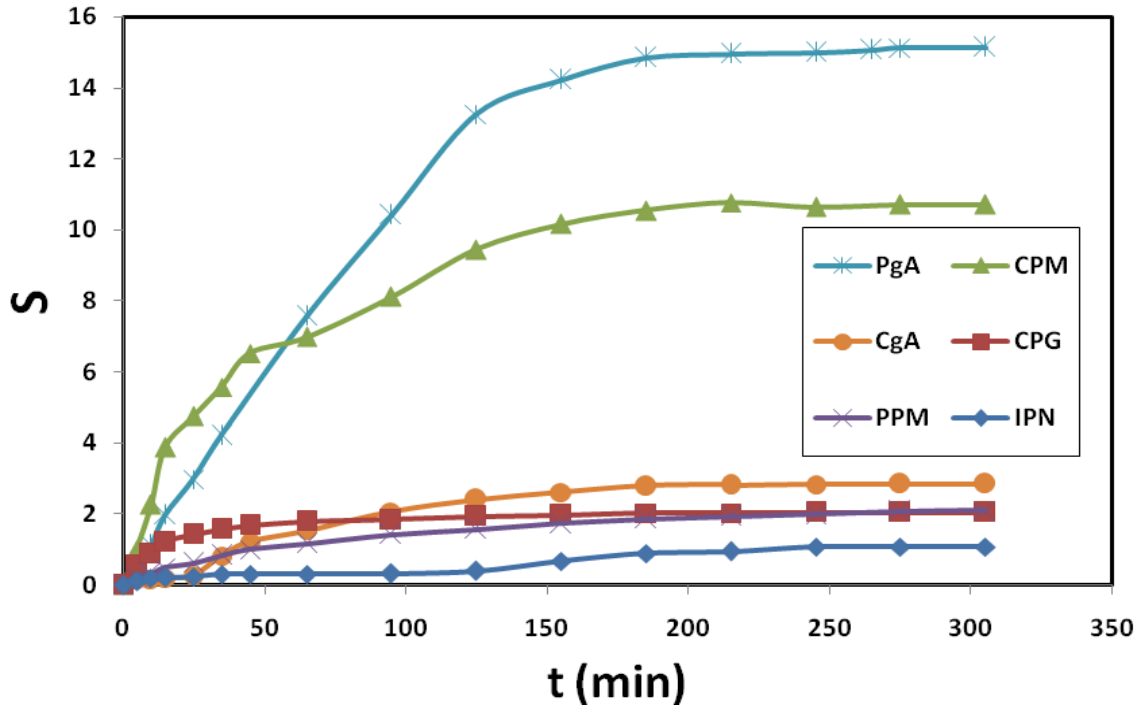

Figure (45): Degree of swelling for all hydrogels in water at R.T

The electric properties of all hydrogels were measured by LCR Meters

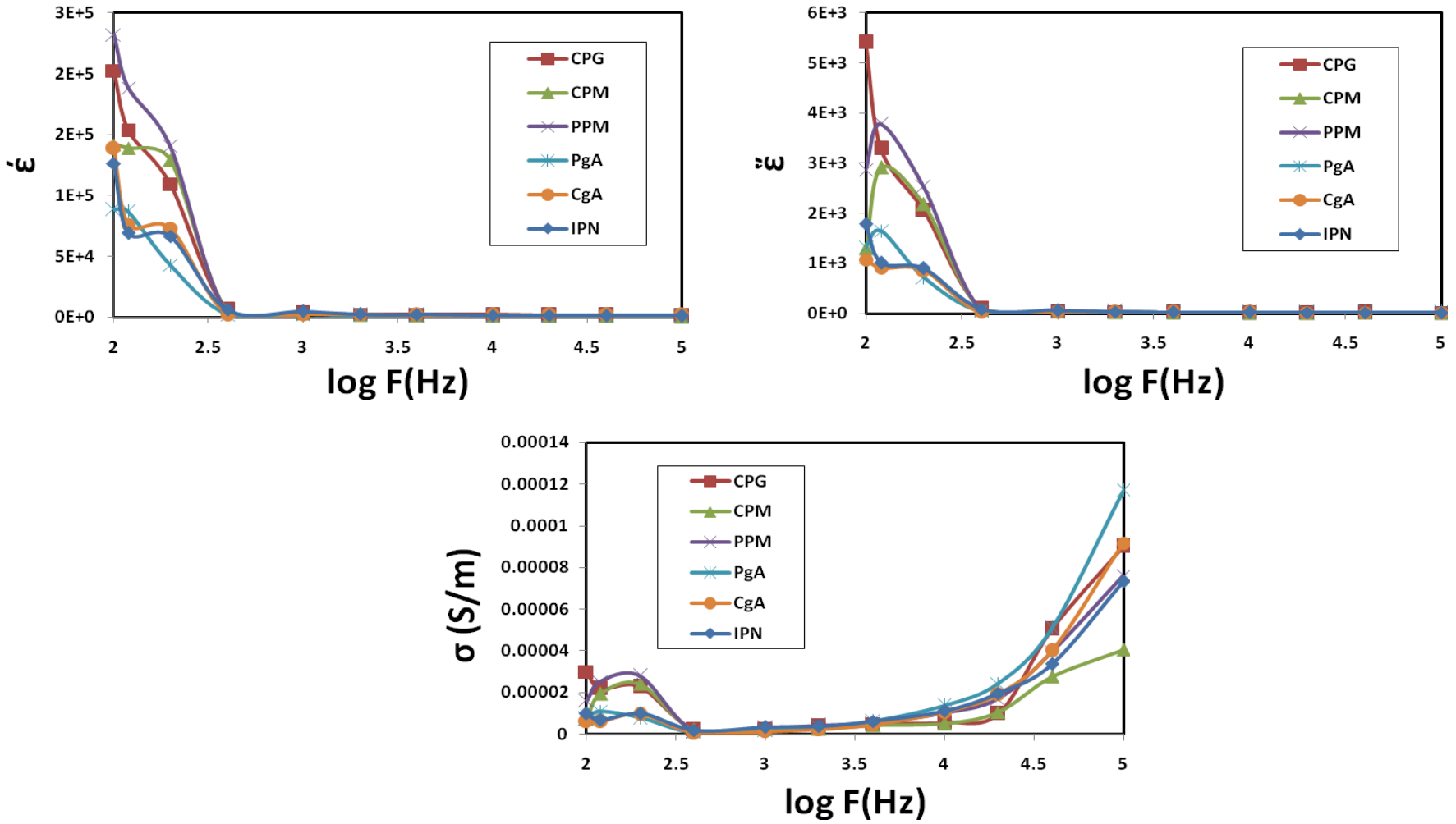

Figure (46): Real permittivity, Imaginary permittivity, and AC conductivity versus log frequency for hydrogels

Synthesis of conductive hydrogels

1. Synthesis of conductive hydrogels /PANI

In brief, mixed solutions of hydrogel and polyaniline with mechanical stirring in ice bath.

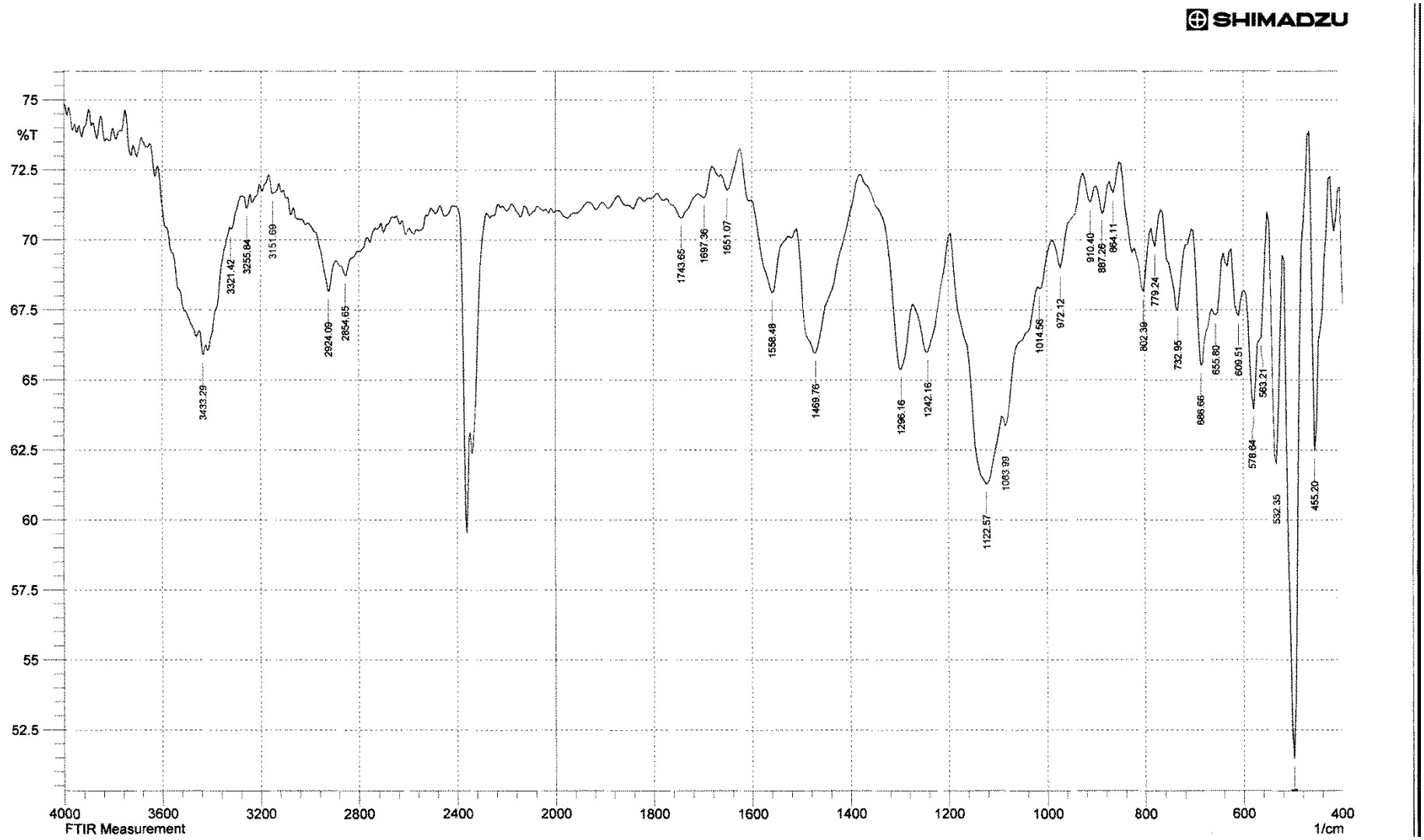

Figure (47): FT-IR spectrum of conductive hydrogel PgA/PANI film

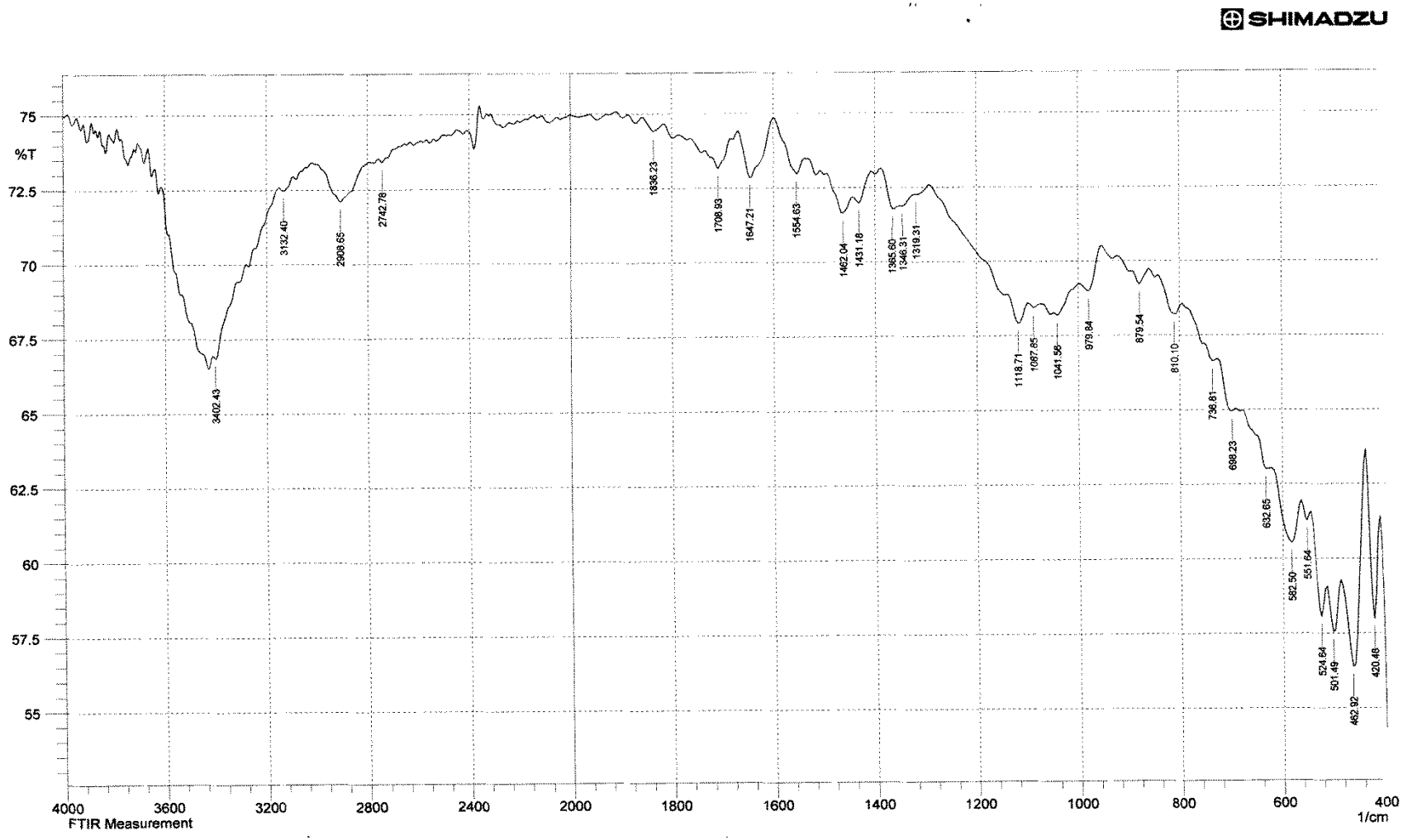

Figure (48): FT-IR spectrum of conductive hydrogel of PPM /PANI film

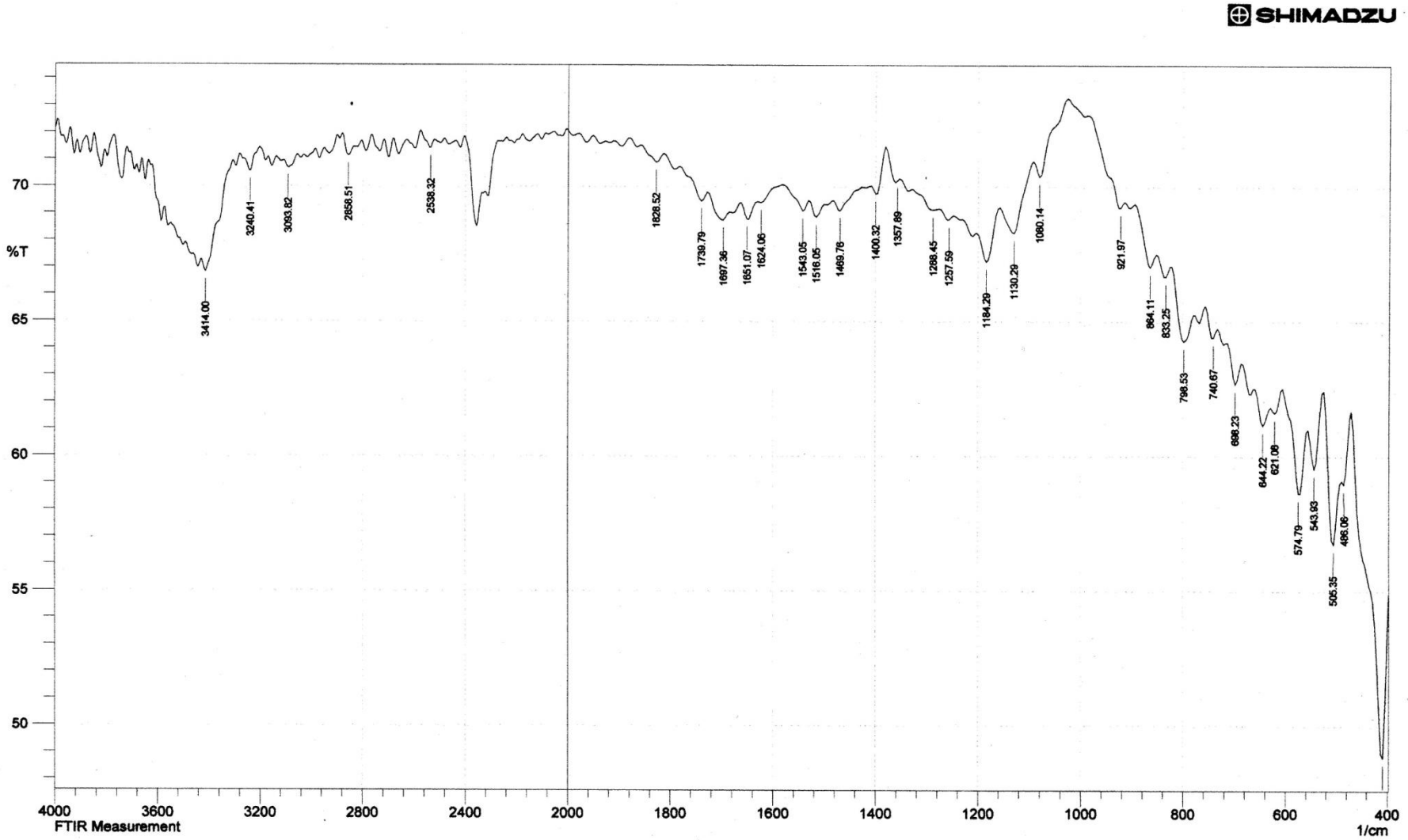

Figure (49): FT-IR spectrum of conductive hydrogel of CPG /PANI film

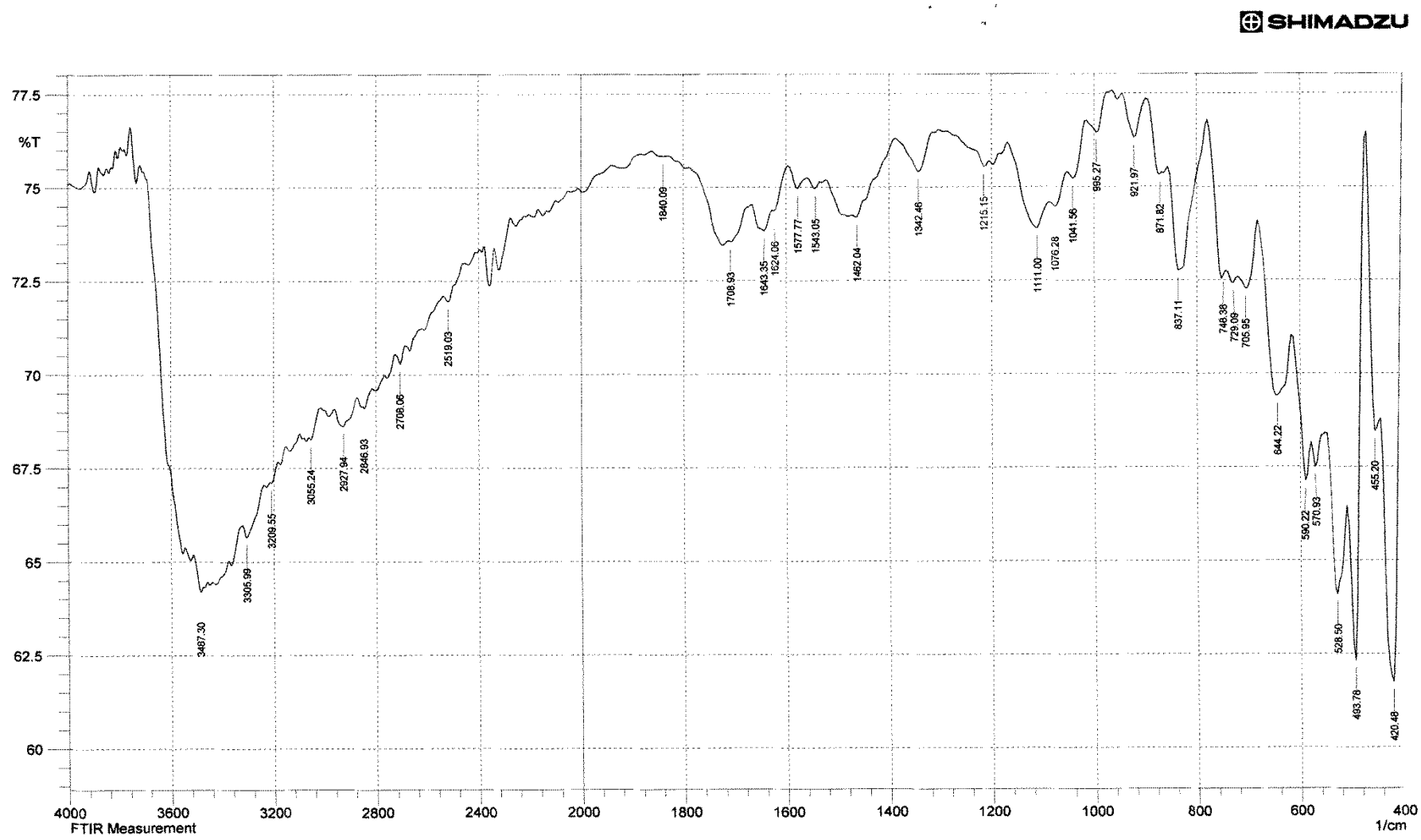

Figure (50): FT-IR spectrum of CPM/PANI film

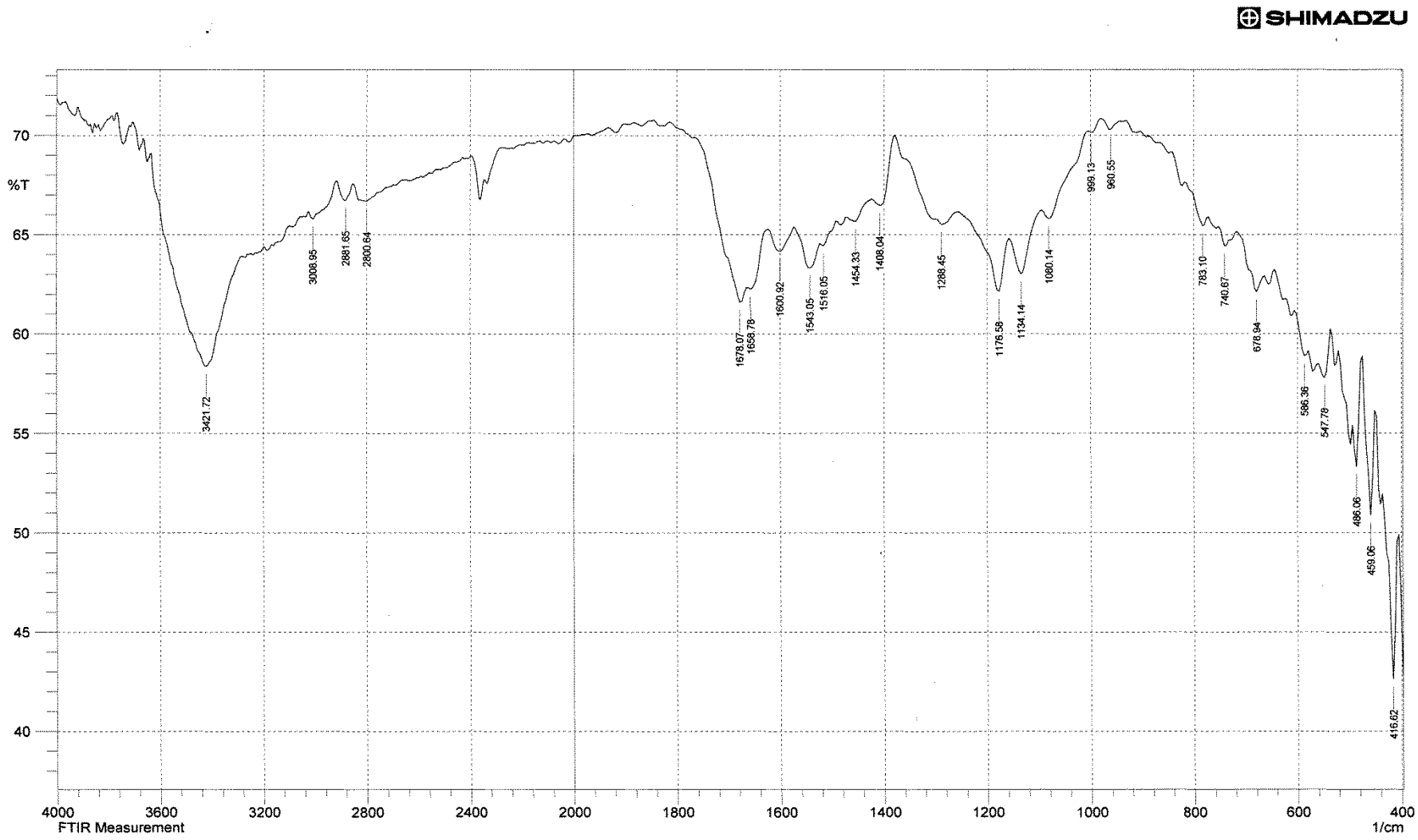

Figure (51): FT-IR spectrum of conductive hydrogel CgA/PANI film

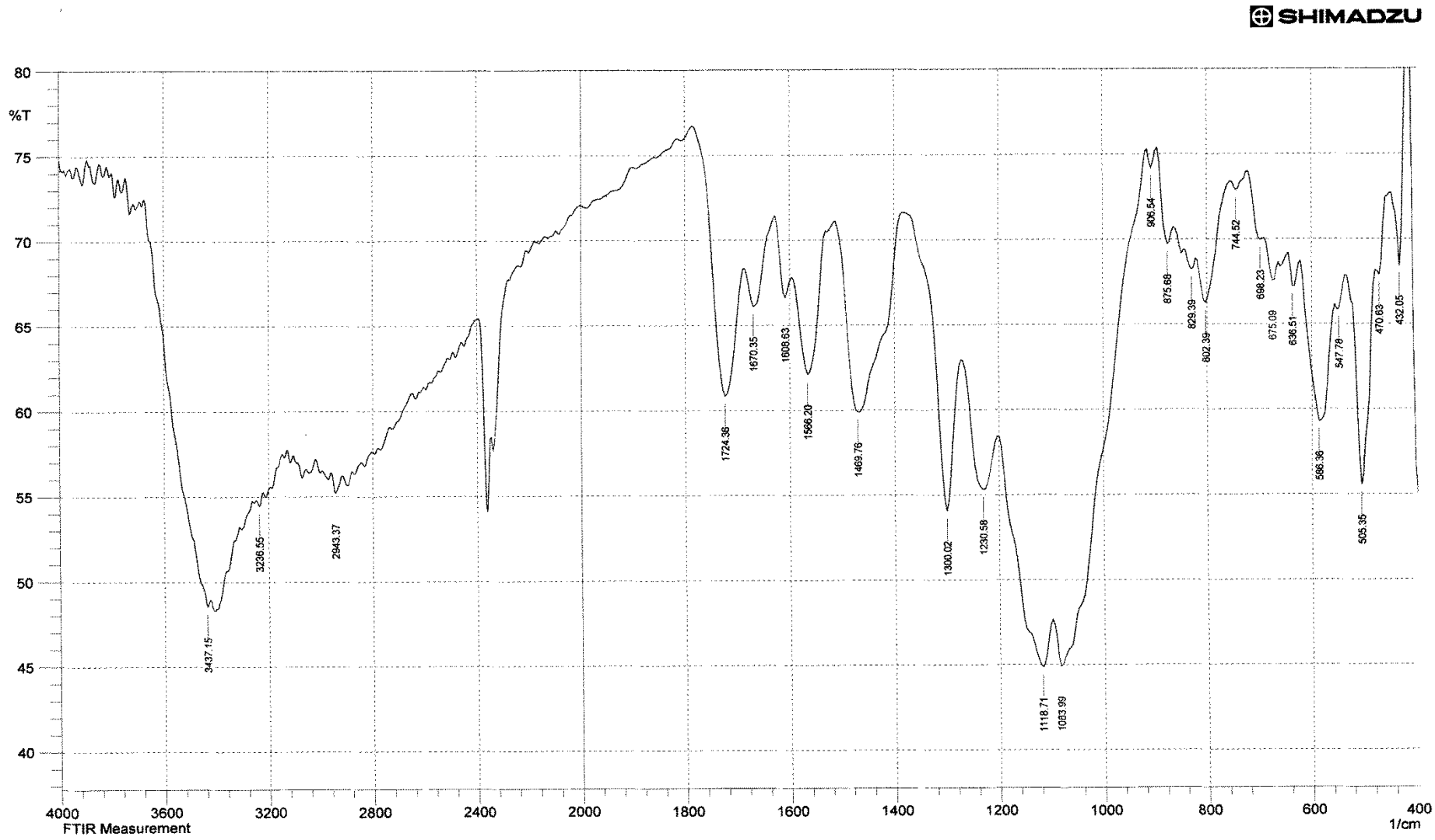

Figure (52): FT-IR spectrum of conductive hydrogel of IPN/PANI film

Table (1): Characteristics FTIR absorption bands (cm^{-1}) contain stretching vibrations& bending vibrations of hydrogels/PANI composite

Samples	O-H	N-H	CH-	C=O	C-O	C-N	peaks other
PgA/PANI	3433	New peak at 3255 to aromatic	2924,2854 aliphatic, New peak at 3151 to aromatic	1743	1651	1242aliphatic, New peak at 1296 for aromatic	Q at 1558 B at 1469 N=Q=N at 1122overlap with C-O acetal
PPM/PANI	Stretching at 3402 ,bending at 1431	Overlaps with O-H	New peak for aromatic at 3132, aliphatic at 2908, bending at 1348	Shift to 1647 to pectin and 1708 to PVA	1087	Aliphatic at 1319, aromatic at 1365	Q at1554 B at 1482 N=Q=N at 1118
CPG/PANI	3414, bending at 1400	New peak at 3240 for aromatic, Bending shift to 1516 weak	2858aliphatic, new peak for aromatic at 3093	1697 (chitosan amide),1739(remaining acetate for PVA)	Shift to 1080, shift to 1130 for secondary alcohol, overlap with alcoholic of PVA	1257 aliphatic, new peak at 1288 for aromatic	Schiff base (C=N) shift to 1651, Q at 1543,B at 1449,N=Q=N at 1184
CPM/PANI	3487	3305 aliphatic , new peak at 3209 for aromatic, bending shift to1577	Shift to 2927, new peak at 3055 for aromatic	Shift to 1643 chitosan amide , shift and weaker to 1708 to PVA	Shift to 1041, disappeared peak for secondary alcohol	1215 for aliphatic, new peak at 1342 for aromatic	Q at 1543, B at 1482, N=Q=N at 1111
CgA/PANI	3421, bending at 1408	Overlap with O-H, bending at 1516	2881 aliphatic, new peak for aromatic at 3008	1678 and 1600	Weaker and shift to 1080, secondary alcohol peak shift and weaker to 1134	Overlaps between aliphatic and aromatic at 1288	Q at 1543, B at 1454, N=Q=N at 1176
IPN/PANI	3437	Stretching 3228, bending at 1608	2943	1670 for poly acryl amide, 1724 for poly acrylic acid	1083	1230 aliphatic, new peak for aromatic at 1300	Q at 1556, B at 1469, N=Q=N at 1118

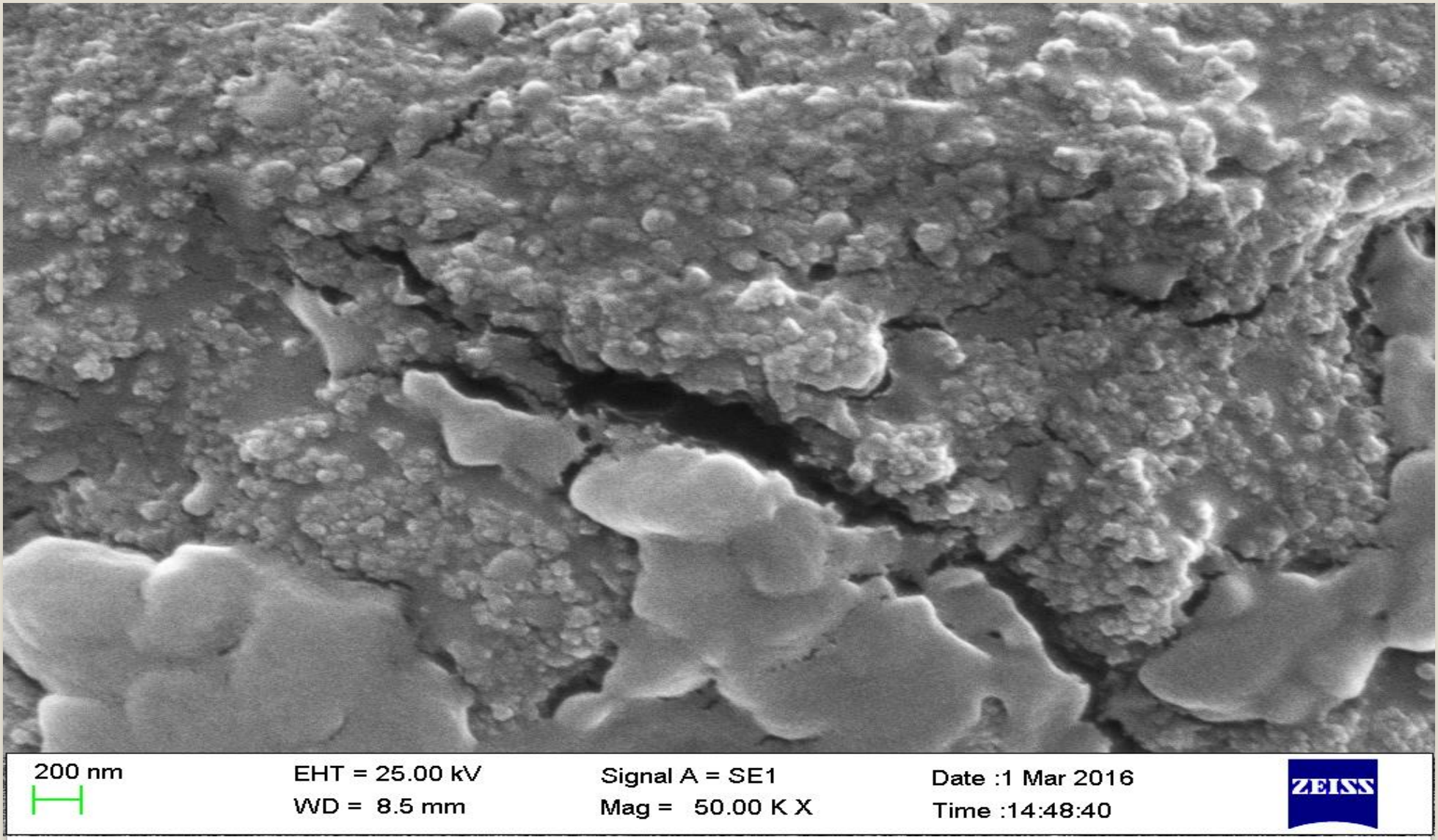

Figure (53): SEM photomicrograph of (CPG/PANI) with magnification 50 KX

(a)

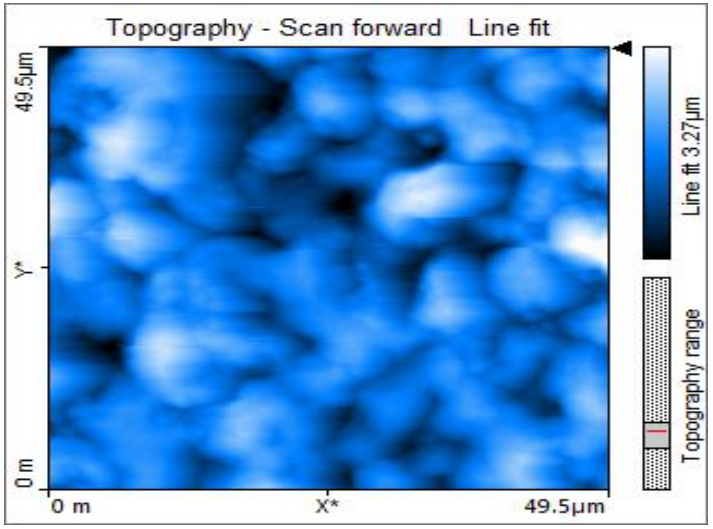

(b)

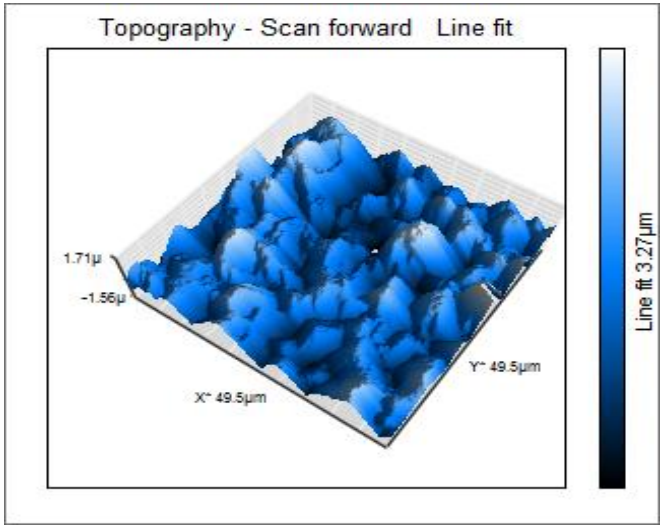

(c)

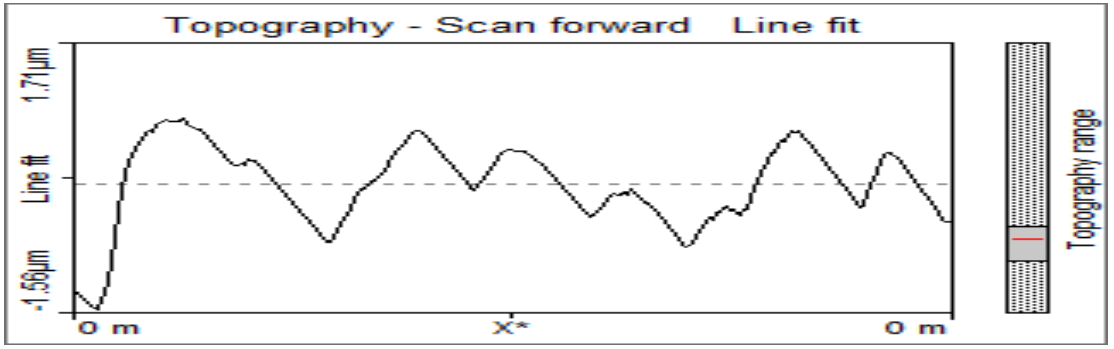

Figure (54): AFM photomicrograph of (CPG/PANI), (a): scan topography, b: 3D topography, & (c): line graph topography

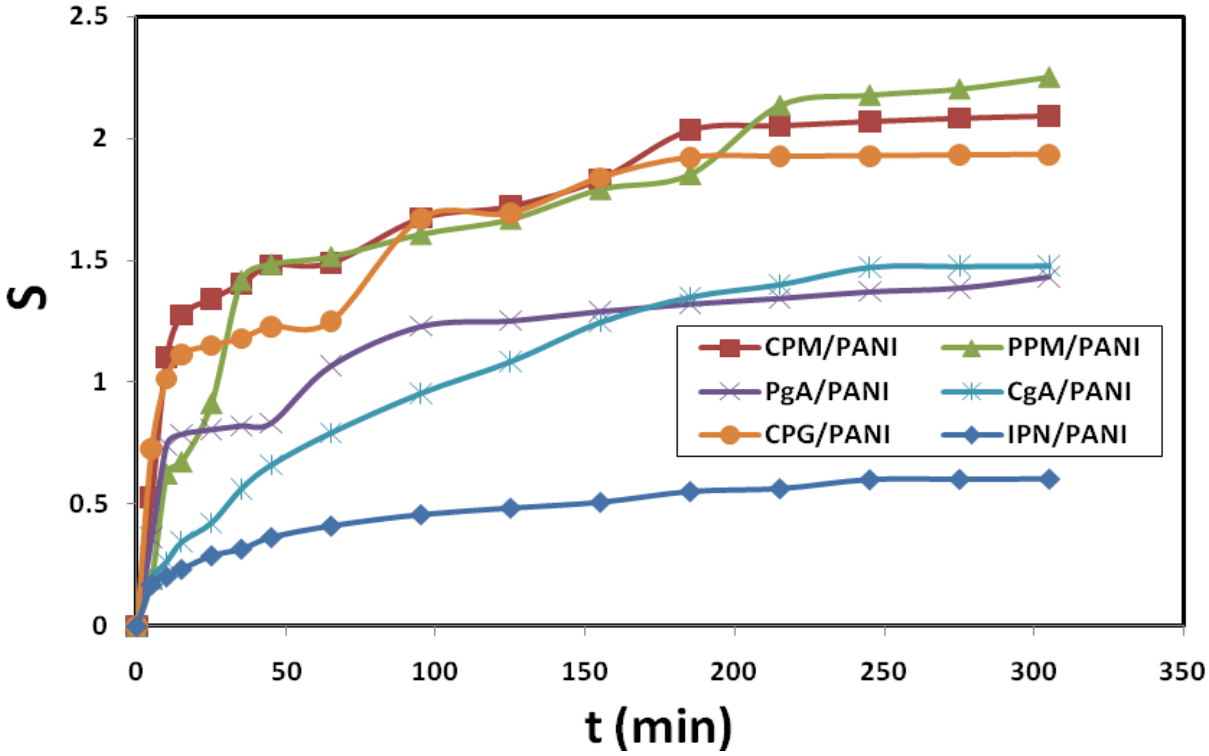

Figure (55): Degree of swelling for PANI composites in water at R.T.

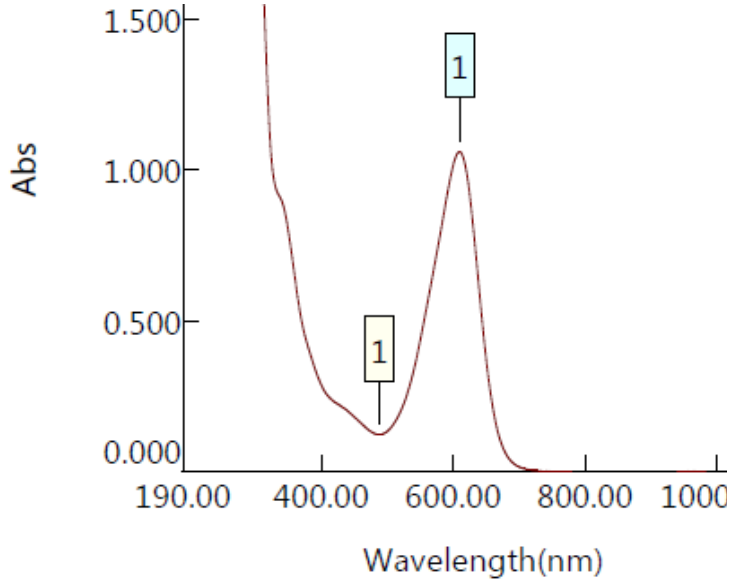

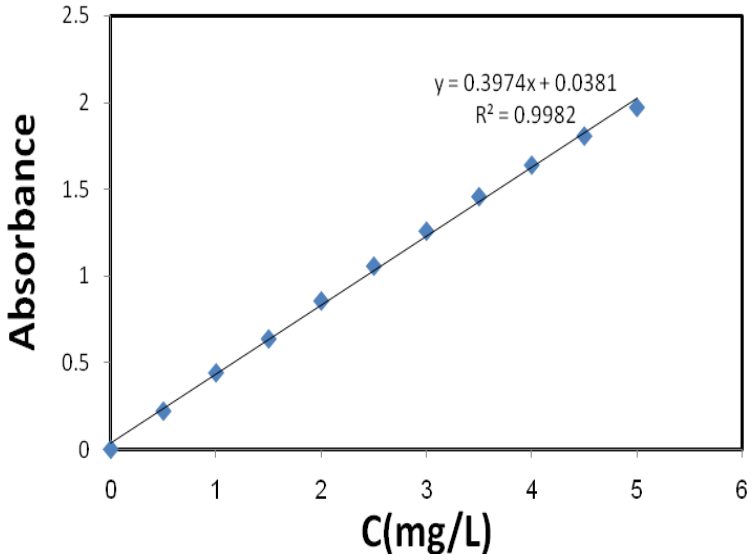

Figure (56): UV-Vis. Spectrum of indigo carmine and calibration curve

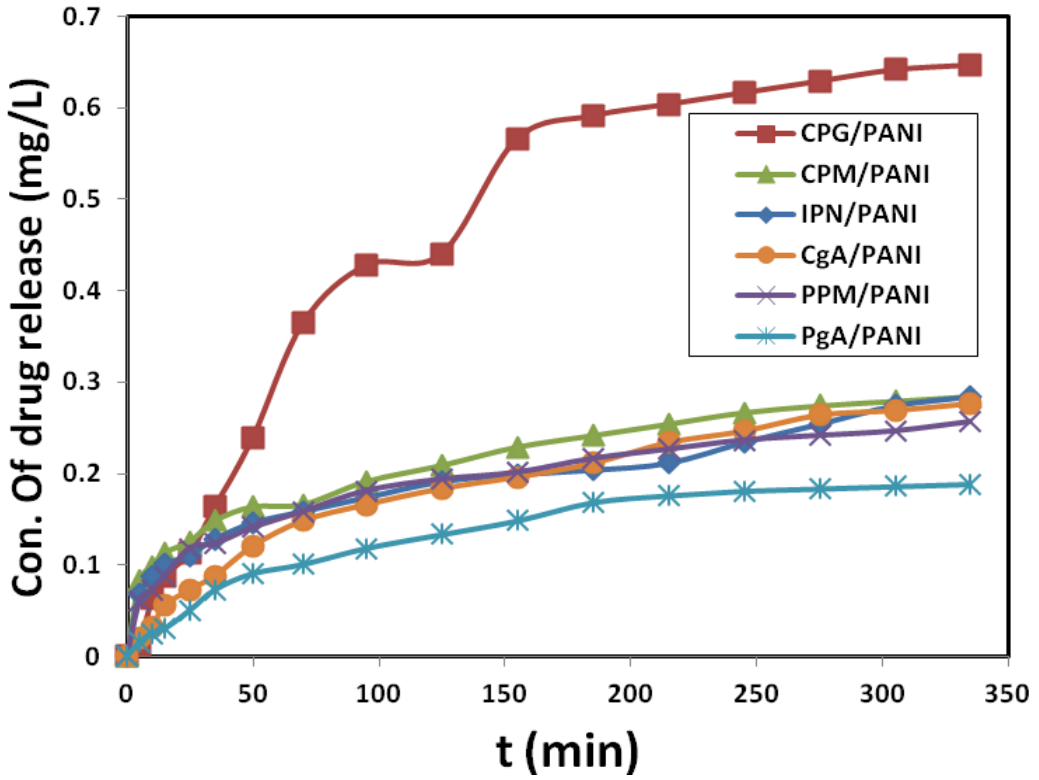

Figure (57): Indigo release from PANI composites at R.T. and Voltage=8

Synthesis of coated Fe_3O_4 with conductive hydrogel (CPG/Fe_3O_4/PANI)

In brief, CPG hydrogel solution was mixed with dispersion solution of Fe_3O_4 MNPs (2.5 w/v %) by mechanical stirring for (1h) at (2500 rpm.). with continuous mixing with mechanical stirrer was added poly aniline solution at (0-2) ˚ C until color of solution convert to black green then added glutaraldehyde as crosslinking agent.

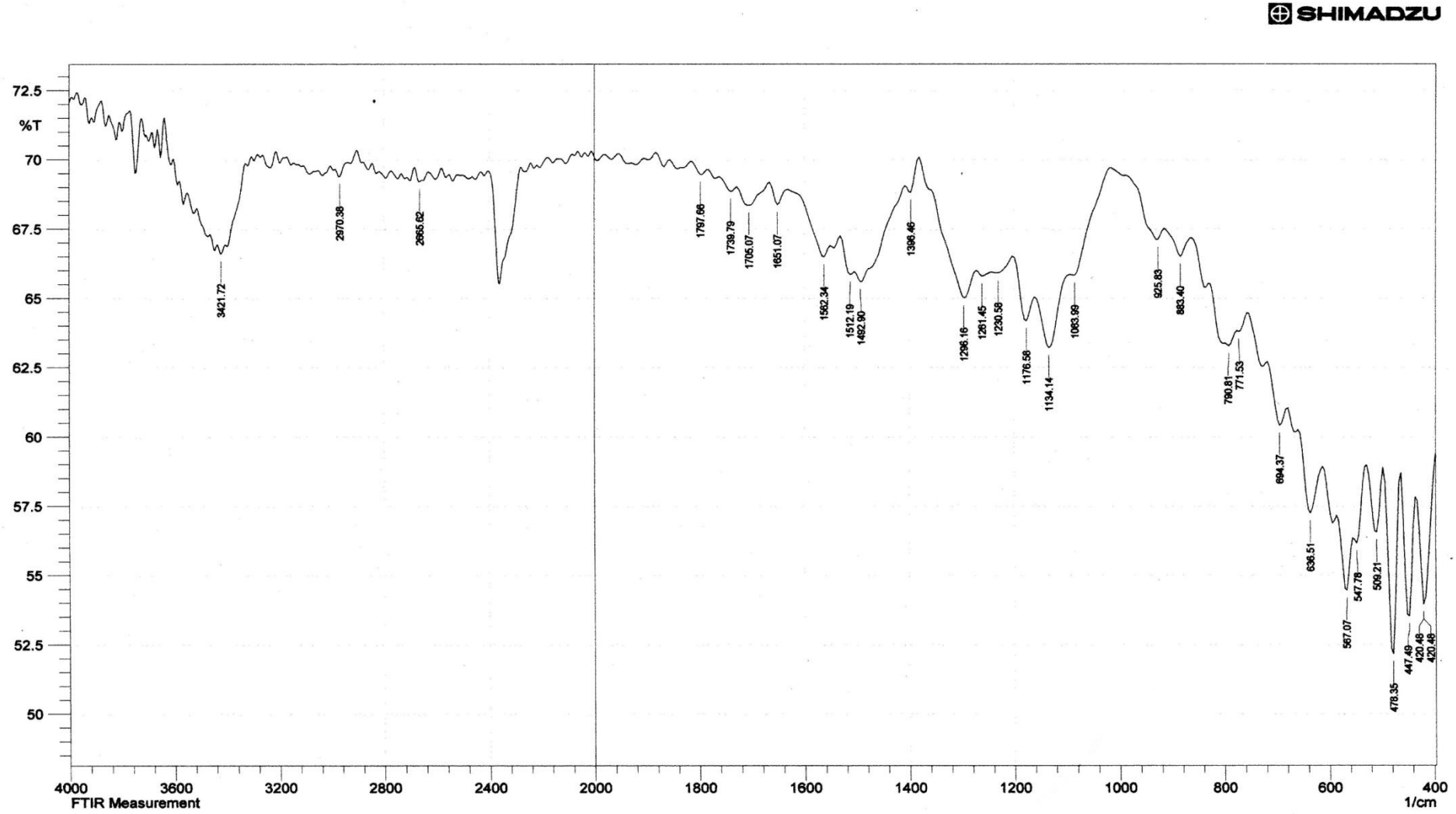

Figure (58): FT-IR spectrum of CPG/Fe_3O_4/PANI

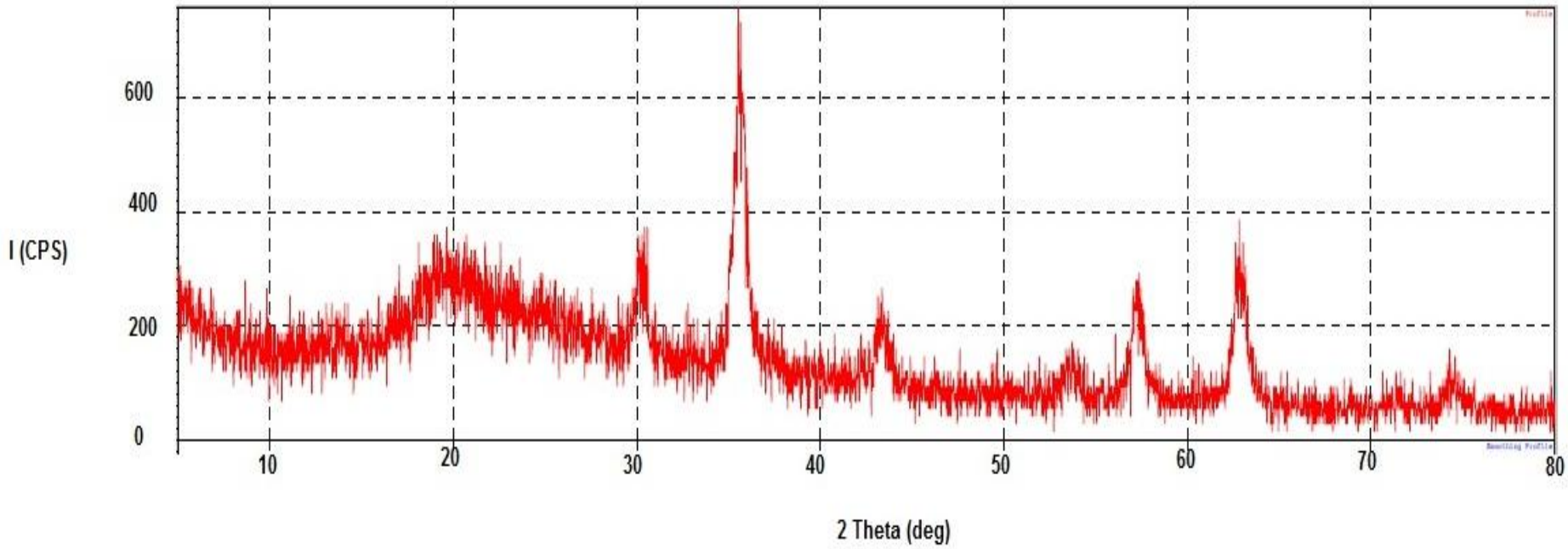

Figure (59): XRD for CPG/Fe_3O_4/PANI

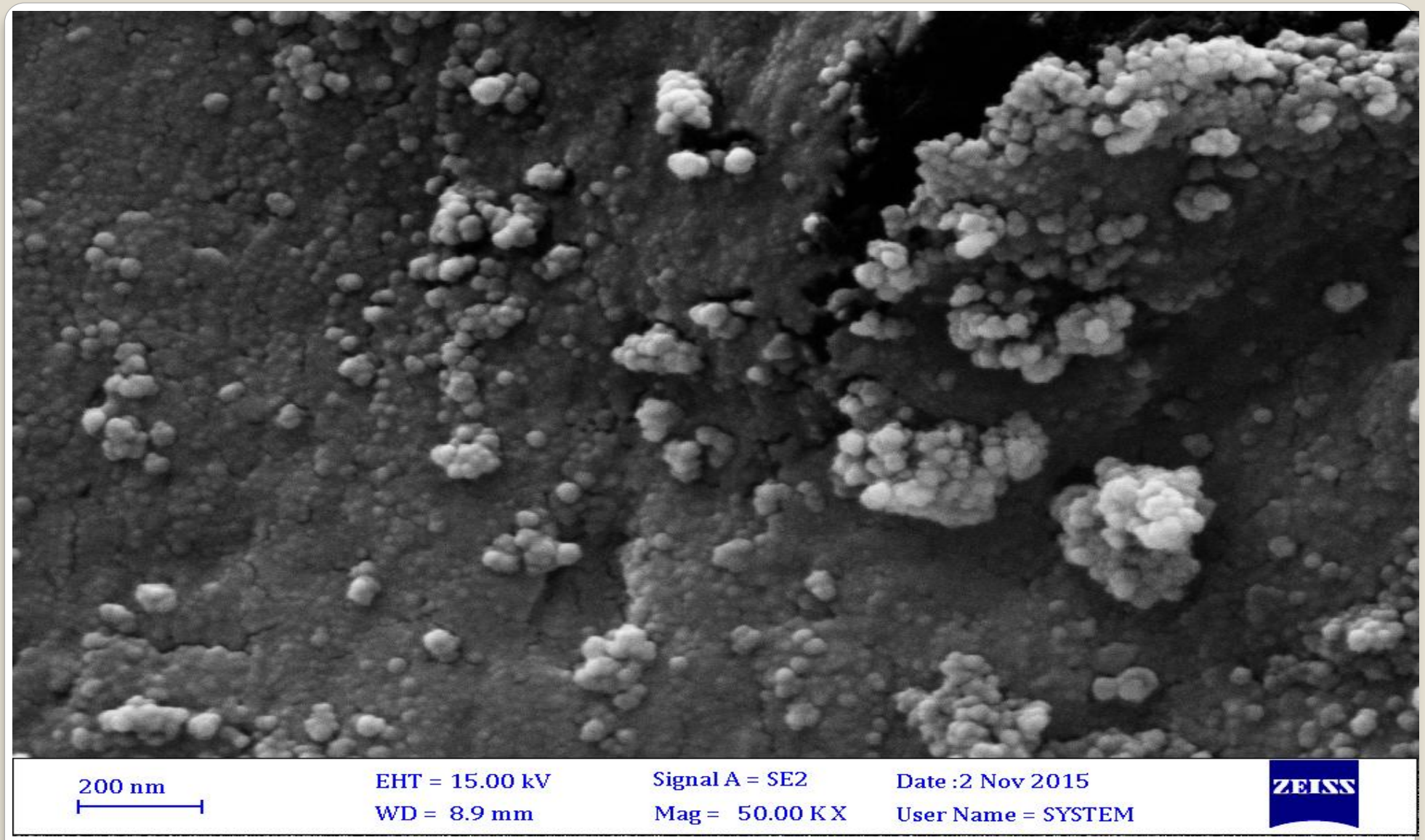

Figure (60): SEM photomicrograph of Coated Fe_3O_4 form (CPG/Fe_3O_4/PANI) with magnification 50 KX

The SEM & EDS results of coated magnetite nanoparticles was shown the type and weight percent of elements present in the selected area of the sample at SEM micrographs. The coated sample analysis consisted new elements (C, N, Cl) due to conductive hydrogel.

(a)

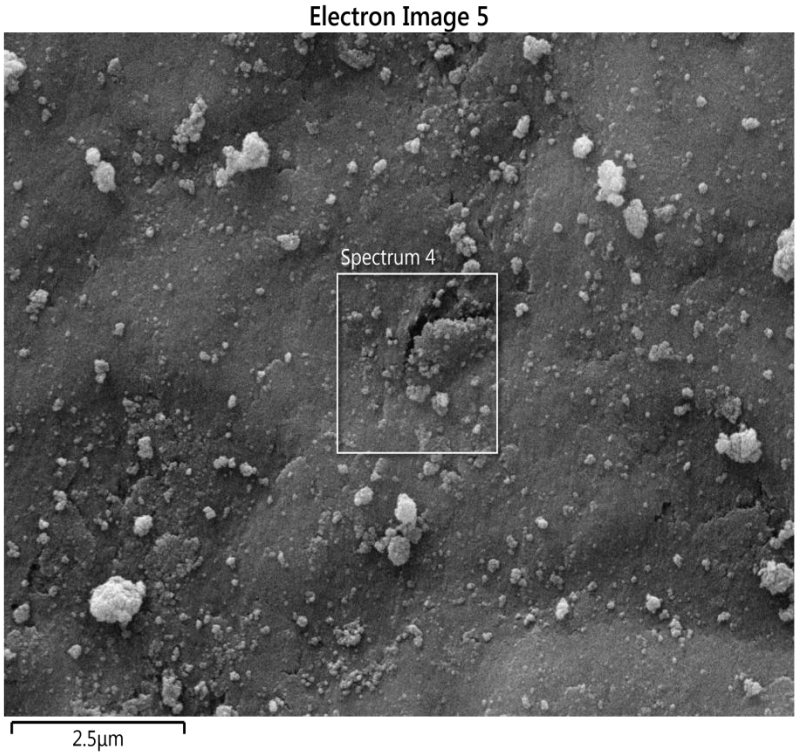

(b)

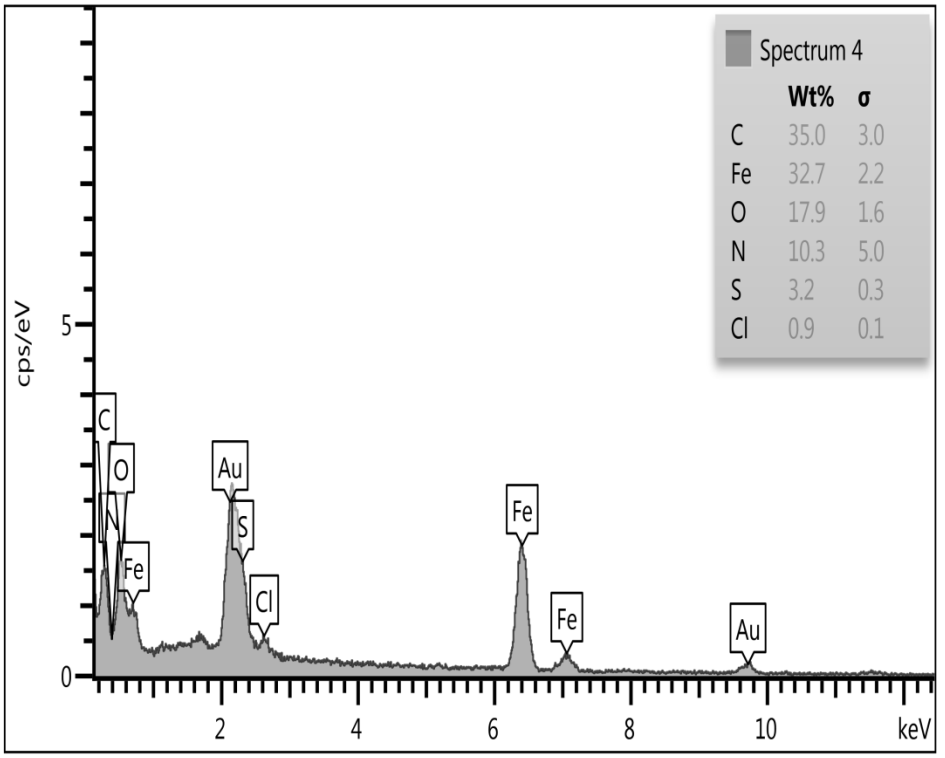

Figure (61): (a) SEM and (b) EDS for coated Fe_3O_4 form (CPG/Fe_3O_4/PANI)

In this figure show magnetite nanoparticles coated with conductive hydrogel and very clear to recognize the coating and the core of the nanoparticle.

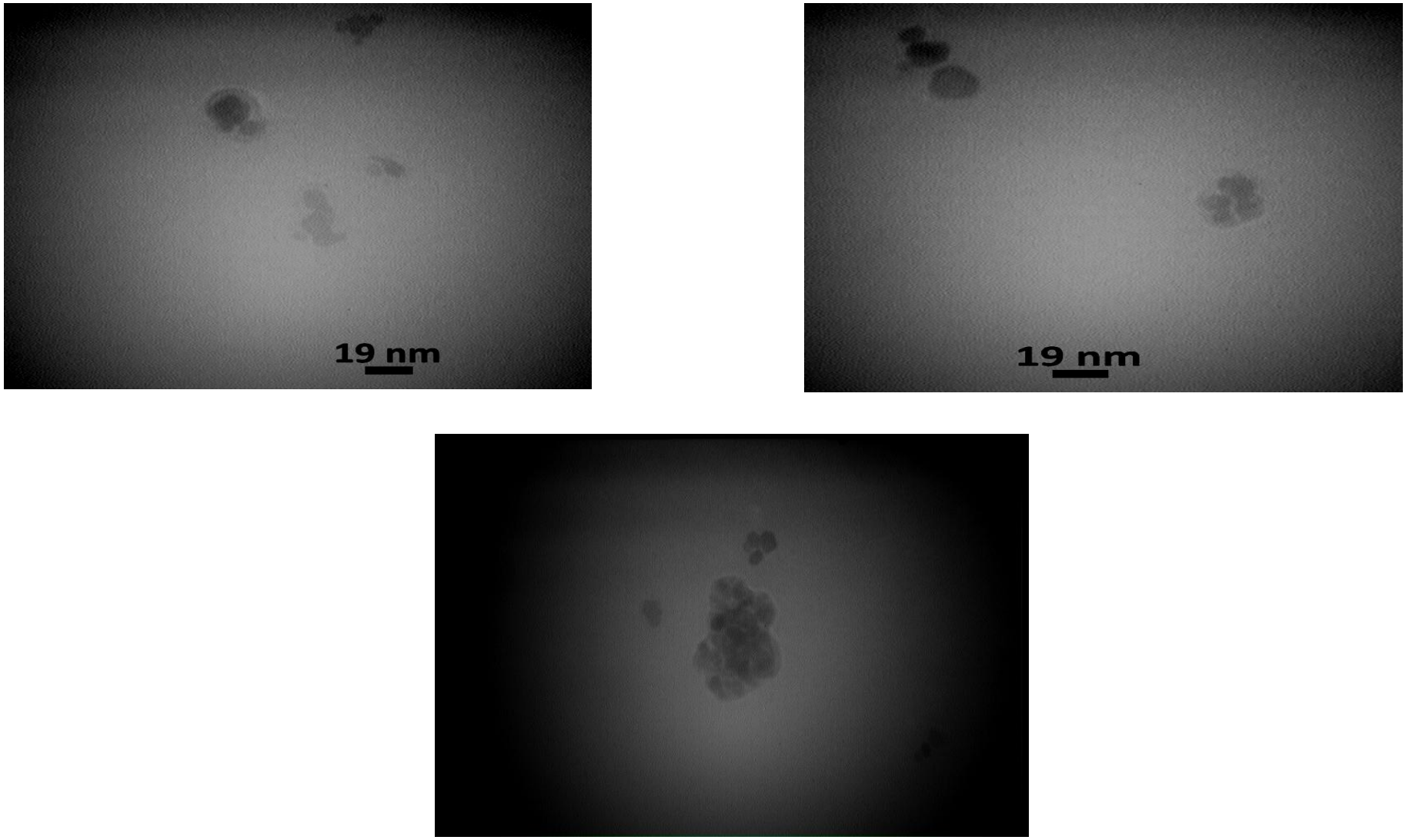

Figure (62): TEM photomicrographs of Coated Fe_3O_4 form (CPG/Fe_3O_4/PANI)

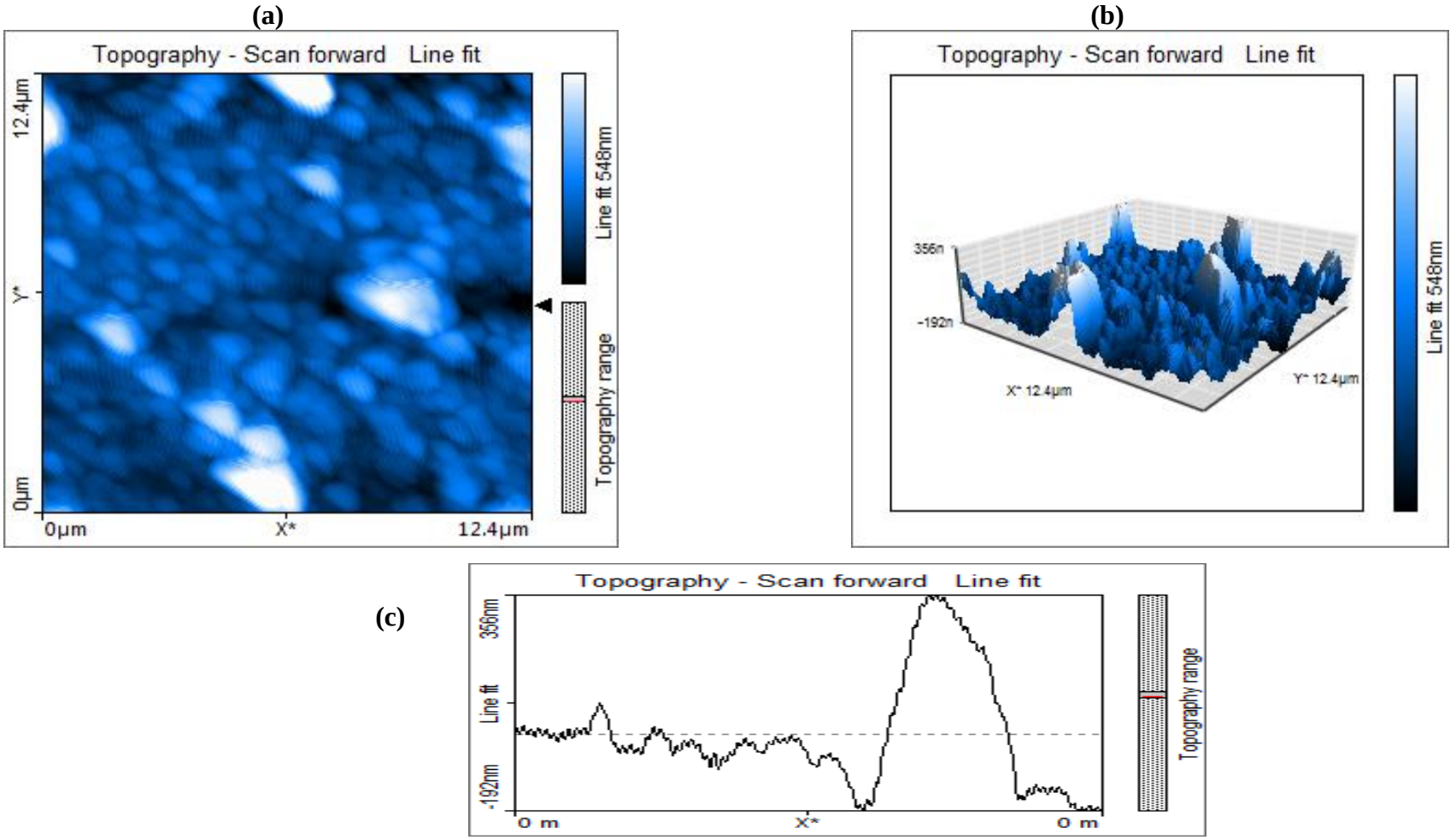

Figure (63): AFM photomicrograph of accumulation of $(CPG/Fe_3O_4/PANI)_{,}$ (a): scan topography, (b): 3D topography, & (c): line graph topography

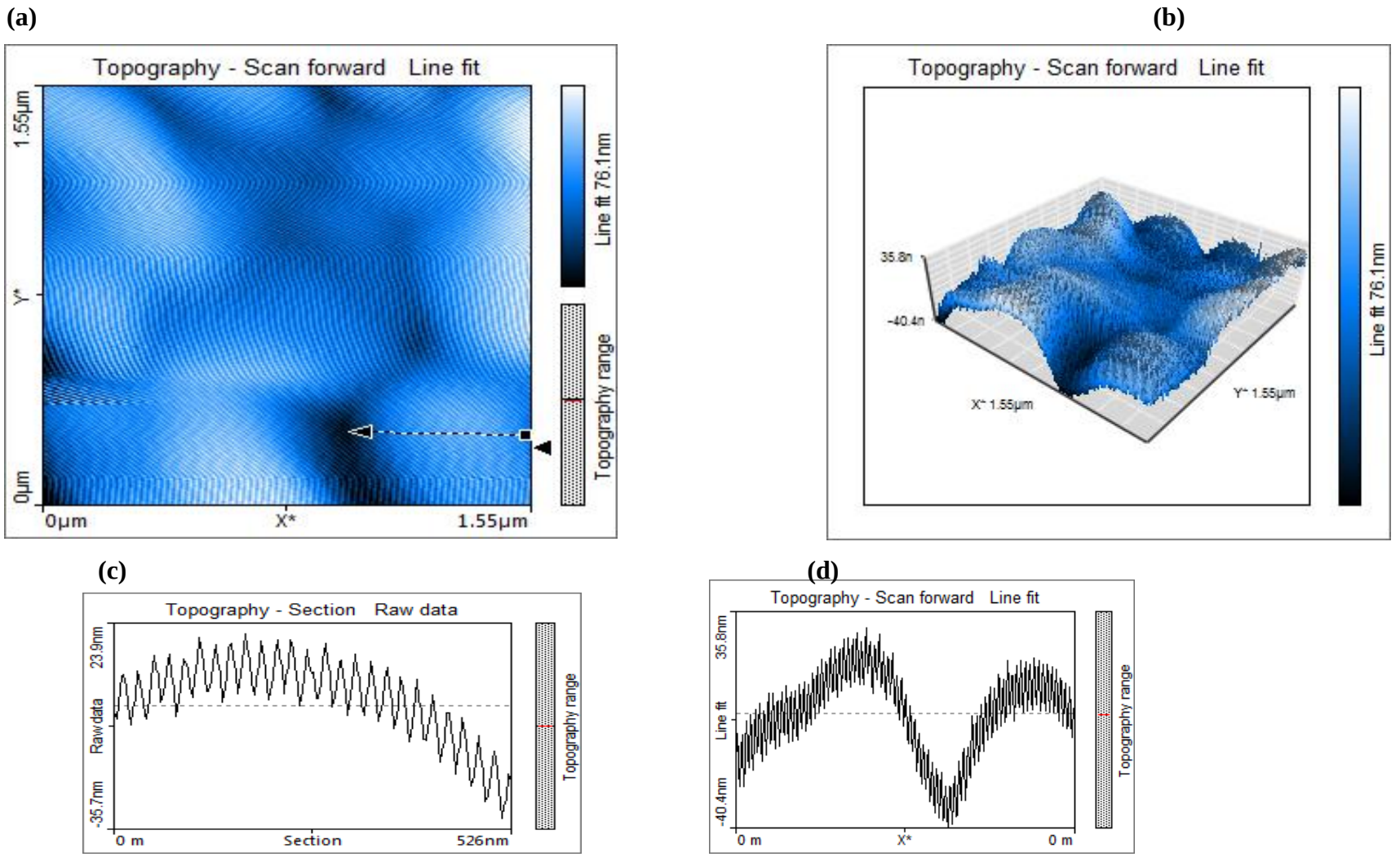

Figure (64): AFM photomicrograph of coated Fe_3O_4 form (CPG/Fe_3O_4/PANI) , (a): scan topography, b: 3D topography, (c): cross-section topography, & (d): line graph topography

Saturation magnetization of coated magnetite nanoparticle was equal to (17.53514 emu g^{-1} at applied field 8499.915 Oe) which has been significantly decreased compared to that of the pure Fe_3O_4 was equal to (59.79764 emu g-1 at applied field 8500.56 Oe) which can be assigned to hydrogel coating magnetite.

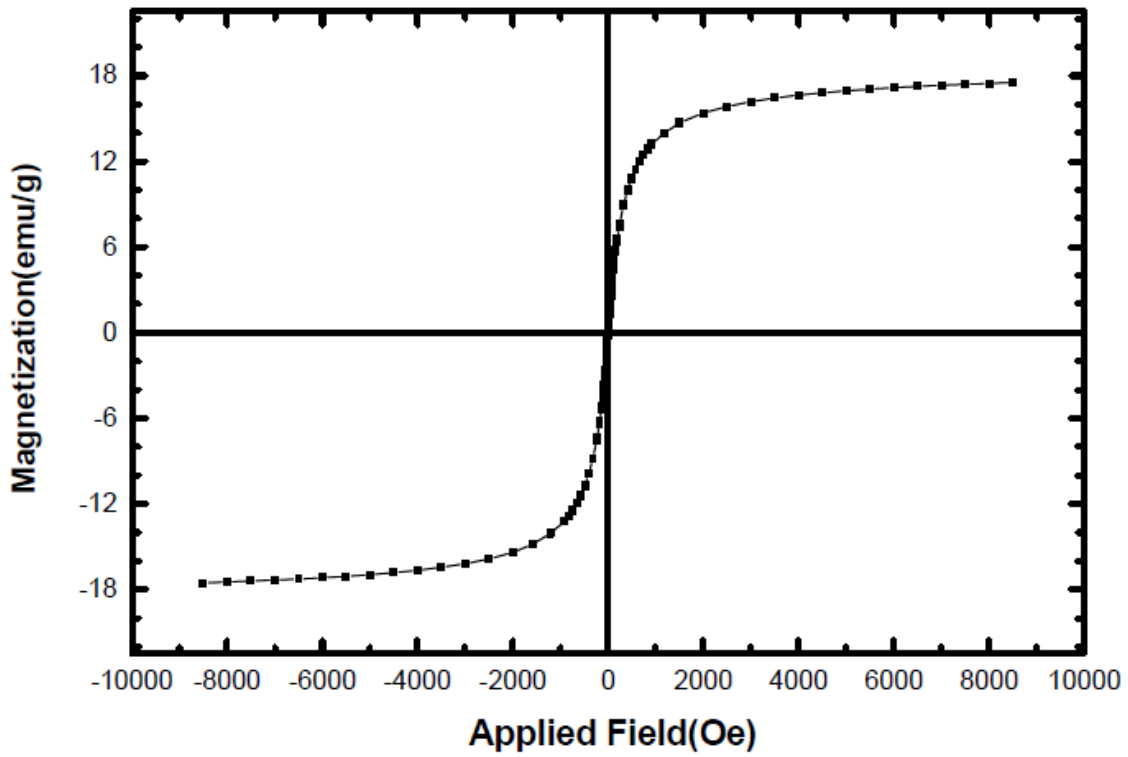

Figure (65): Hysteresis loop of coated form (CPG/Fe_3O_4/PANI)

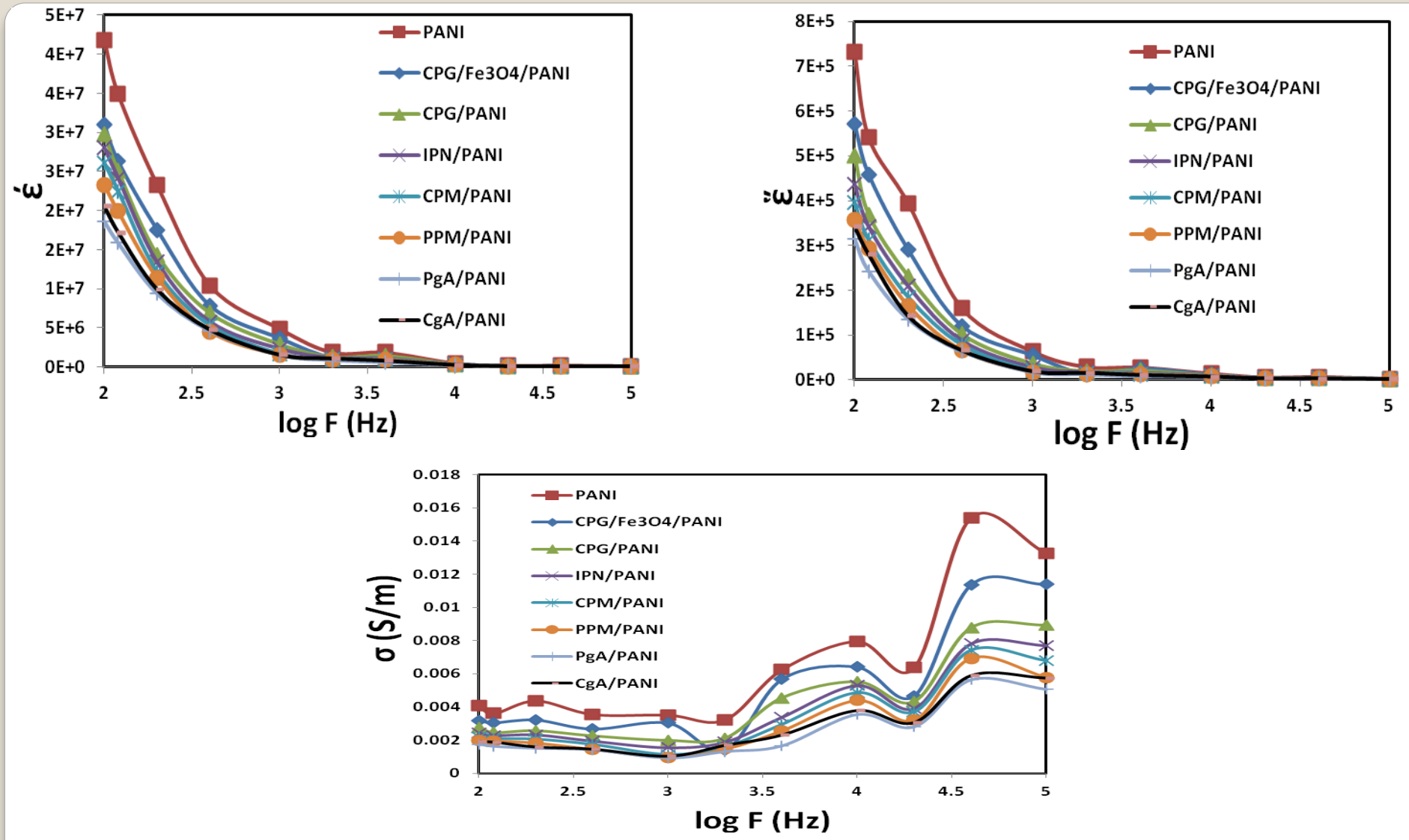

Figure (66): Real permittivity , Imaginary permittivity , and AC conductivity versus log frequency for PANI and composites

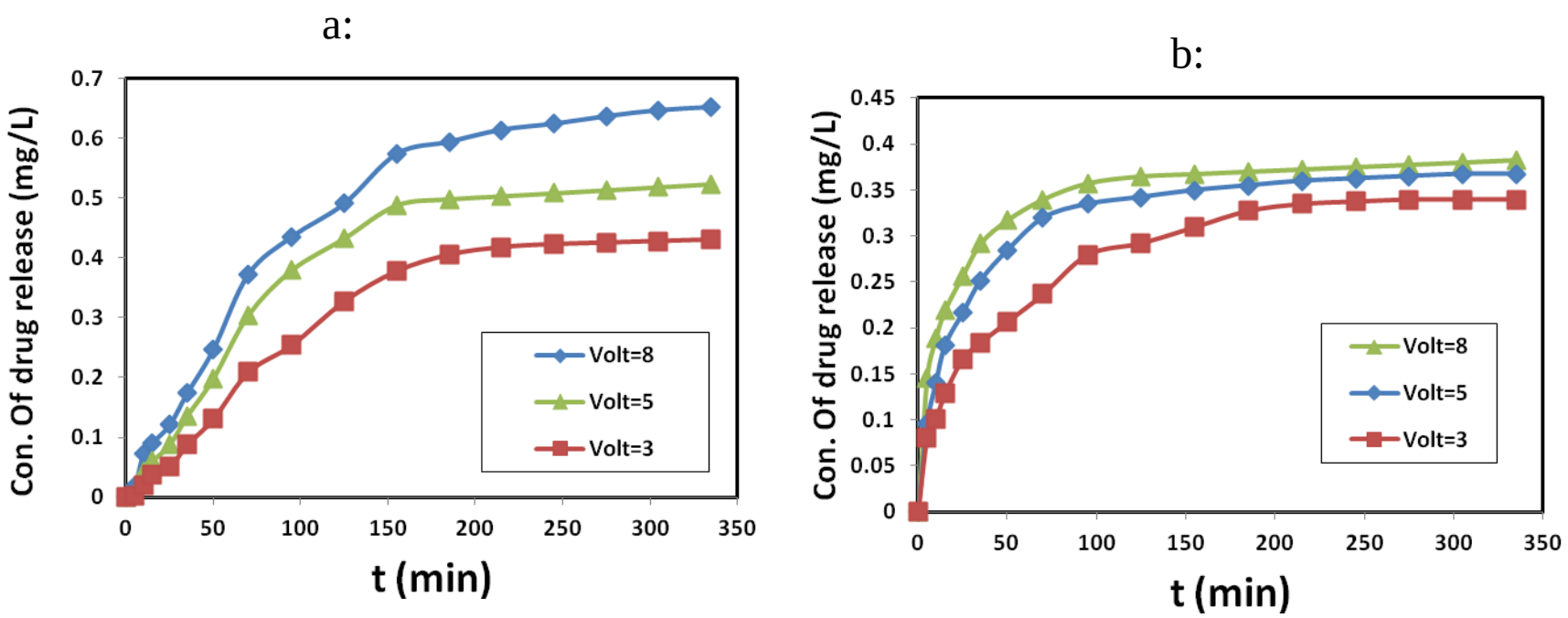

Figure (67): Indigo release from a: CPG/PANI and b: (CPG/Fe_3O_4/PANI) composite at 37ºC and difference voltages

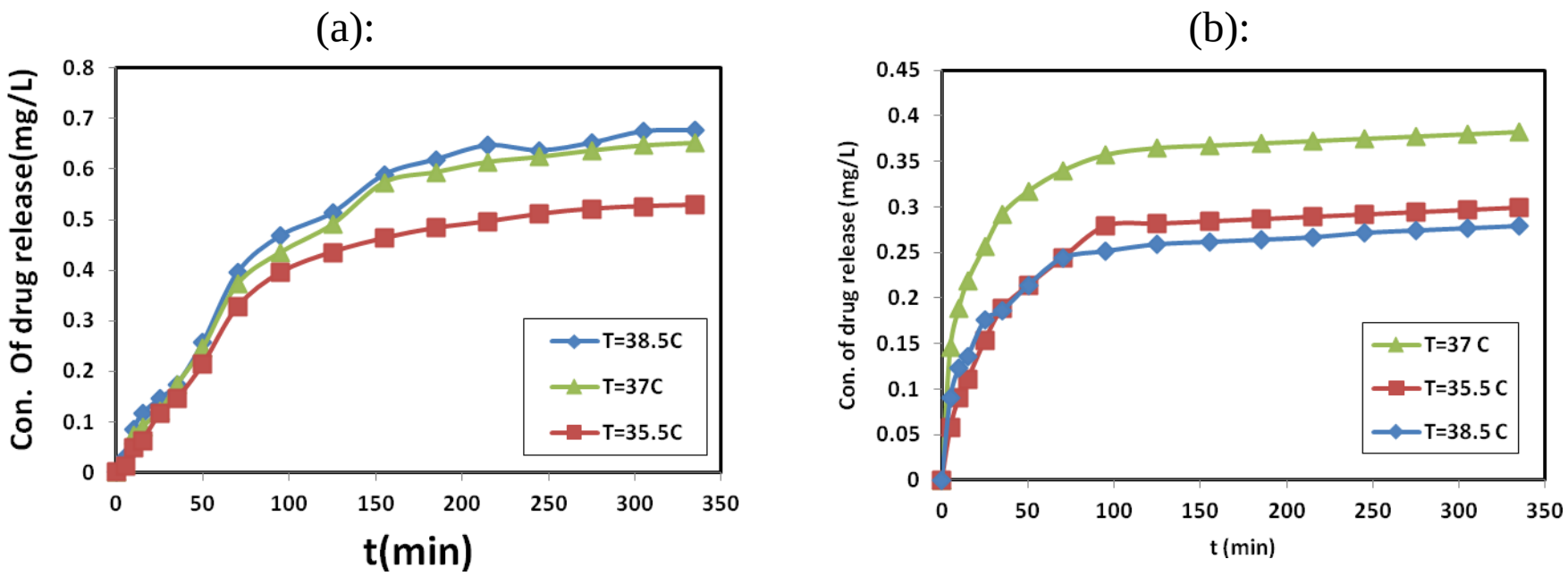

Figure (68): Indigo release from (a): CPG/PANI and (b) : (CPG/Fe_3O_4/ PANI) composite at different temperature and 8V

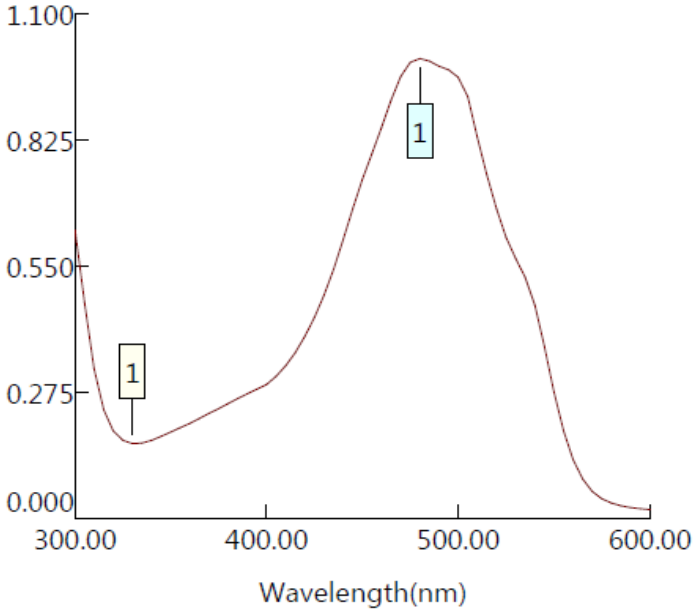

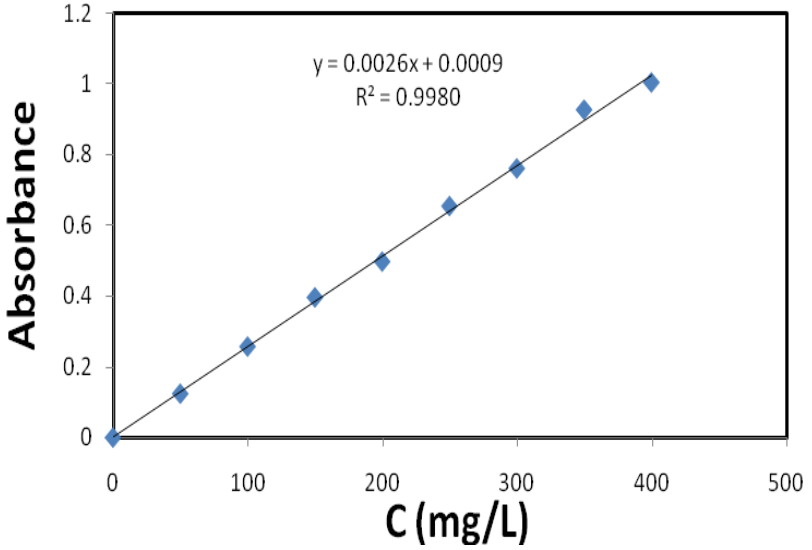

Figure (69): UV-Vis. Spectrum of doxorubicin hydrochloride and calibration curve

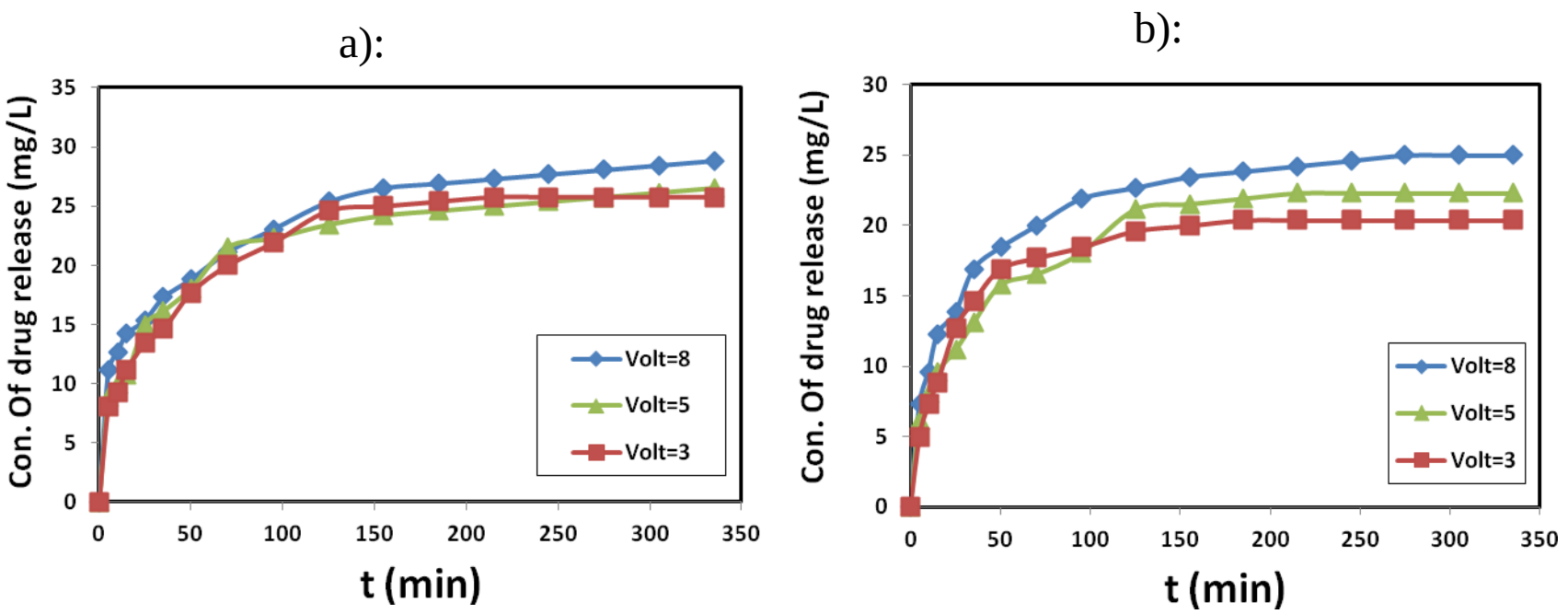

Figure (70): Doxorubicin hydrochloride release from (a): CPG/PANI and (b): (CPG/ Fe_3O_4/PANI) composite at different voltages and 37ºC

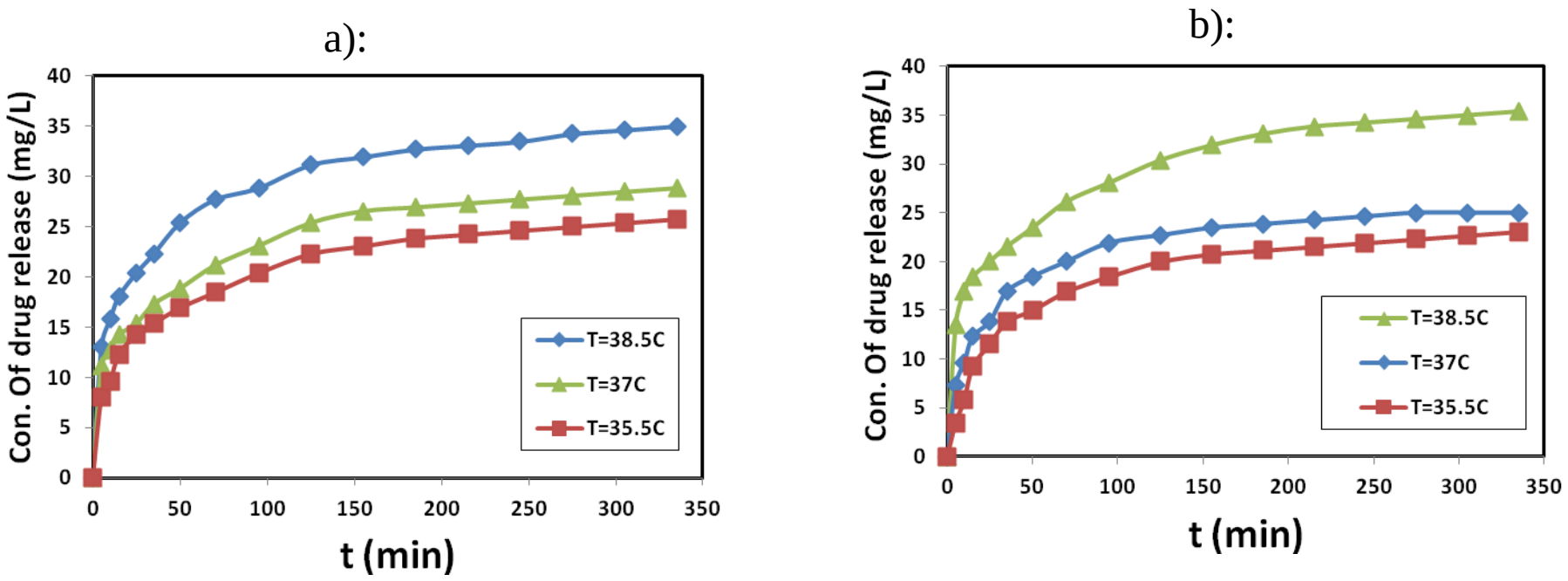

Figure (71): Doxorubicin hydrochloride release from (a): CPG/PANI and (b): (CPG/Fe_3O_4/PANI) composite at different temperatures and 8V

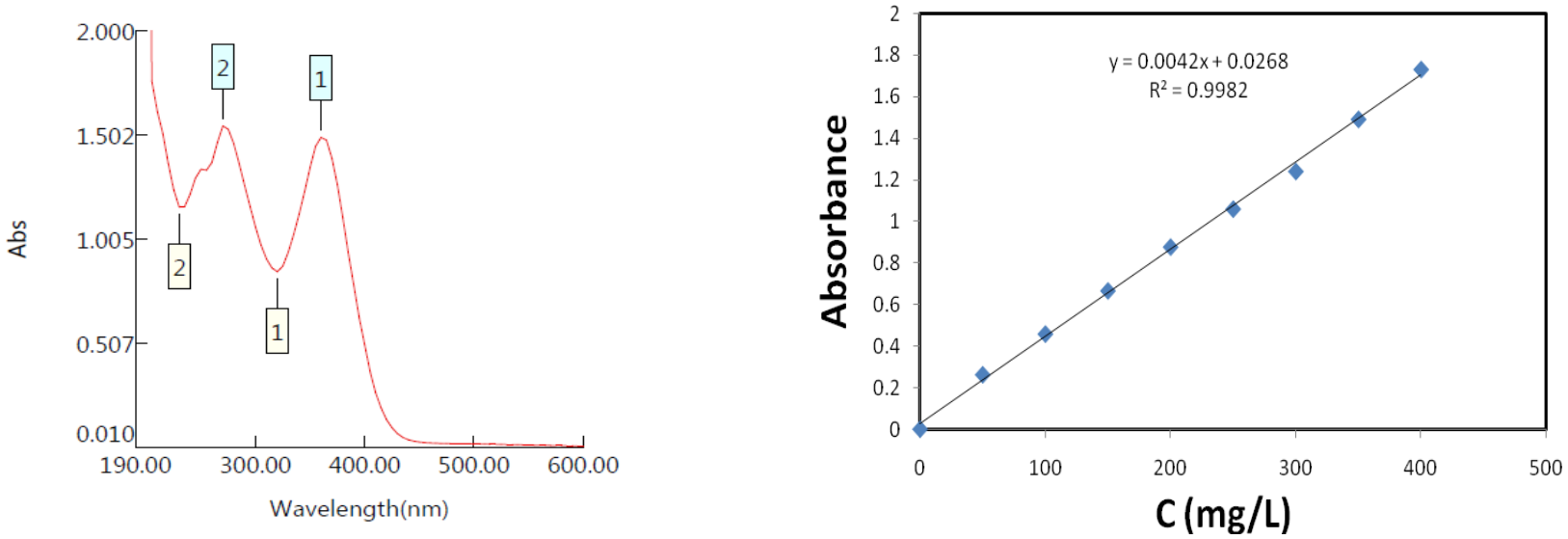

Figure (72): UV-Vis. Spectrum of methotrexate and calibration curve

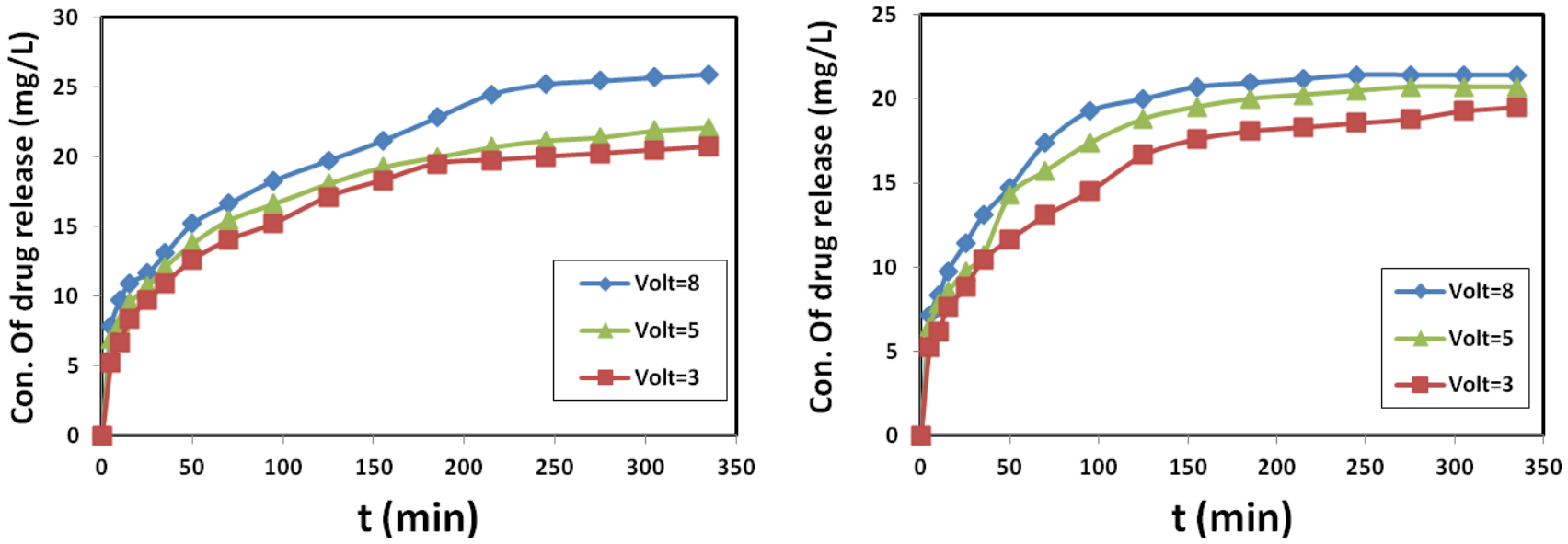

Figure (73): Methotrexate release from (a): CPG/PANI and (b): (CPG/Fe_3O_4/PANI) composite at different Voltages and 37ºC

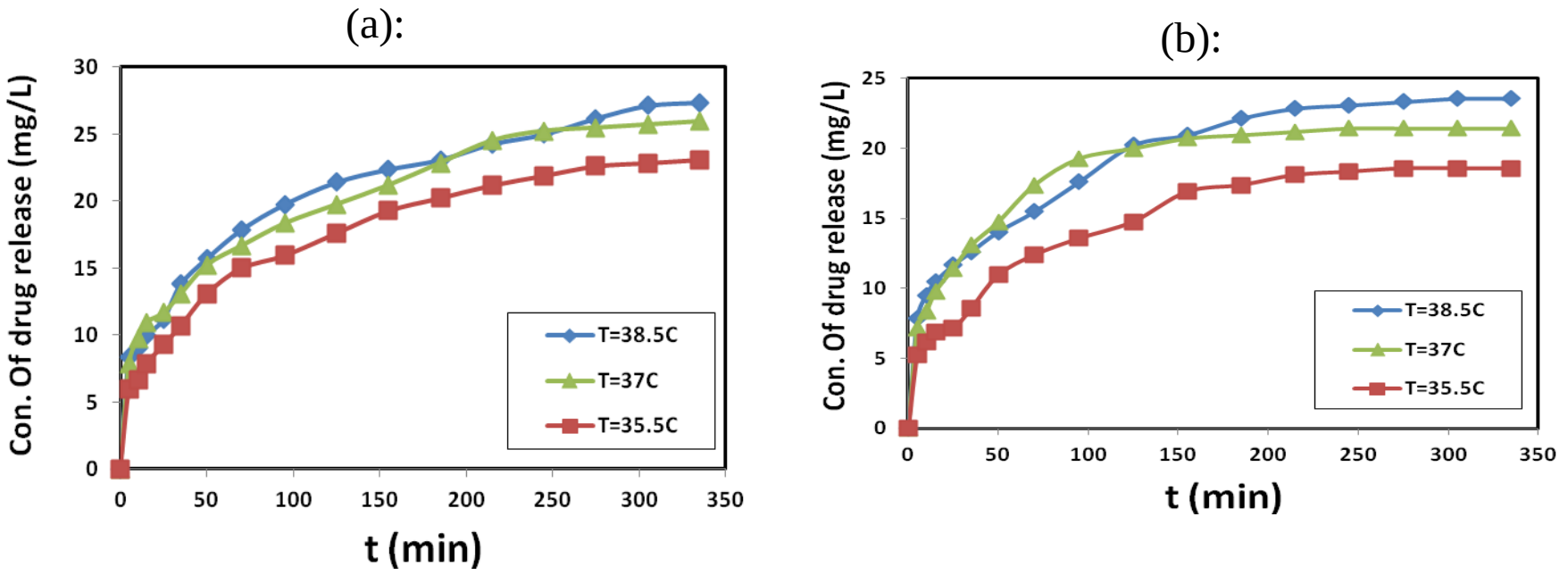

Figure(74): Methotrexate release from (a): CPG/PANI and (b): (CPG/Fe_3O_4/PANI) composite at different temperatures and 8V

Synthesis of conductive hydrogels /G

In brief, hydrogel solution was mixed with dispersion solution of G (0.25w/v %) with mechanical stirring for (1h) at (2500 rpm.).

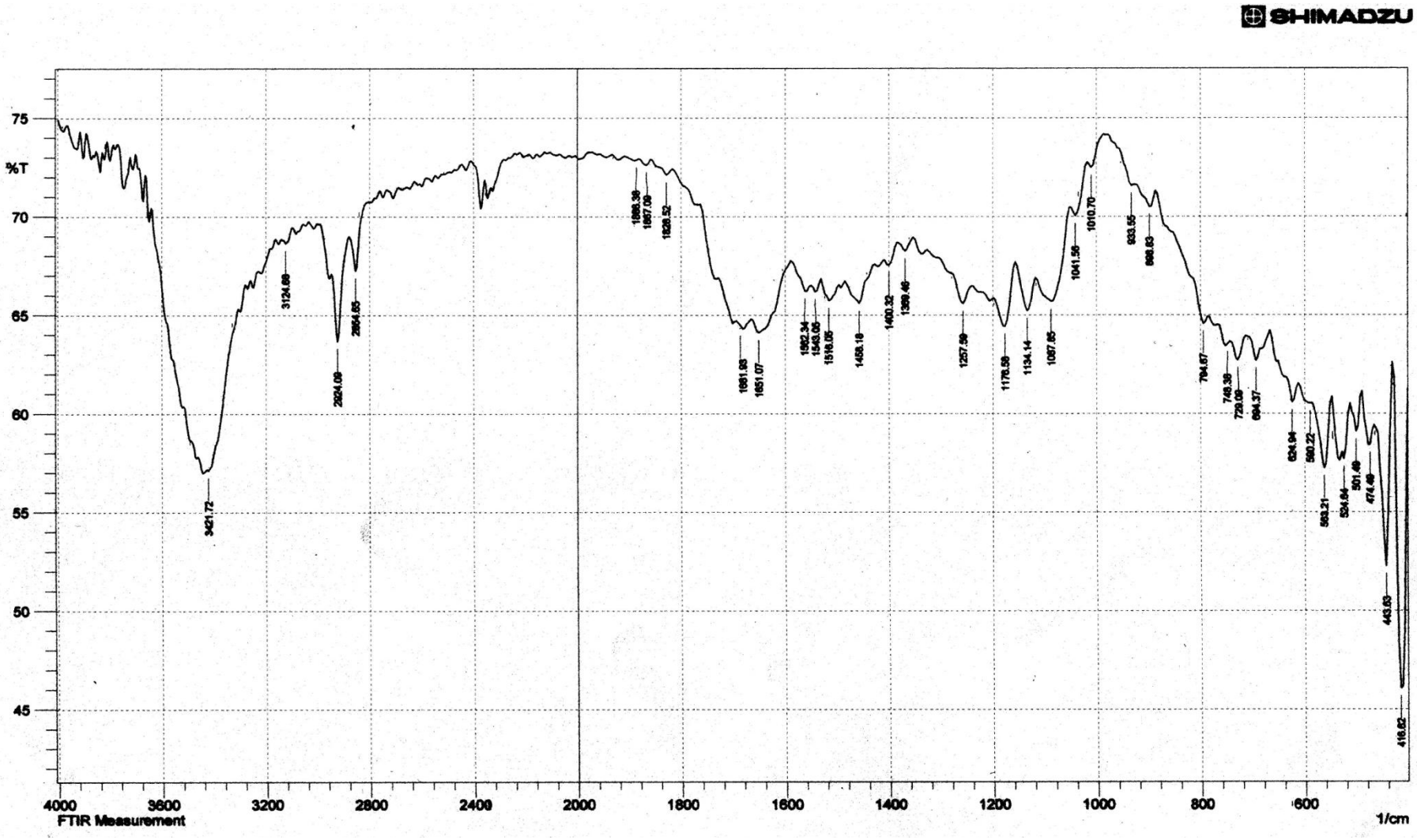

Figure (75): FT-IR spectrum of conductive hydrogel PgA/G film

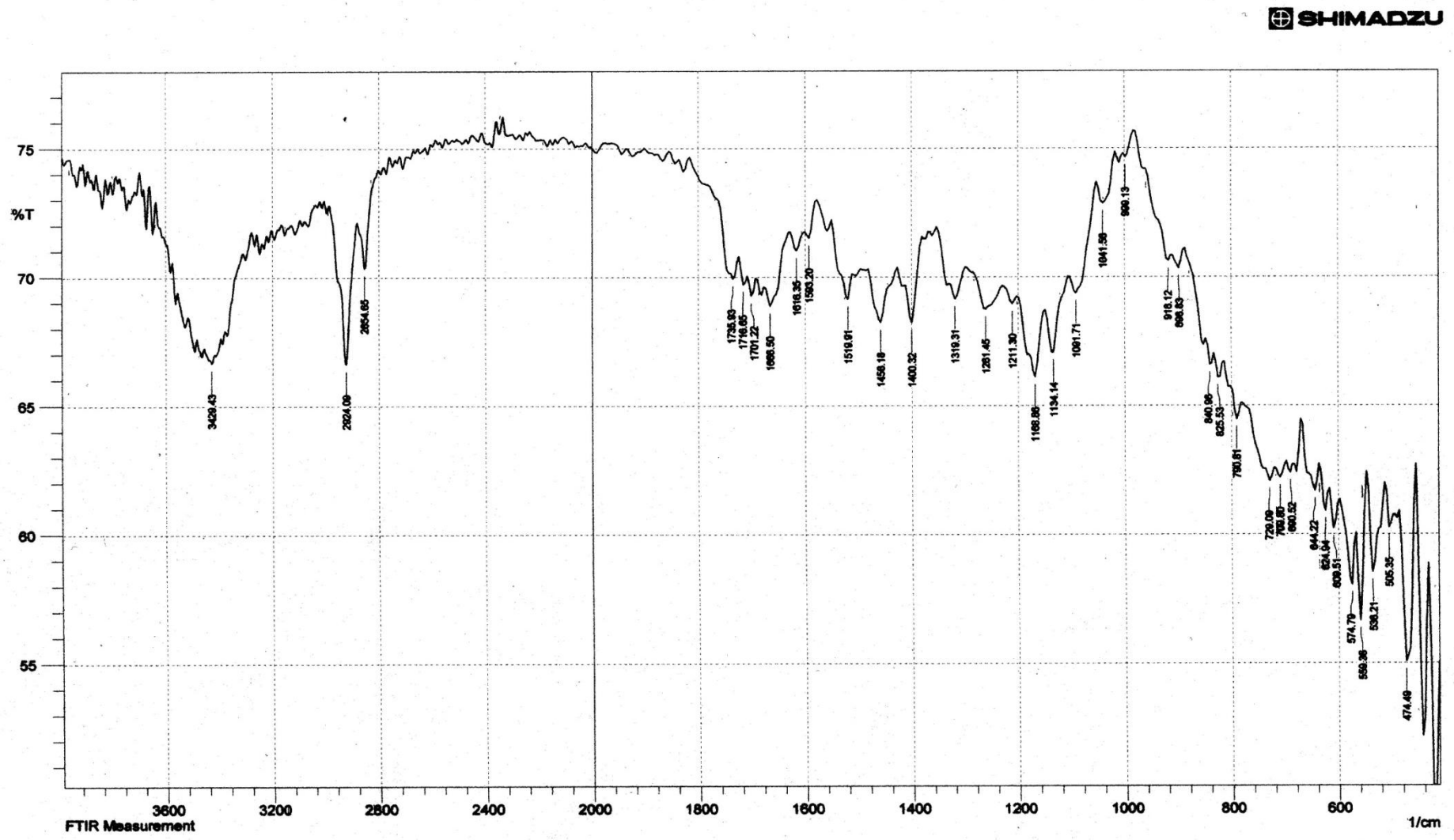

Figure (76): FT-IR spectrum of conductive hydrogel PPM/G film

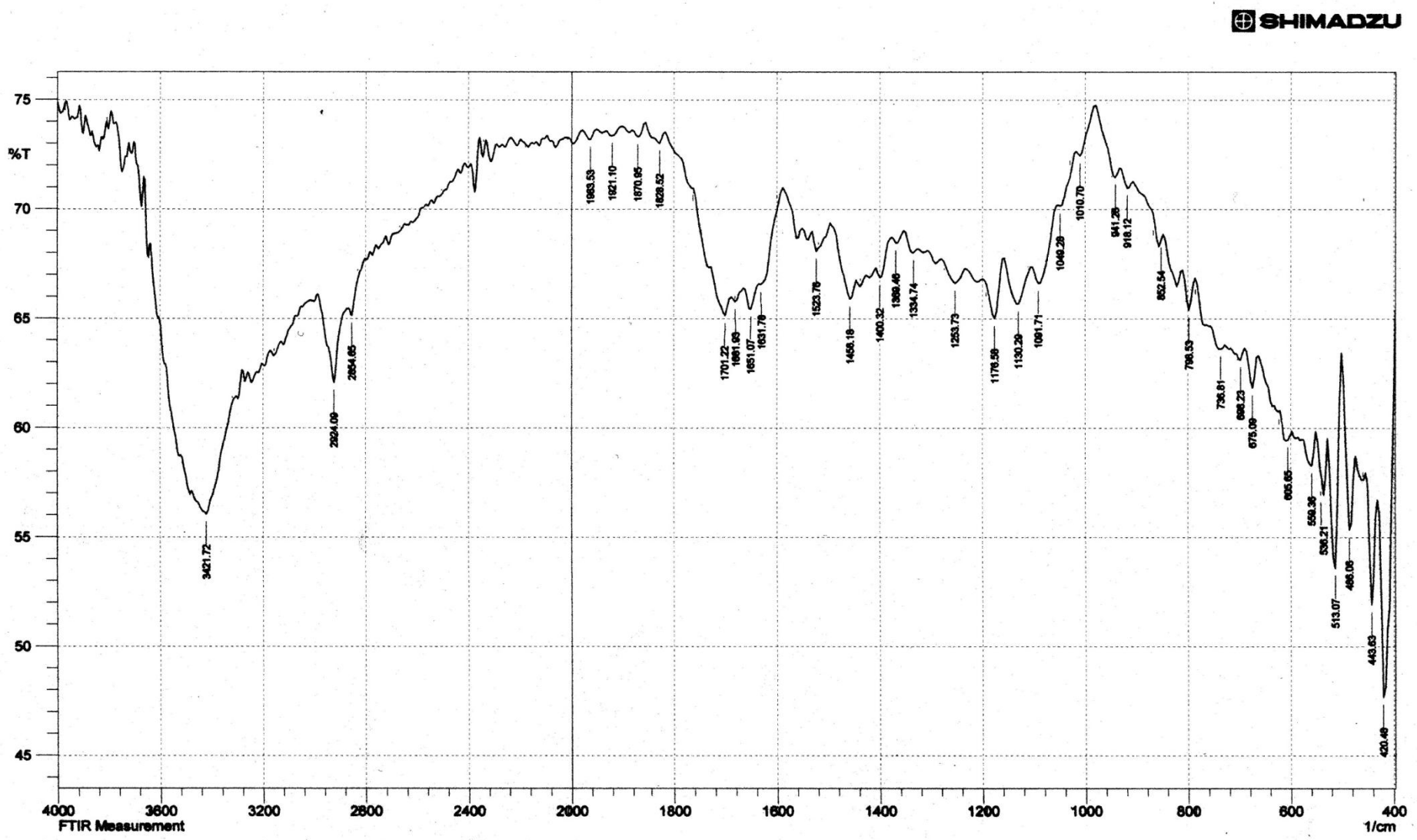

Figure (77): FT-IR spectrum of conductive hydrogel CPG/G film

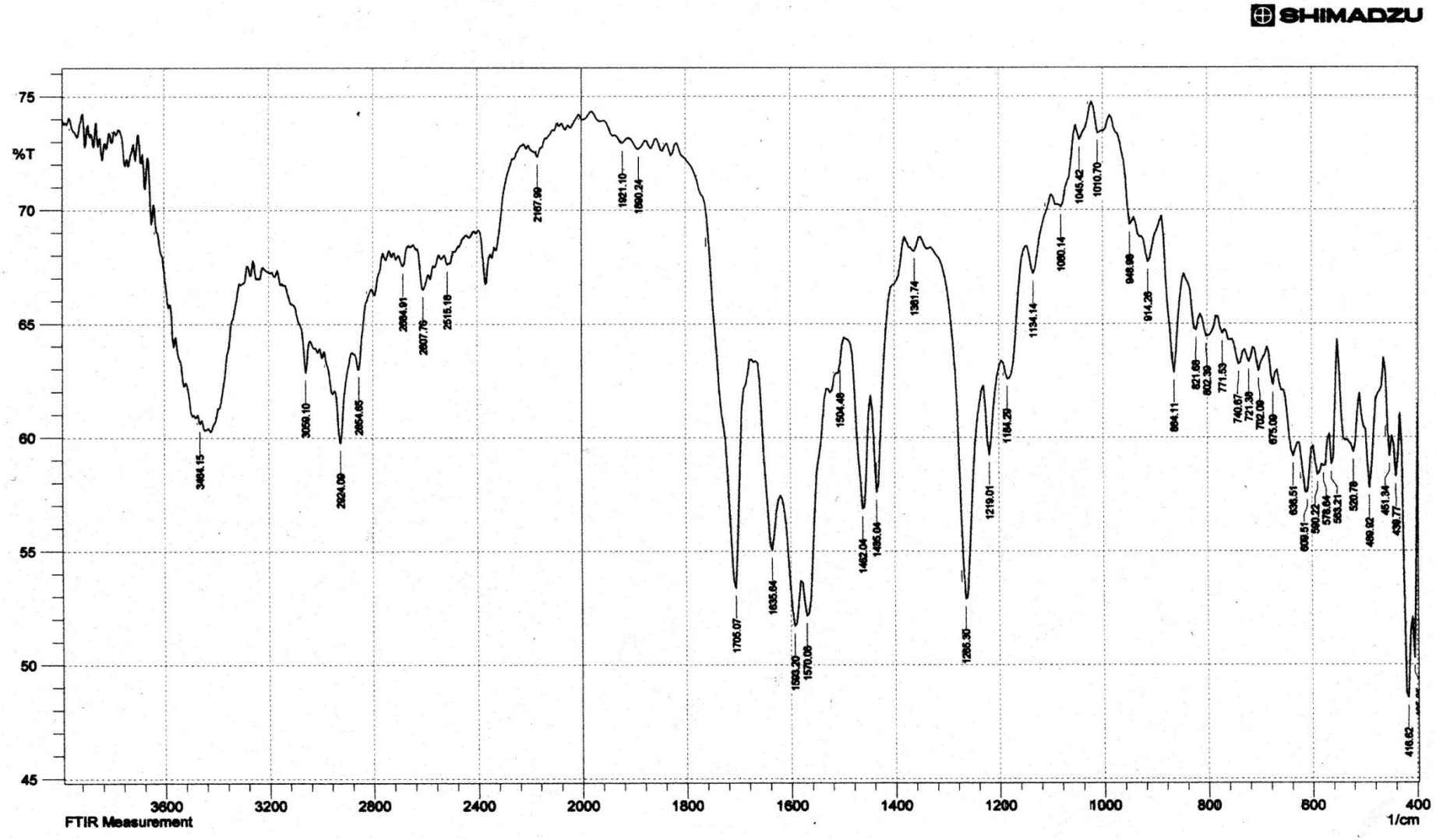

Figure (78): FT-IR spectrum of conductive hydrogel CPM/G film

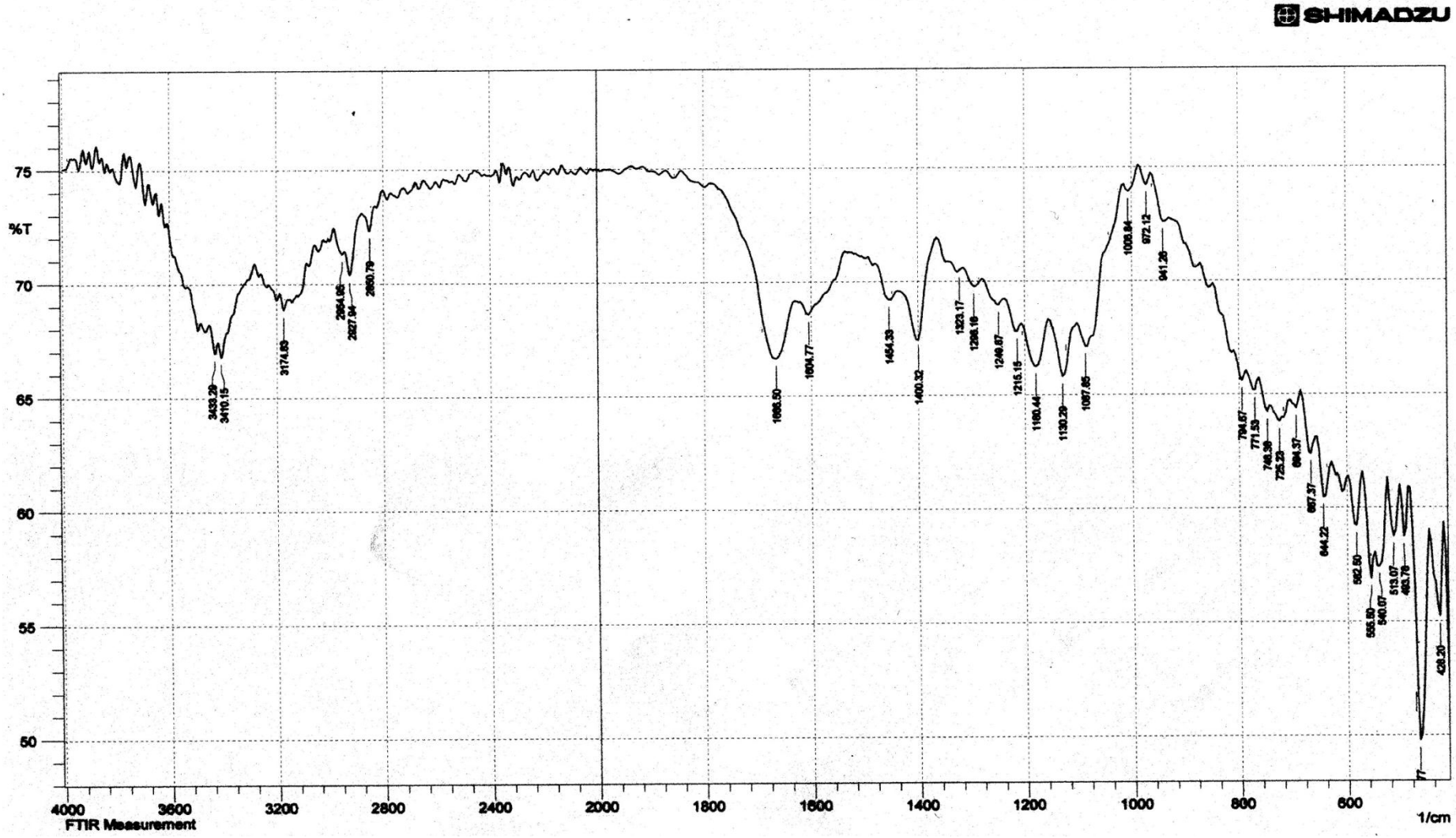

Figure (79): FT-IR spectrum of conductive hydrogel CgA/G film

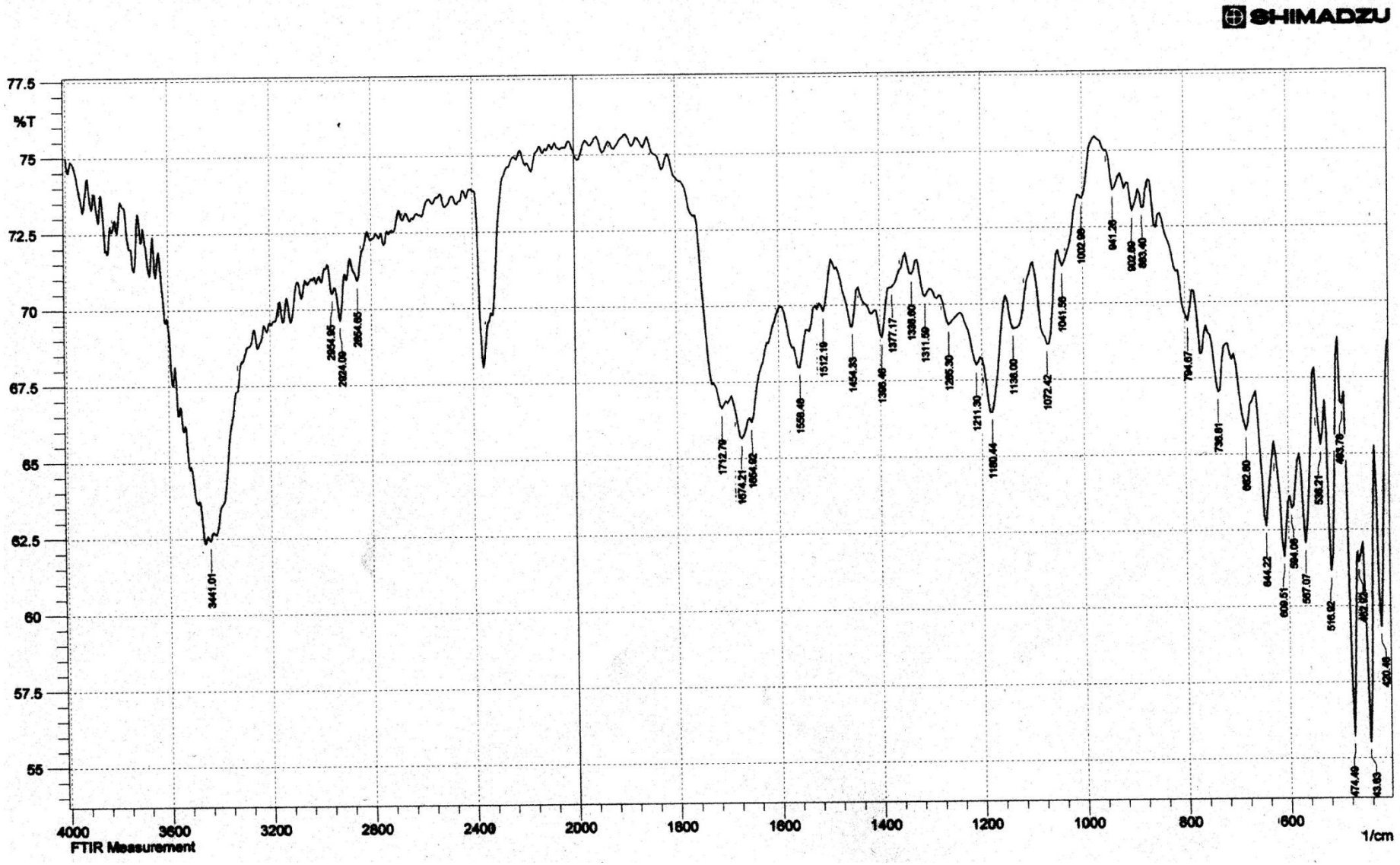

Figure (80): FT-IR spectrum of conductive hydrogel IPN/G film

Table (2): Characteristics FTIR absorption bands (cm^{-1}) contain stretching vibrations& bending vibrations of hydrogels/G composite

Samples	O-H	N-H	CH-	C=O	C-O	C-N	peaks other
PgA/G	3421	Overlaps with O-H	2924,2864 aliphatic, New peak at 3124 aromatic	1651, new peak at 1681 for G	1087 alcoholic, 1176 for acetal ring	1257 1309	C=C of G at 1562, 1543,1516
PPM/G	Stretching at 3429 ,bending at 1400	Overlaps with O-H	New peak for aromatic at 3132, aliphatic at 2924,2854 bending at 1319	Shift to 1716 to pectin and 1665 to PVA, 1735 for ester, new peak at 1701 for G,	Shift to 1091	1261,1319	C=C of G at 1616, 1593,1519
CPG/G	3421, bending at 1400	Overlaps with O-H	2924,2854	New peak at 1701 for G,	Shift to 1091, shift to 1130 for secondary alcohol	1253 , 1334	Schiff base (C=N) shift to 1651, C=C of G at 1661, 1560,1523
CPM/G	3464	Overlaps with O-H	2924,2854 new peak at 3059 for aromatic	1705, 1635	1080	1219 , 1265	C=C for G at 1593, 1570,1504
CgA/G	3433, bending at 1400	3410 , bending at 1454	2954, 2927,2860 aliphatic, new peak for G at 3174	1665 overlaps with C=O of G	1087	1215, 1249,1296,1323	C=C for G at 1604
IPN/G	3441	Overlaps with O-H	2924, 2854	1674 for poly acryl amide, 1712 for poly acrylic acid	1072	1265 , 1311	C=C for G at 1654,1558,1512

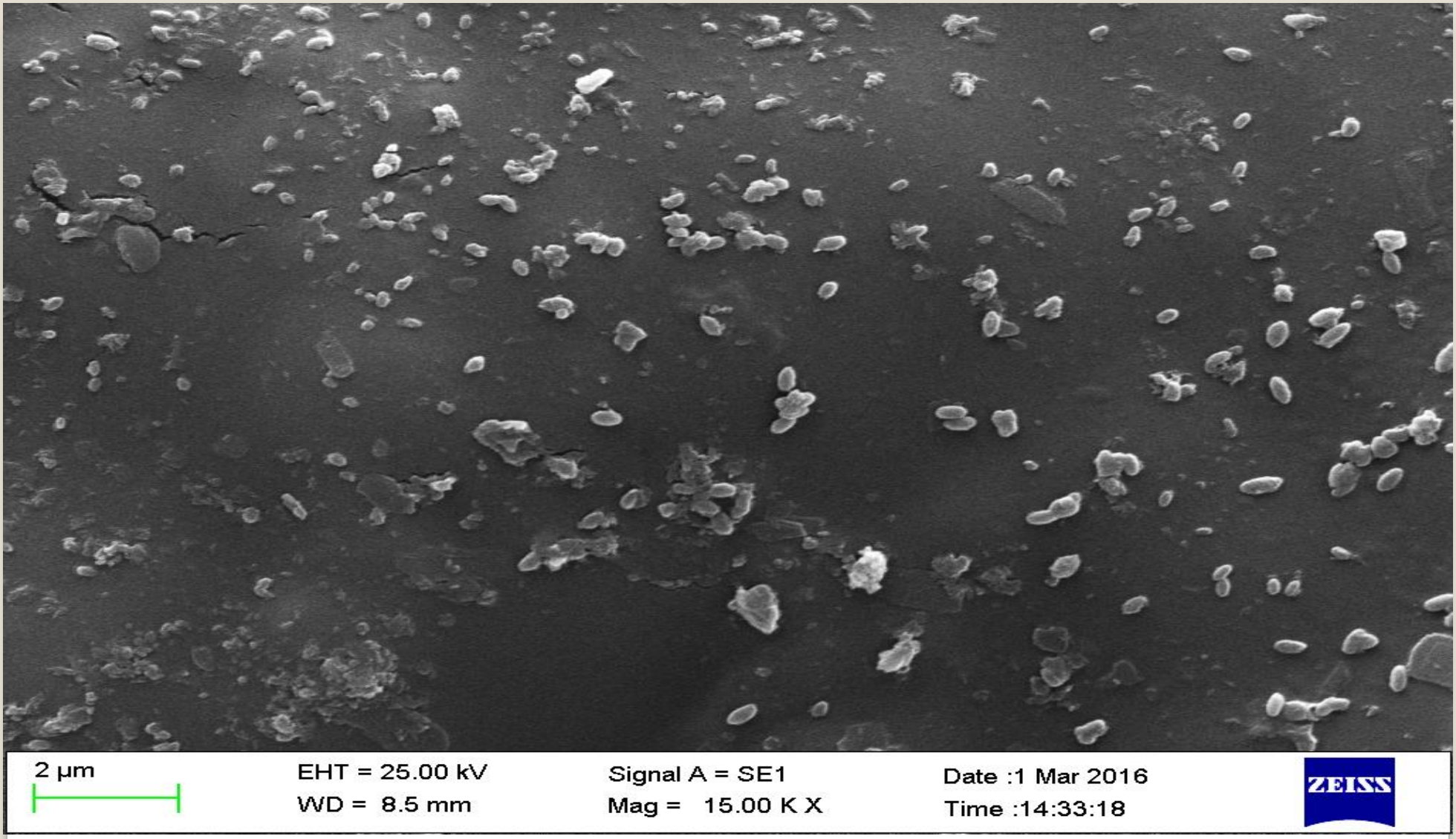

Figure (81): SEM photomicrograph of CPG/G with magnification 15 KX

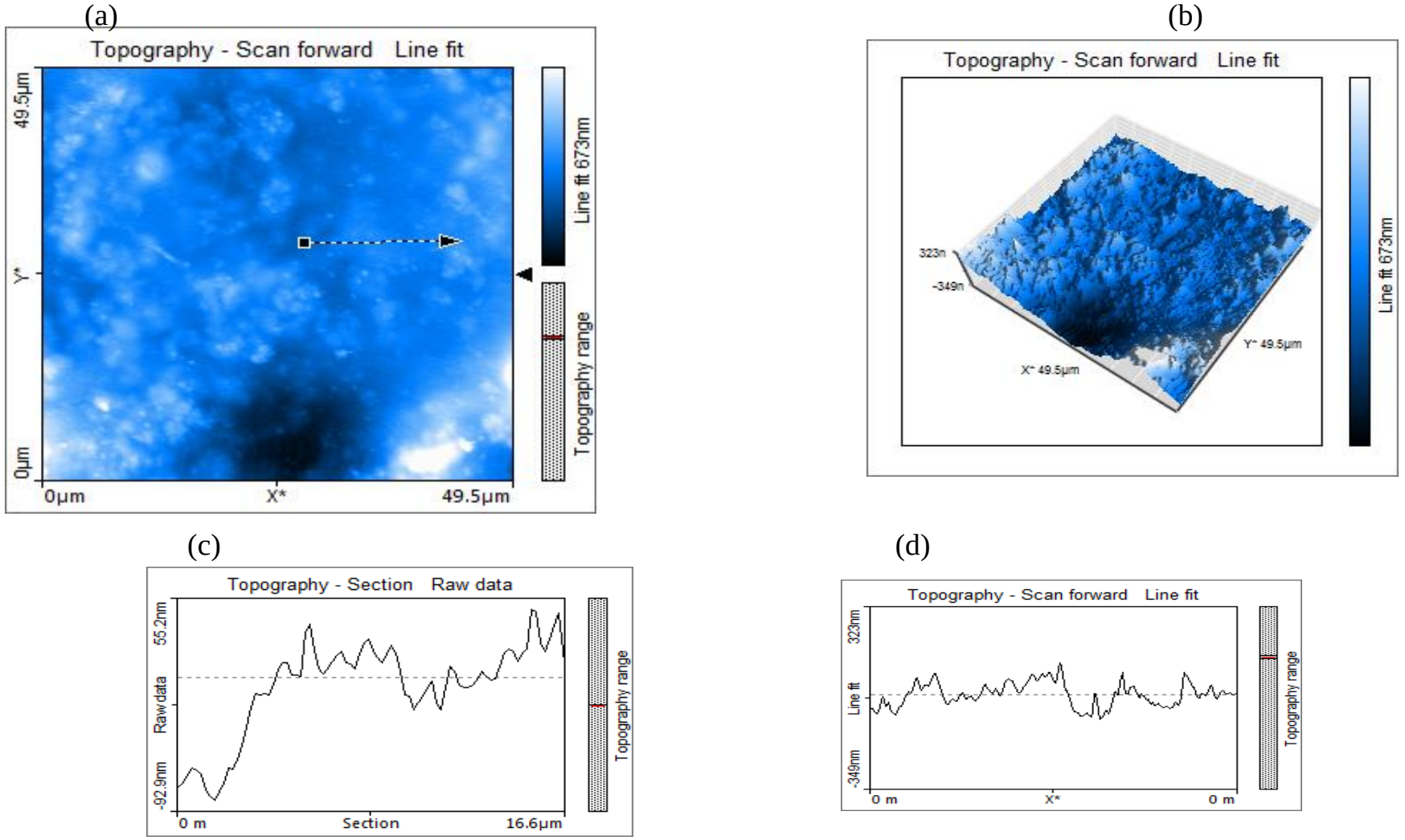

Figure (82): AFM photomicrograph of (CPG/G) , (a): scan topography, b: 3D topography, (c): cross-section topography¸ & (d): line graph topography

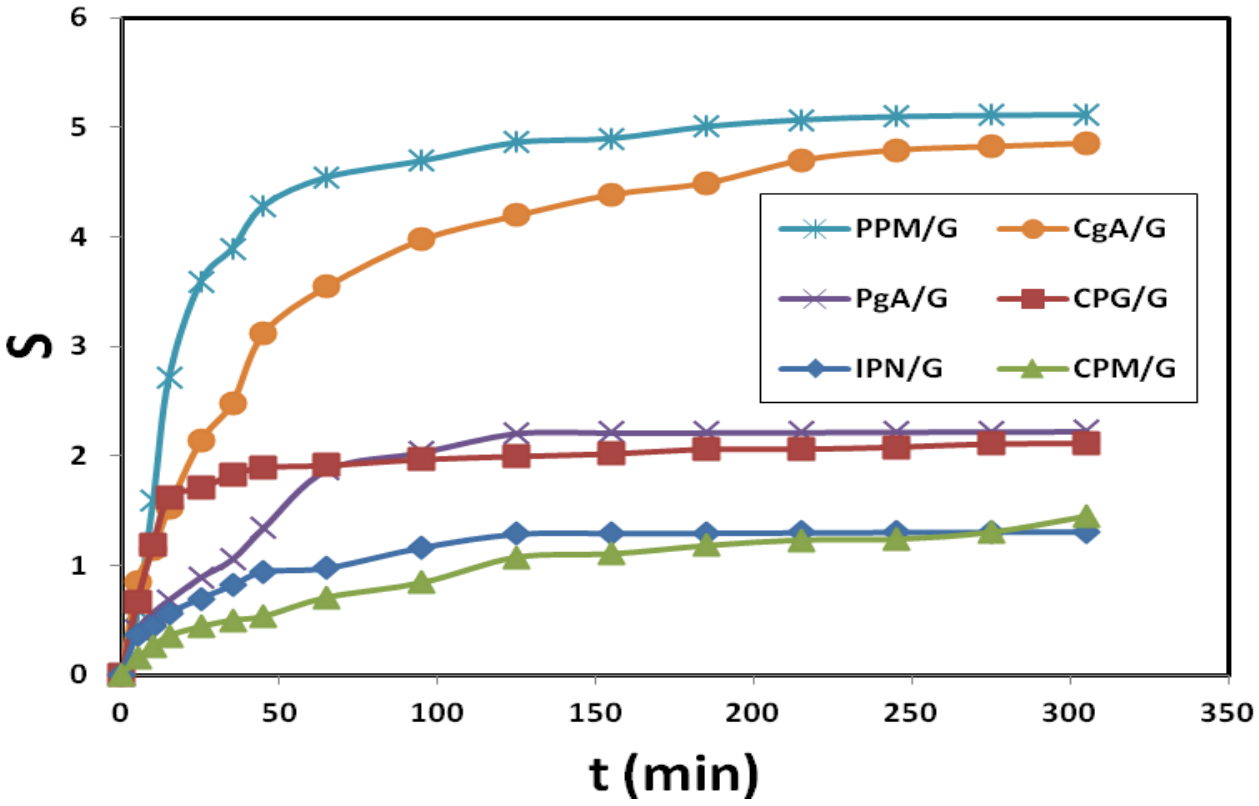

Figure (83): Degree of swelling for G composites in water at R.T.

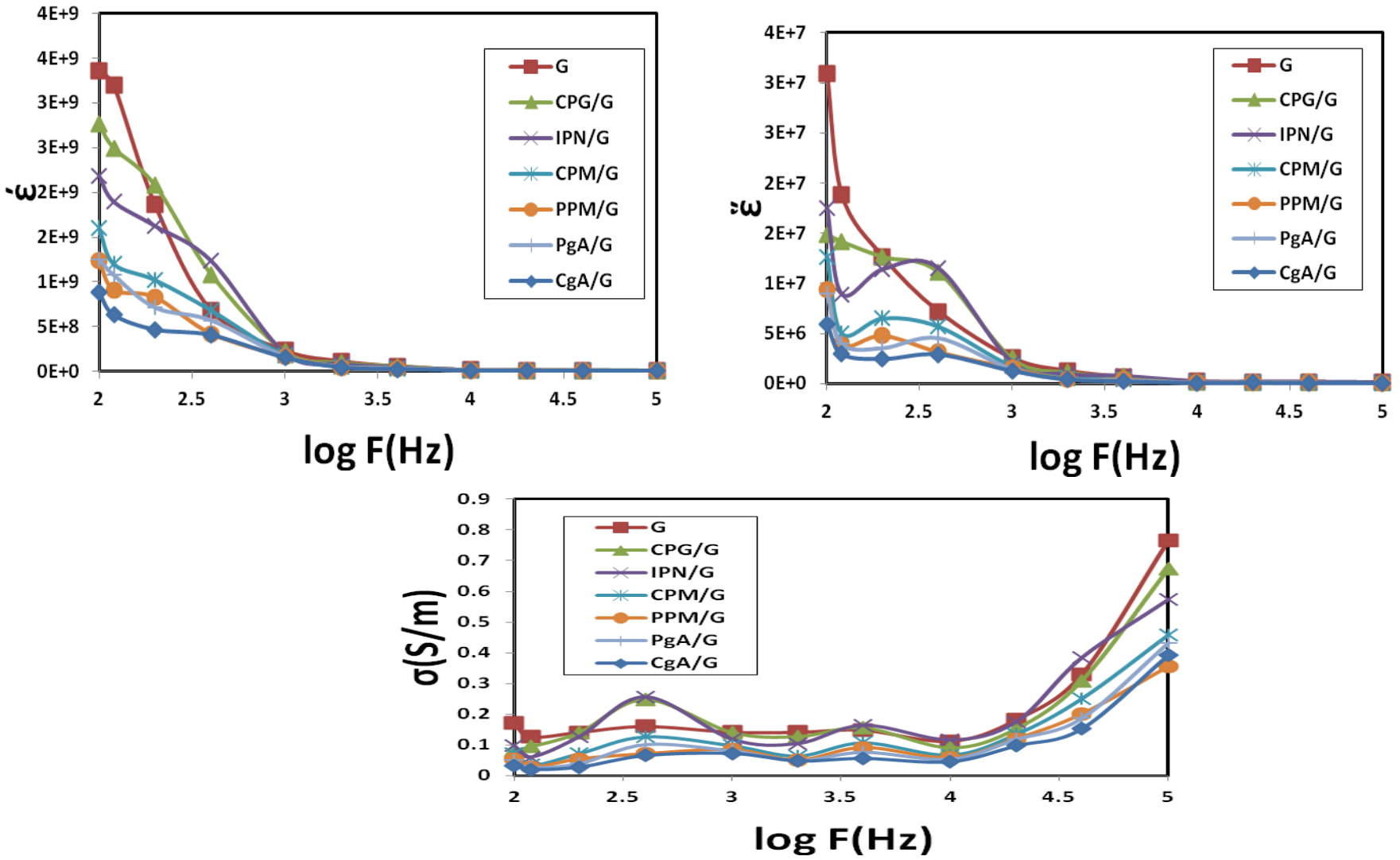

Figure (84): Real permittivity, Imaginary permittivity, and AC conductivity versus log frequency for G and composites

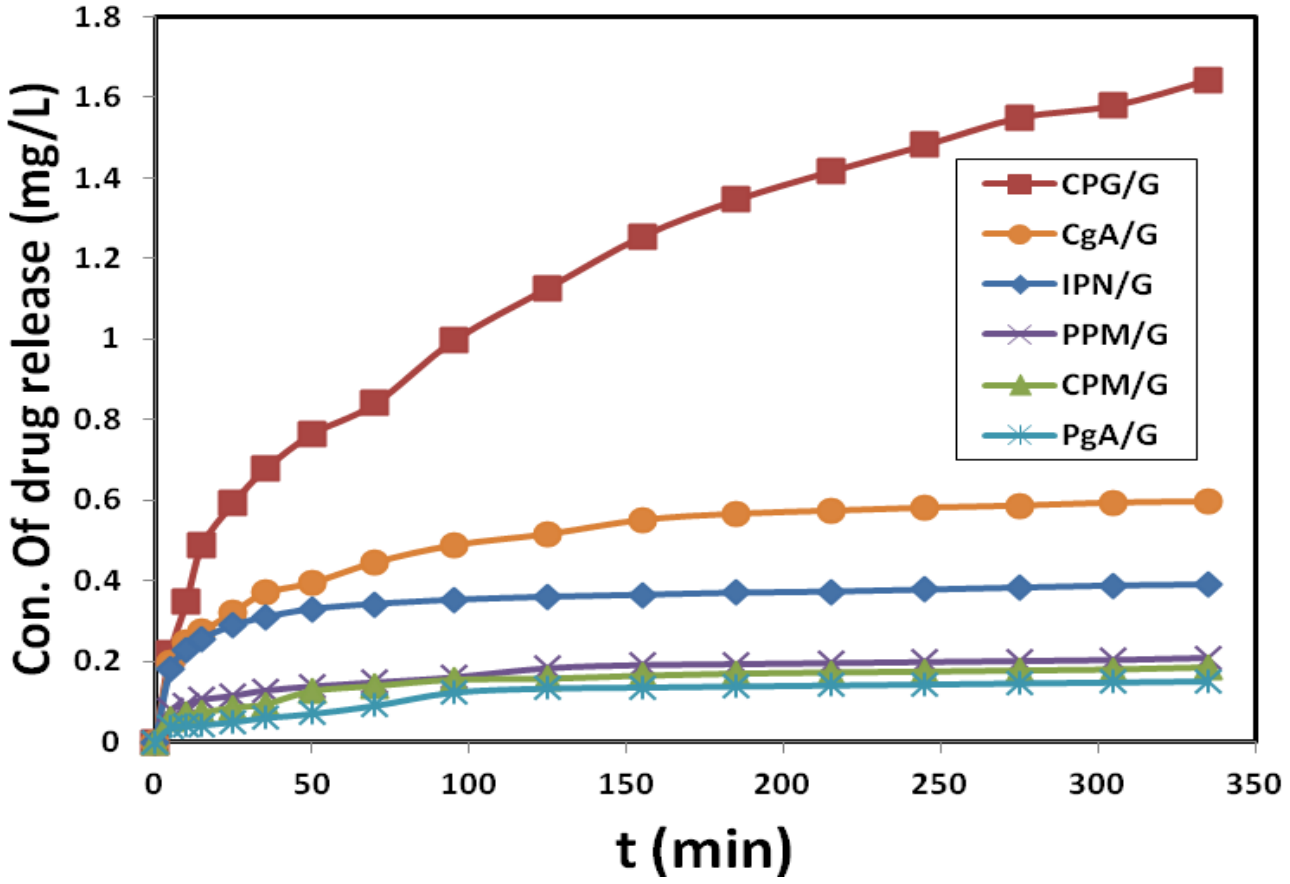

Figure (85): Indigo release from G composites at R.T. and Voltage=2

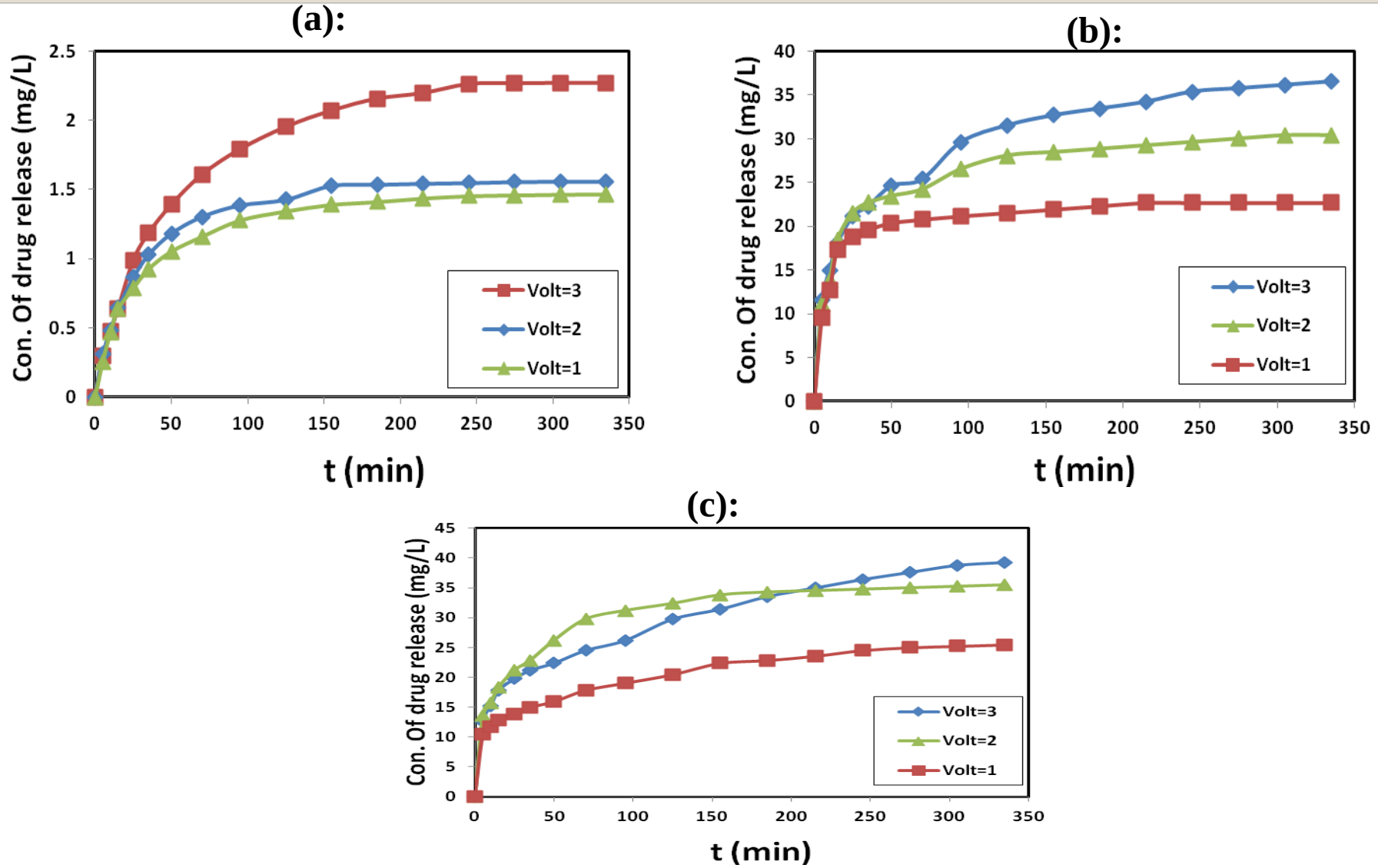

Figure (86): (a): Indigo , (b): Doxorubicin hydrochloride, and **(c):** Methotrexate release from (CPG/G) composite at different Voltages and 37ºC

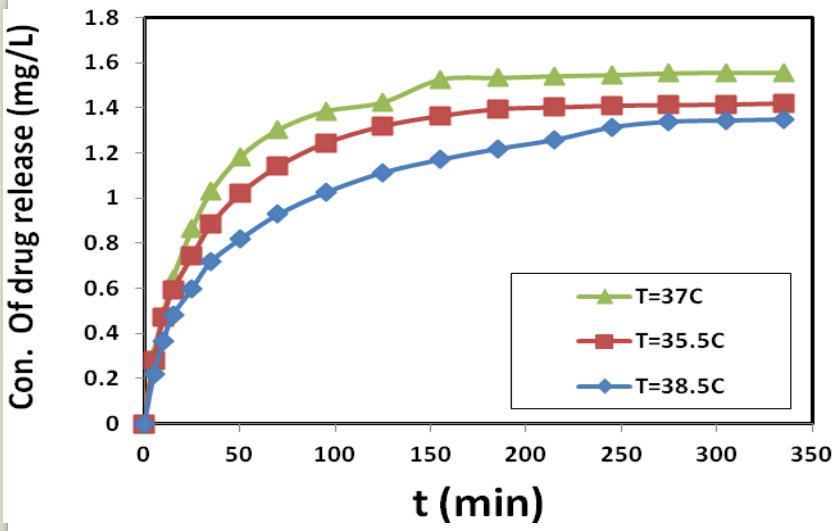

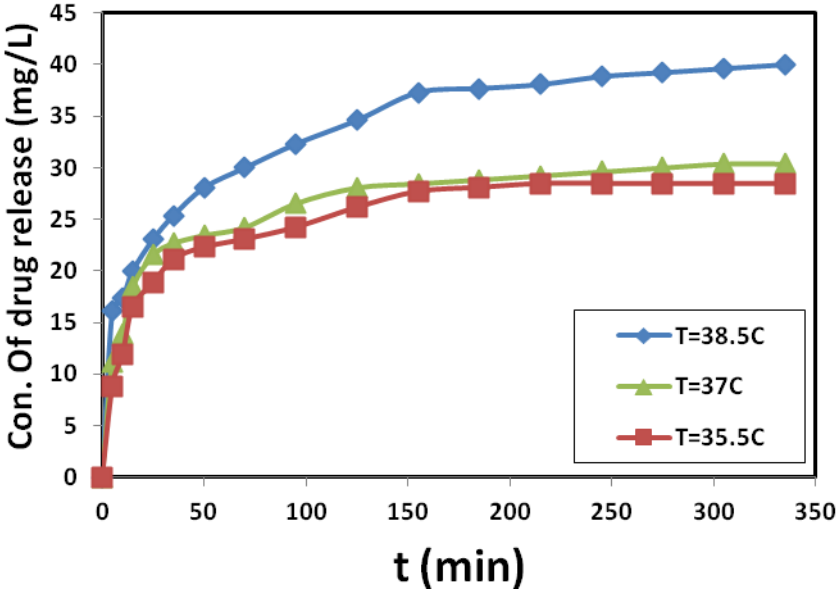

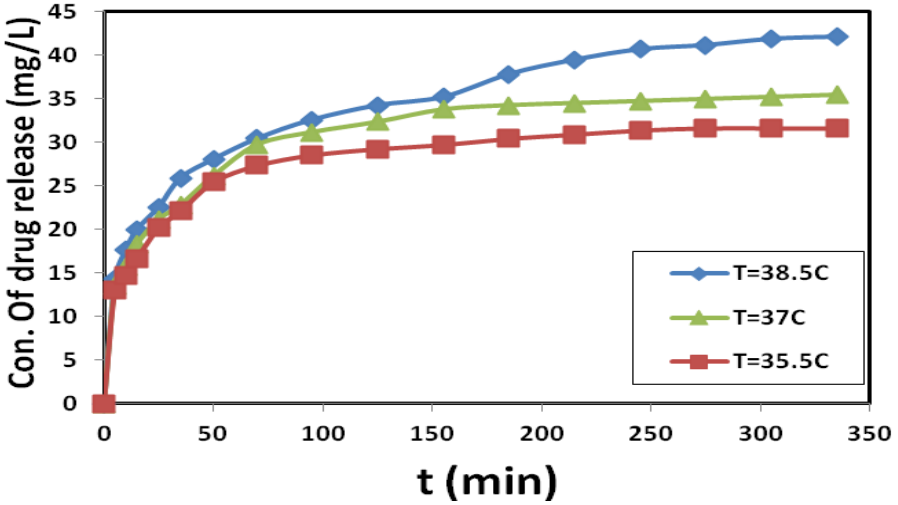

Figure (87): (a) : Indigo, (b): Doxorubicin hydrochloride, and **(c):** Methotrexate release from (CPG/G) composite at different temperatures and 2V

2.8.3 Synthesis of conductive hydrogels /MWCNTs

In brief, hydrogel solution was mixed with dispersion solution of MWCNTs (0.25w/v %) with mechanical stirring for (1h) at (2500 rpm.).

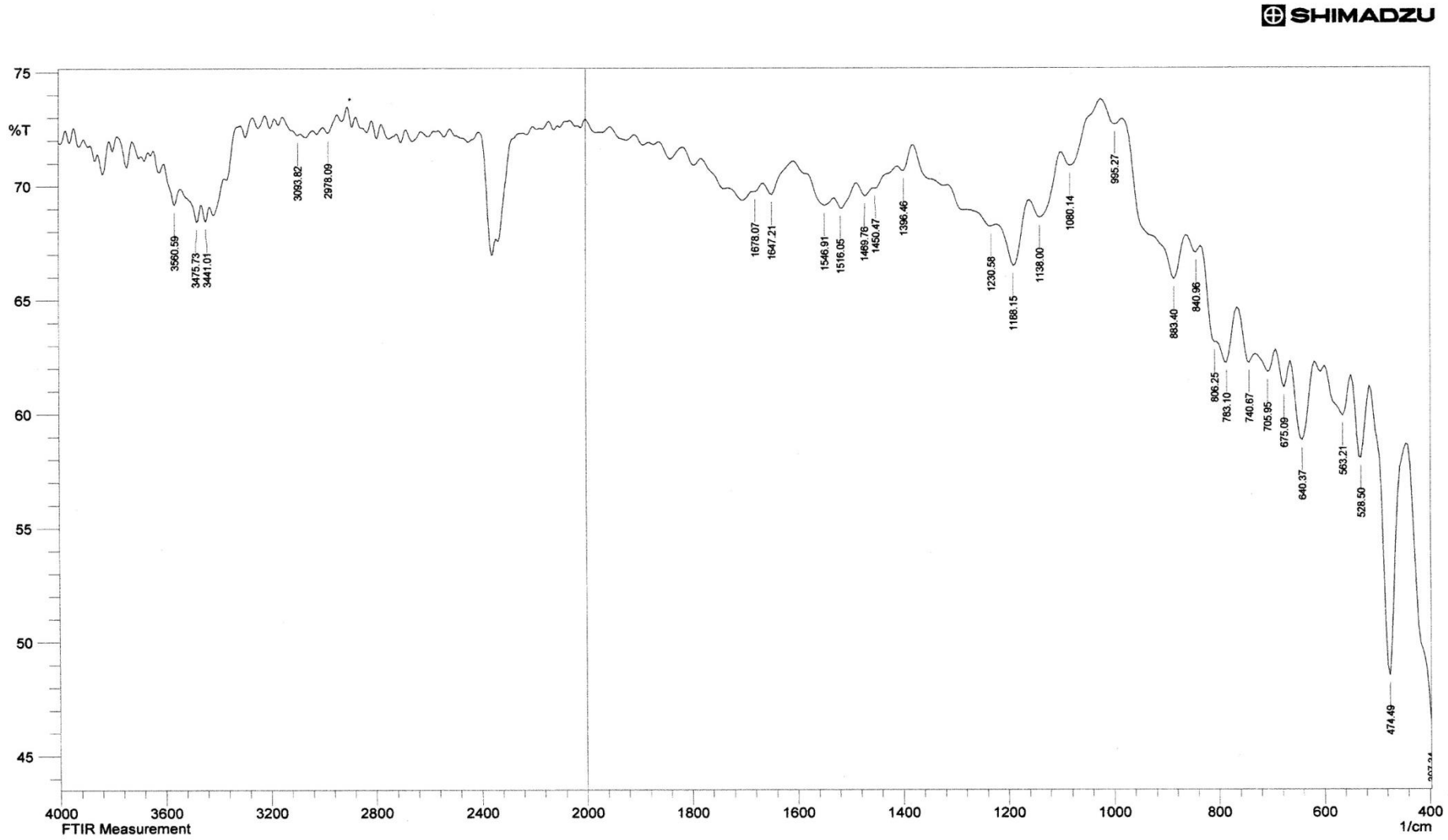

Figure (88): FT-IR spectrum of MWCNTs

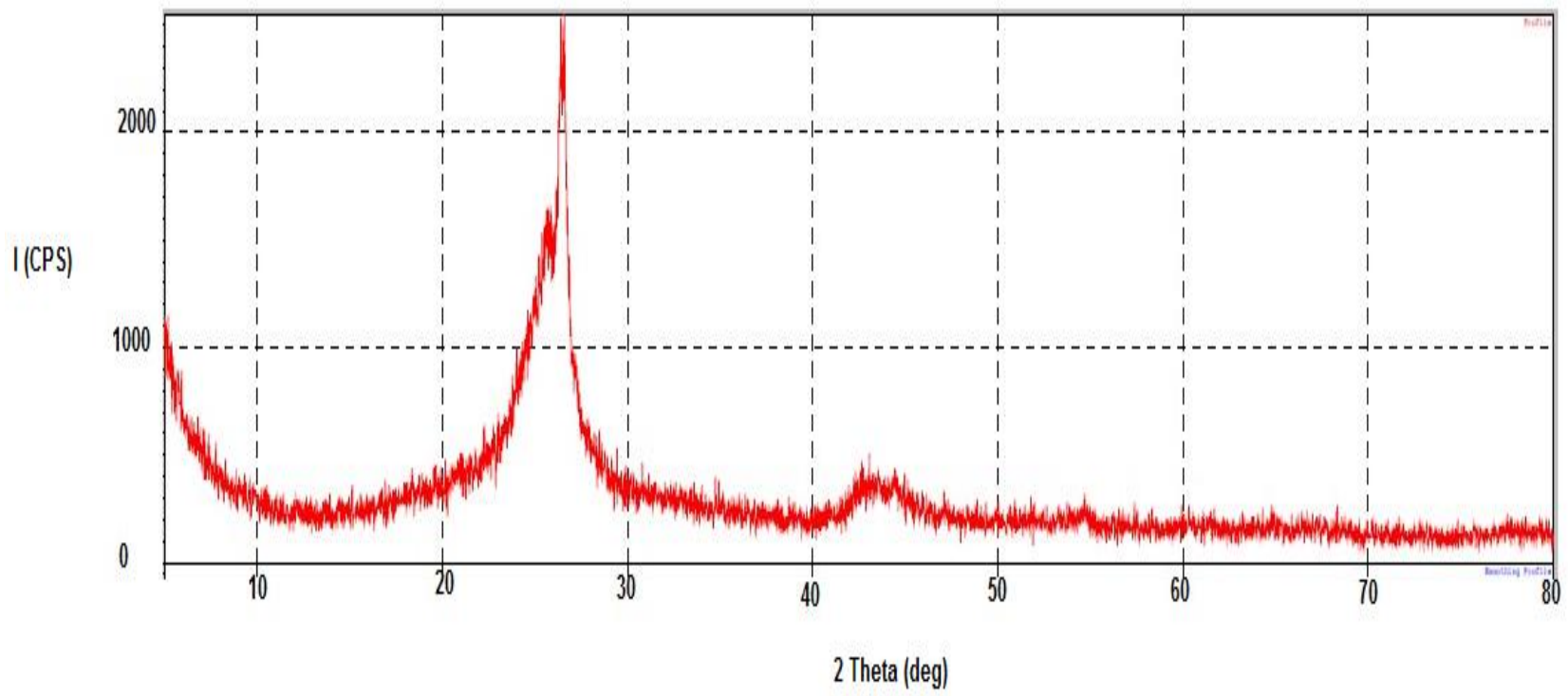

Figure (89): XRD for MWCNTs

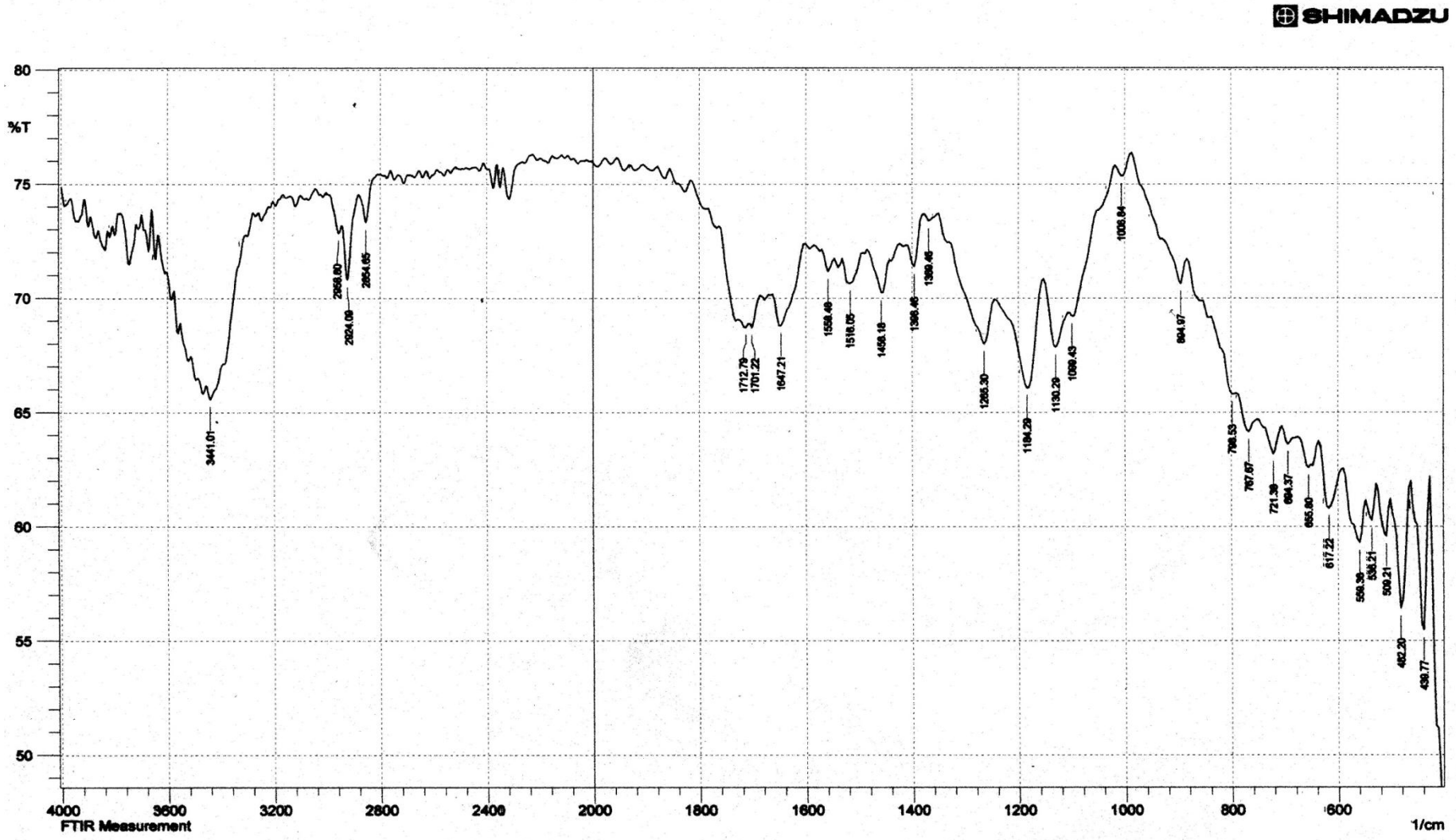

Figure (90): FT-IR spectrum of conductive hydrogel PgA/MWCNTs film

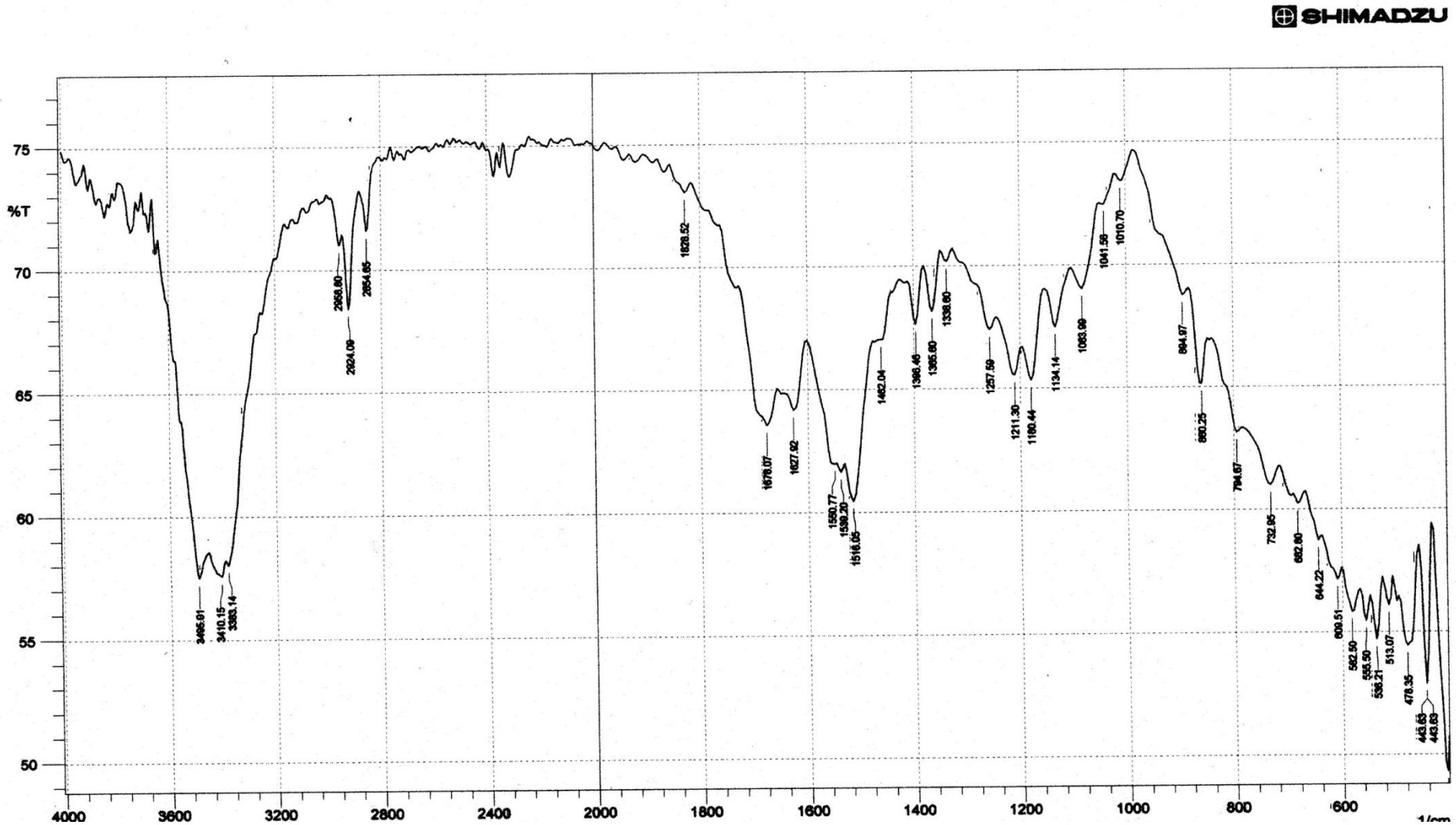

Figure (91): FT-IR spectrum of conductive hydrogel PPM/MWCNTs film

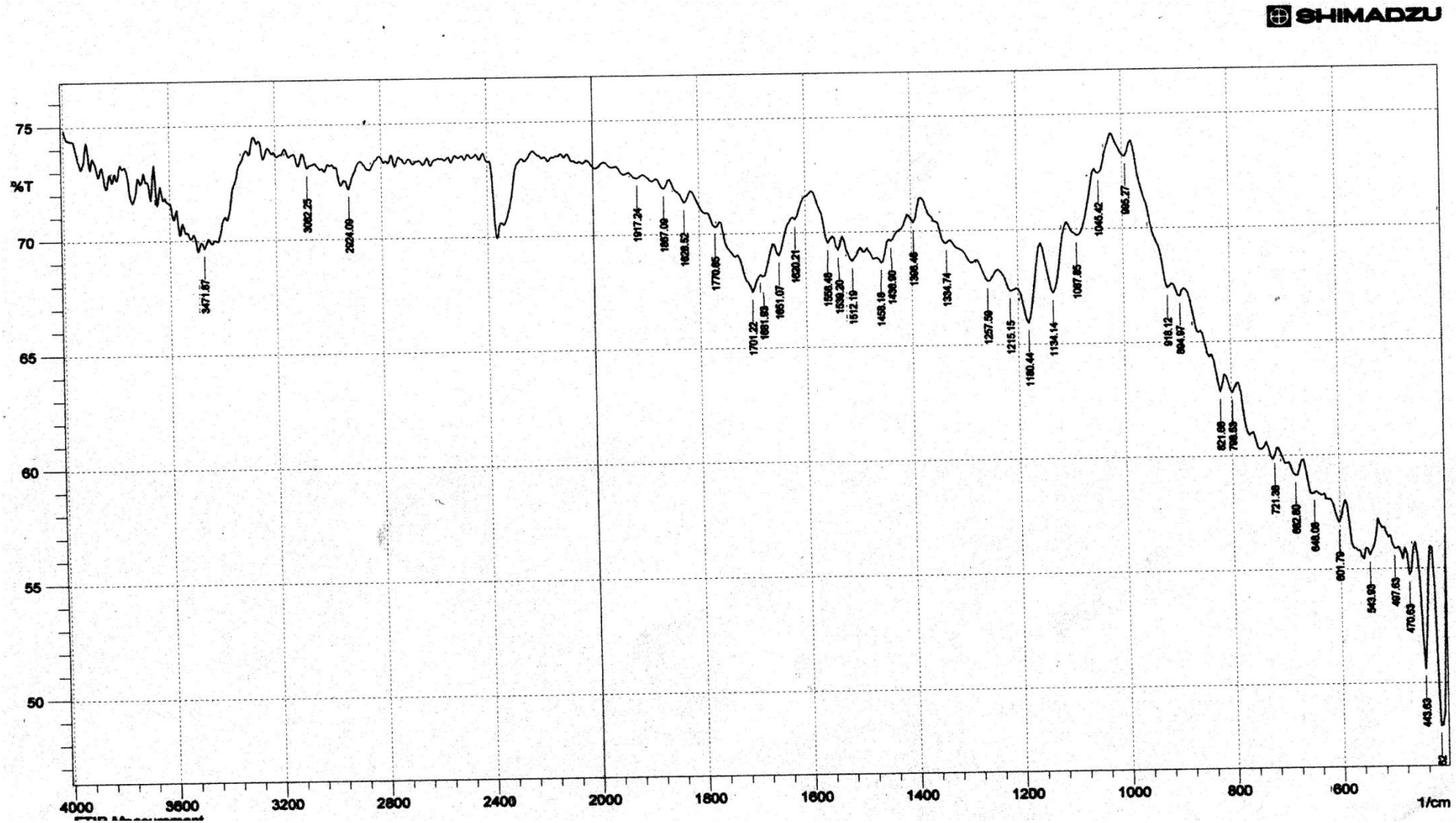

Figure (92): FT-IR spectrum of conductive hydrogel CPG/ MWCNTs film

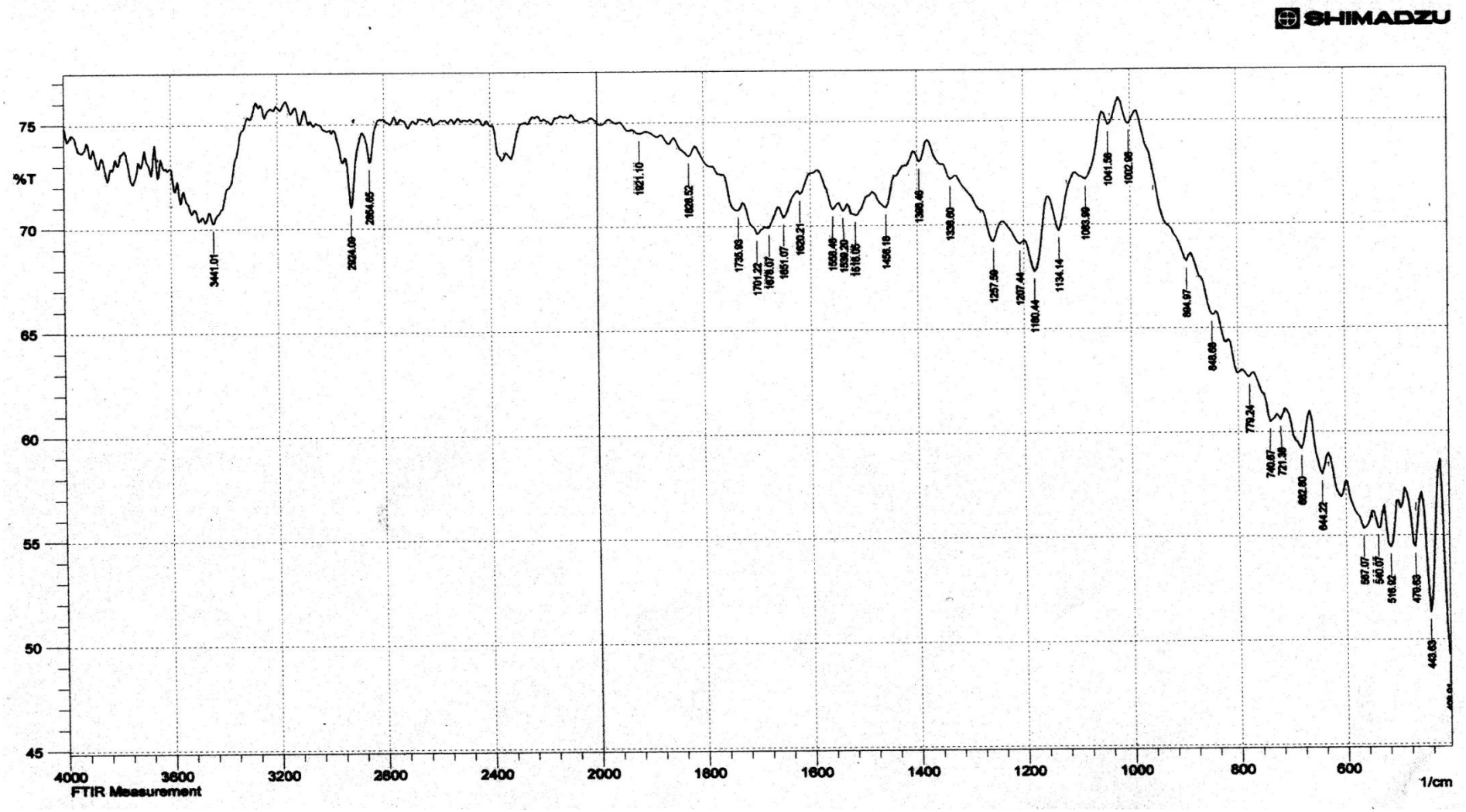

Figure (93): FT-IR spectrum of conductive hydrogel CPM/ MWCNTs film

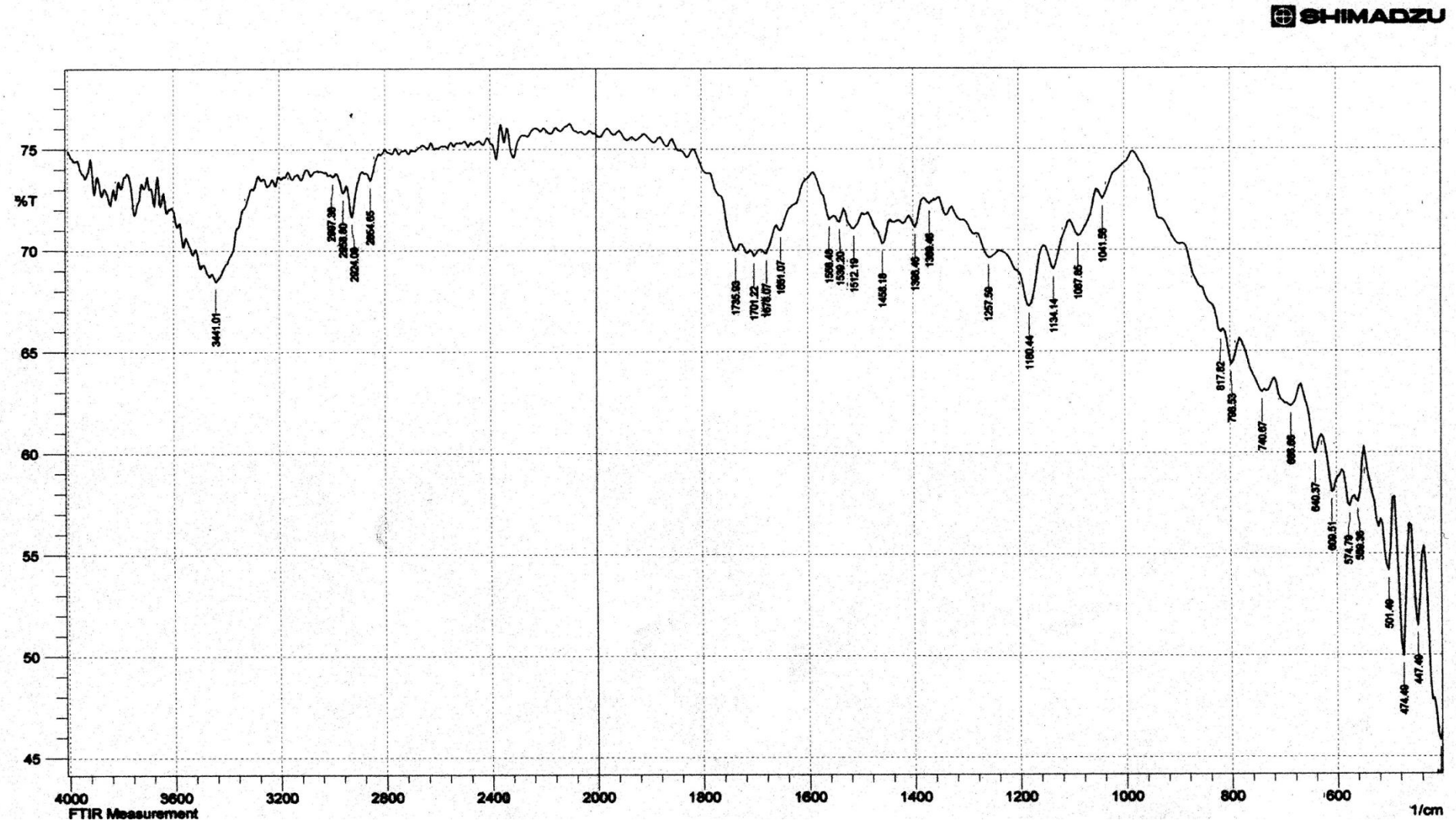

Figure (94): FT-IR spectrum of conductive hydrogel CgA/ MWCNTs film

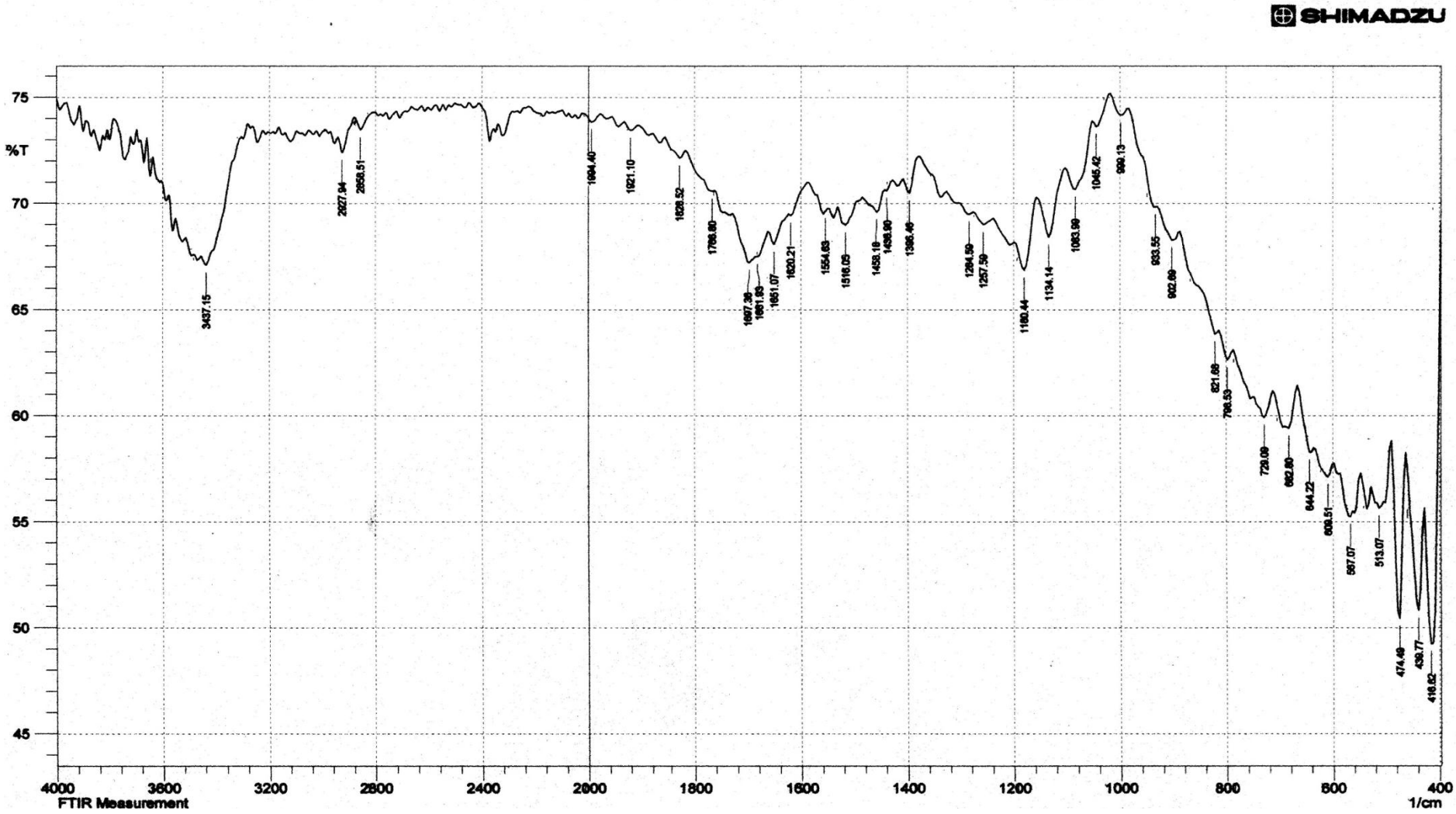

Figure (95): FT-IR spectrum of conductive hydrogel IPN/ MWCNTs film

Table (3): Characteristics FTIR absorption bands (cm^{-1}) contain stretching vibrations& bending vibrations of hydrogels/MWCNTs composite

Samples	O-H	N-H	CH-	C=O	C-O	C-N	peaks other
PgA/MWCNTs	3441	Overlaps with O-H	2956,2924, 2864,	1712,1701	1099 overlaps with C-O for MWCNTs, 1184 for acetal ring	1265 1369	C=C of MWCNTs at 1647,1558 ,1516
PPM/MWCNTs	3495	3410	New peak for MWCNTs at 2958, 2924,2854	Shift to 1667 to pectin and 1627 to PVA,	1041, new peak at 1083 for MWCNTs	1211,1257	C=C of MWCNTs at 1550, 1539,1516
CPG/MWCNTs	3471	Overlaps with O-H	3062, 2924	1701	Shift to 1045, shift to 1134 for secondary alcohol, new peak at 1087 for MWCNTs	1257 , 1334	Schiff base (C=N) shift to 1651, C=C of MWCNTs at 1681, 1620,1539 ,1512
CPM/MWCNTs	3441	Overlaps with O-H	2924,2854	1735, 1701,	Shift to 1041, new peak at 1083 for MWCNTs	1336,1257	C=C for MWCNTs at 1678,1651 ,1620, 1558, 1539, 1516
CgA/MWCNTs	3441	Overlaps with O-H, bending at 1456	2997, 2958 for MWCNTs, 2924,2864	1735,1701	1041 , new peak at 1087 for MWCNTs	1257,1369	C=C for MWCNTs at 1676, 1651,1556 ,1512
IPN/MWCNTs	3437	Overlaps with O-H	2927, 2856	1661for poly acryl amide, 1697 for poly acrylic acid	1045, new peak at 1083 for MWCNTs	1264 , 1396	C=C for MWCNTs at 1651,1620 ,1554,1516

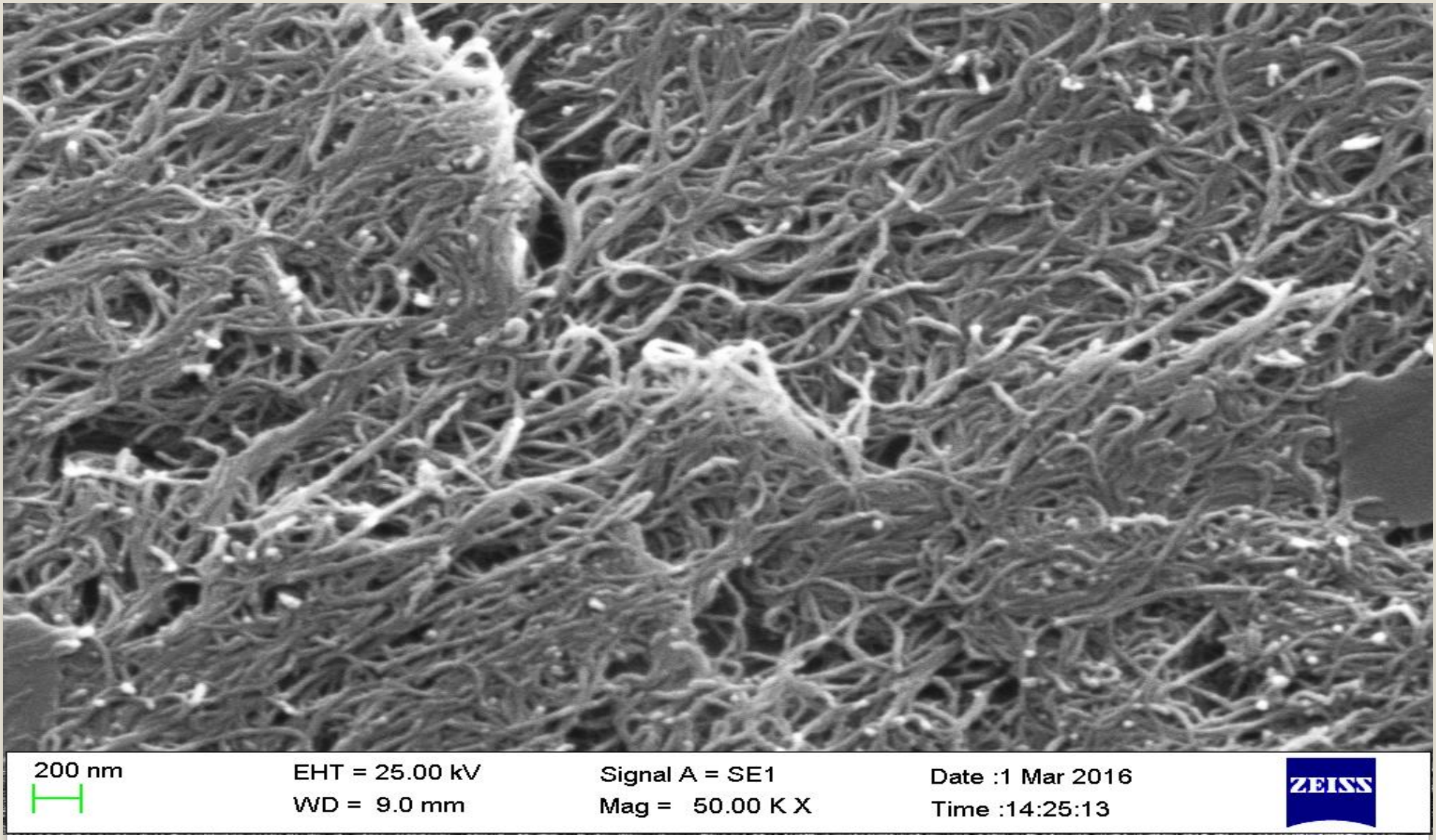

Figure (96): SEM photomicrograph of MWCNTs with magnification 50 KX

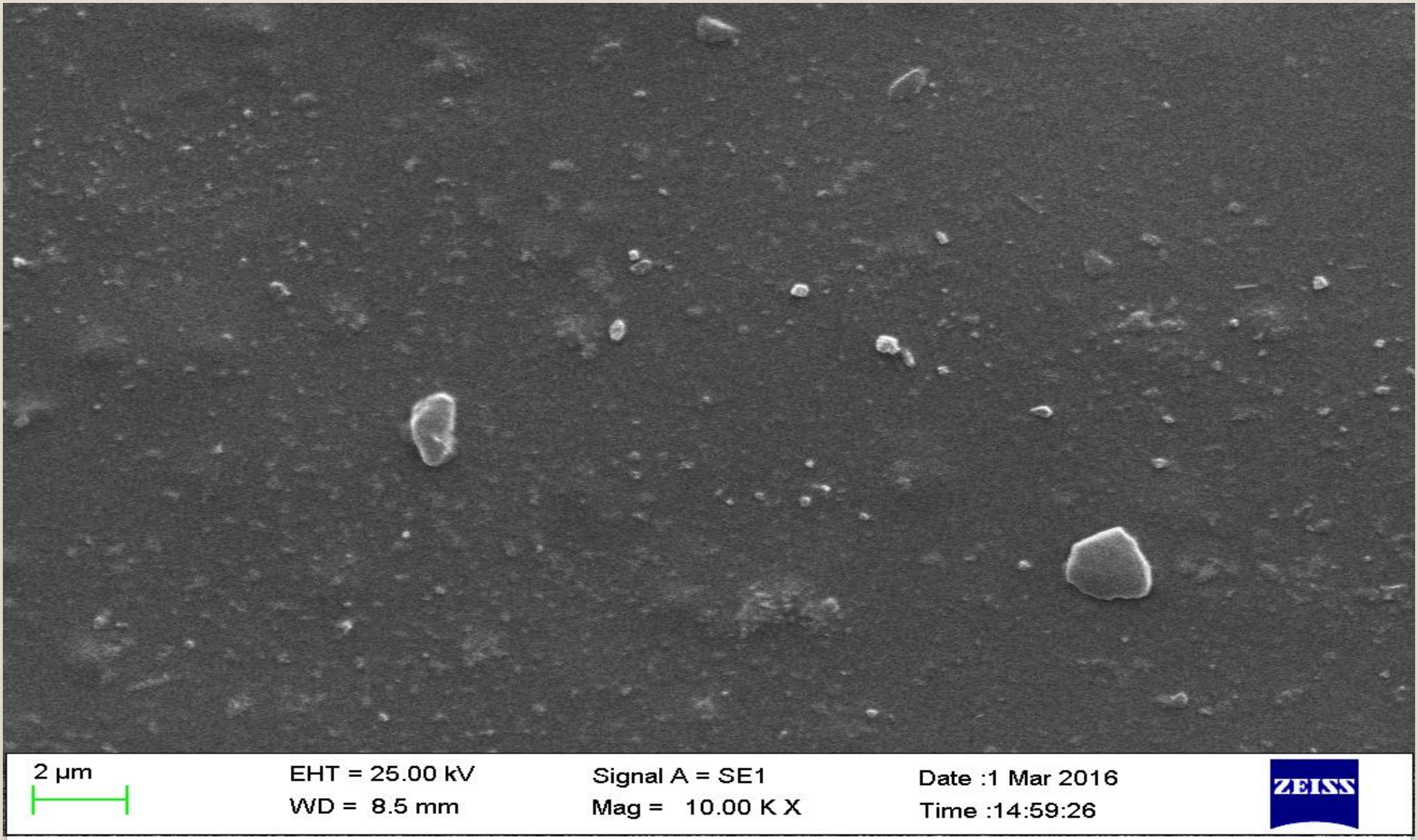

Figure (97): SEM photomicrograph of CPG/ MWCNTs with magnification 10 KX

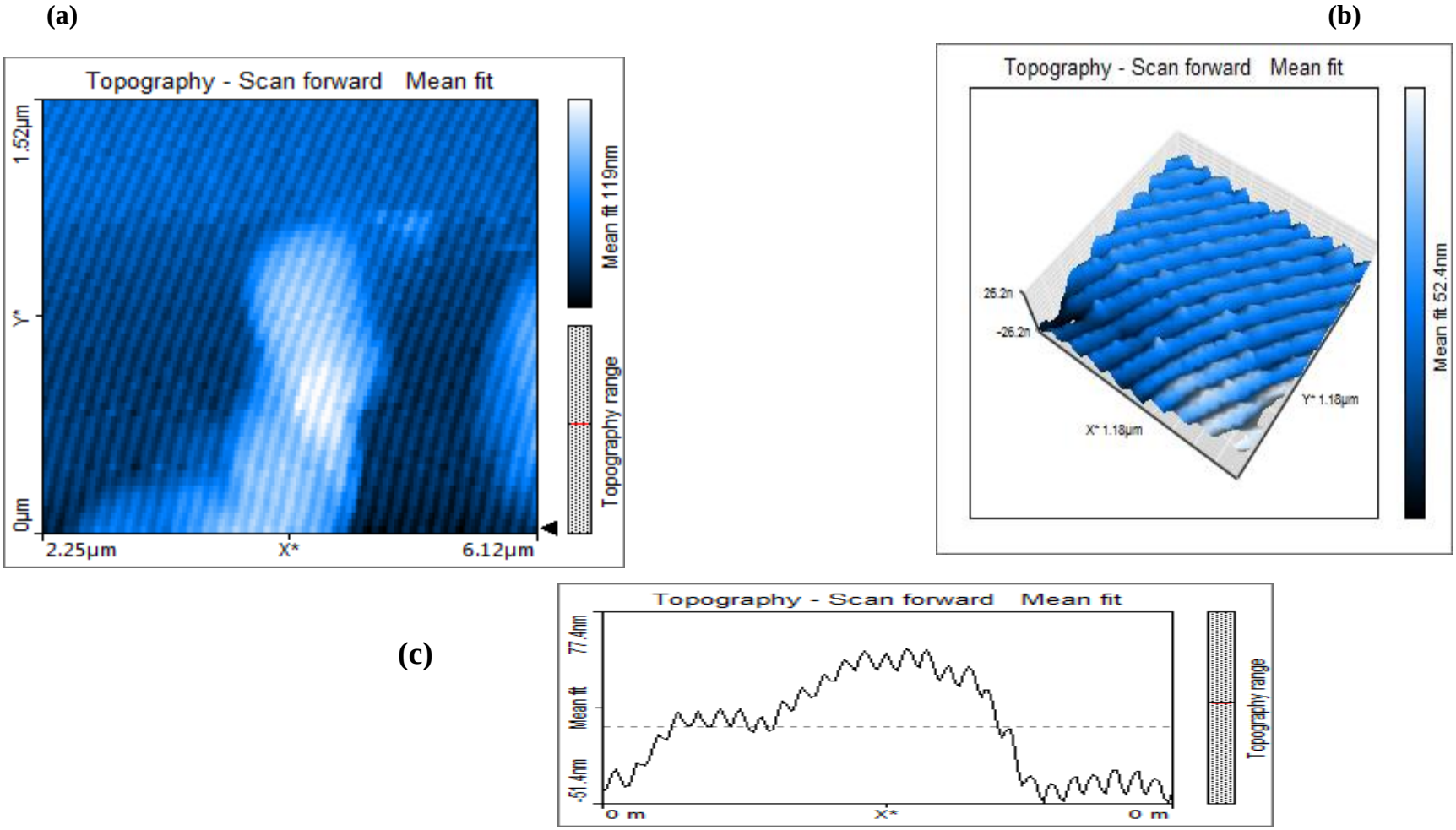

Figure (98): AFM photomicrograph of MWCNTs, (a): scan topography, b: 3D topography, & (c): line graph topography

(a)

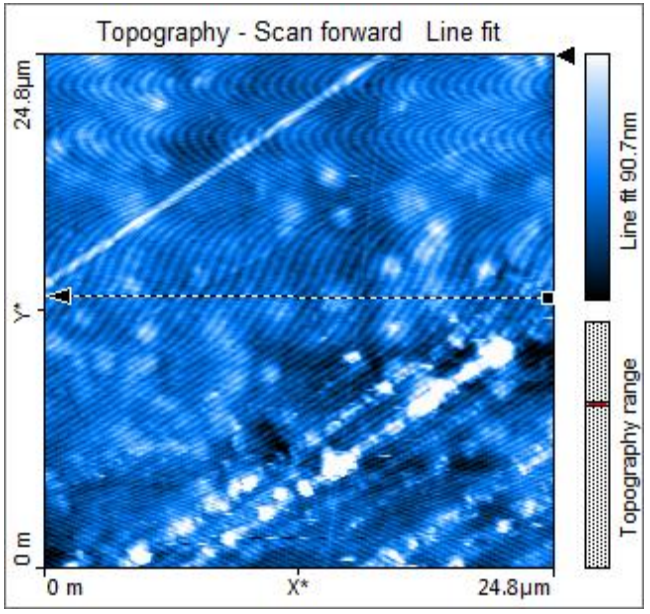

(b)

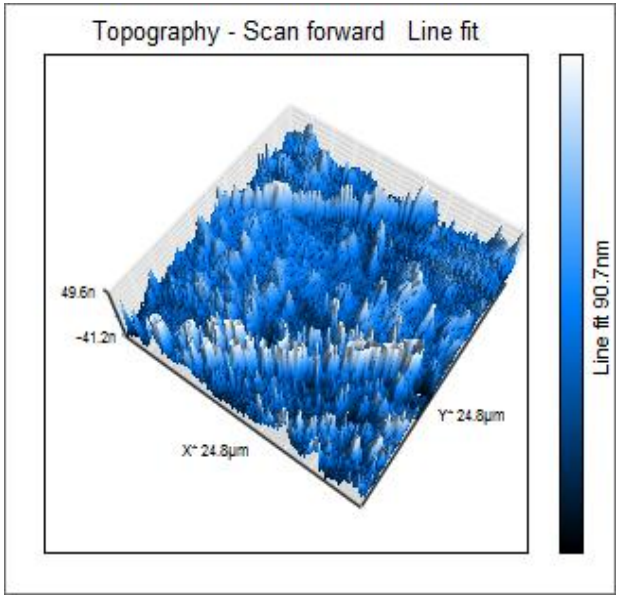

(c)

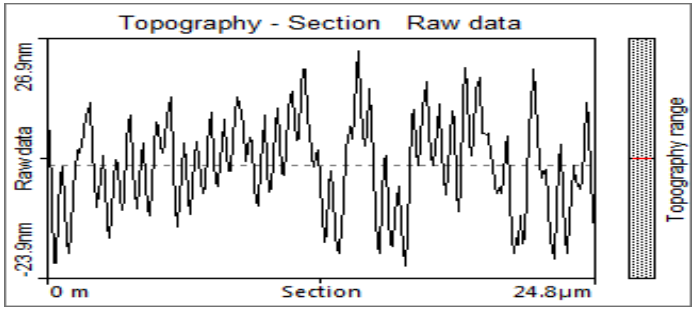

(d)

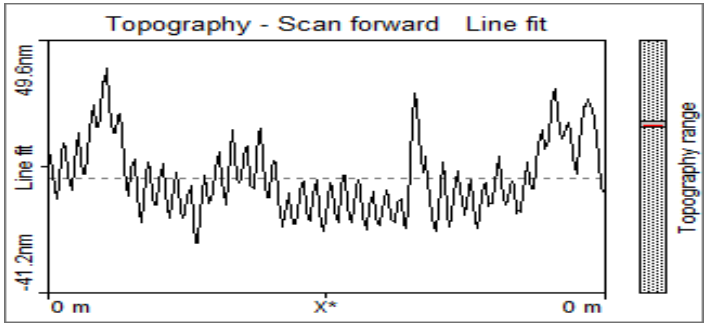

Figure (99): AFM photomicrograph of (CPG/MWCNTs) , (a): scan topography, b: 3D topography, (c): cross-section topography , & (d): line graph topography

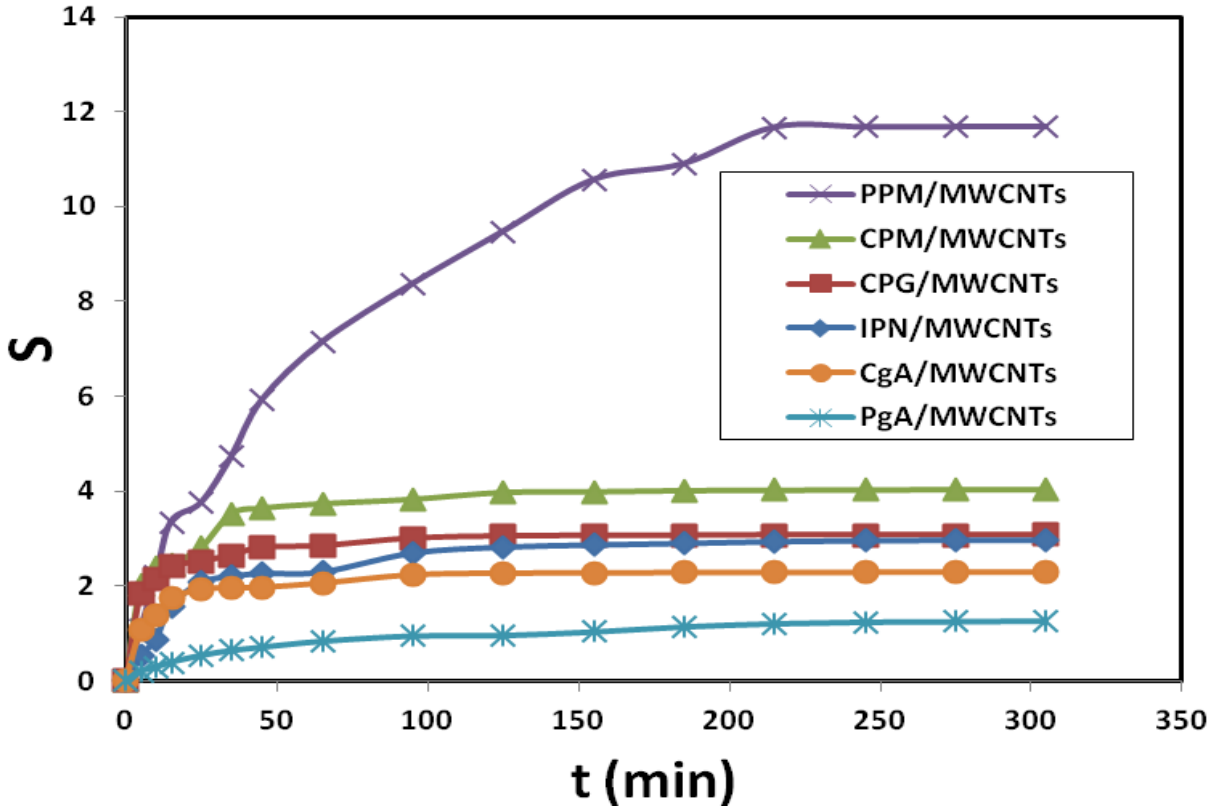

Figure (100): Degree of swelling for MWCNTs composites in water at R. T.

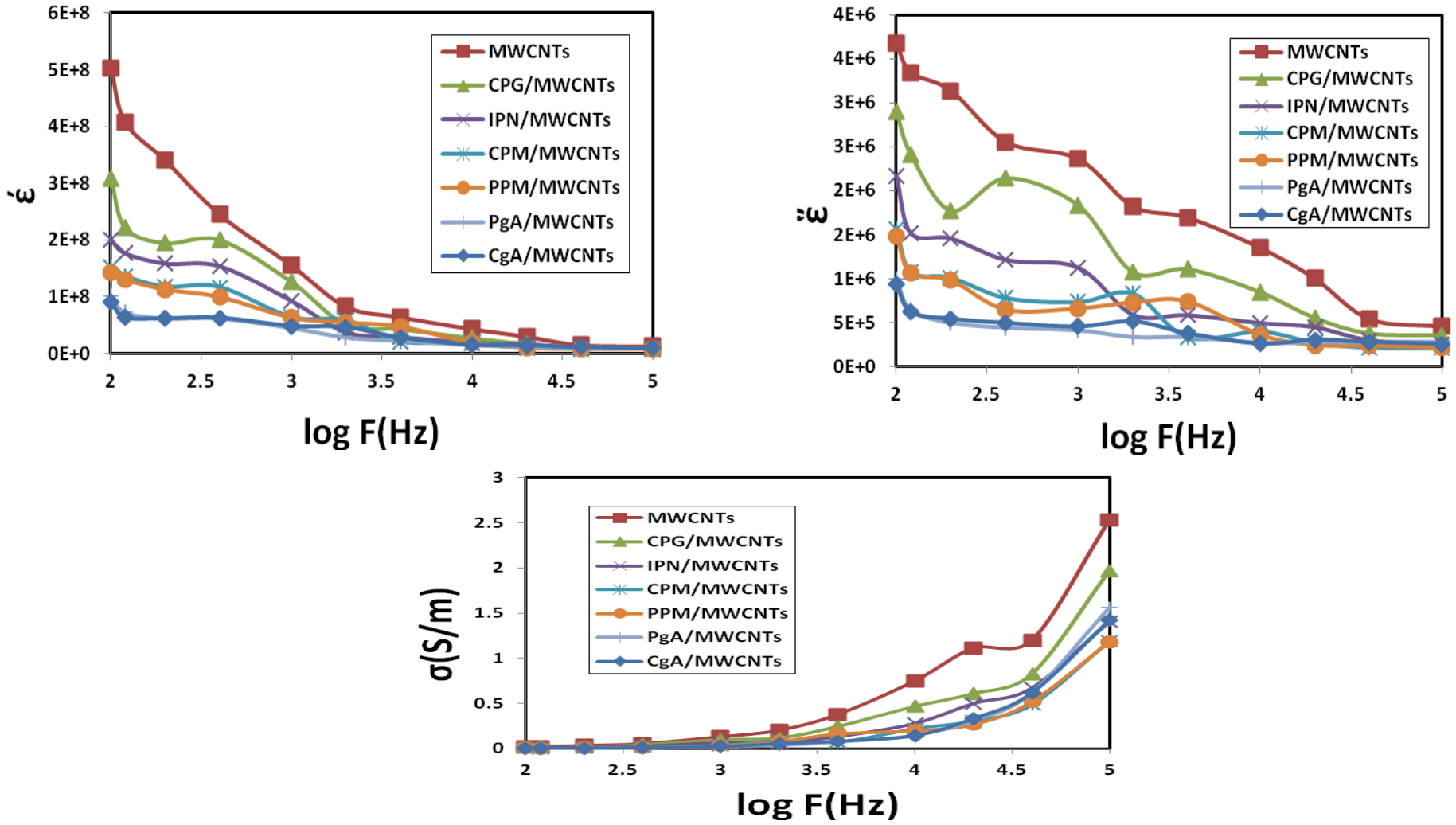

Figure (101): Real permittivity, Imaginary permittivity, and AC conductivity versus log frequency for MWCNTs and composites

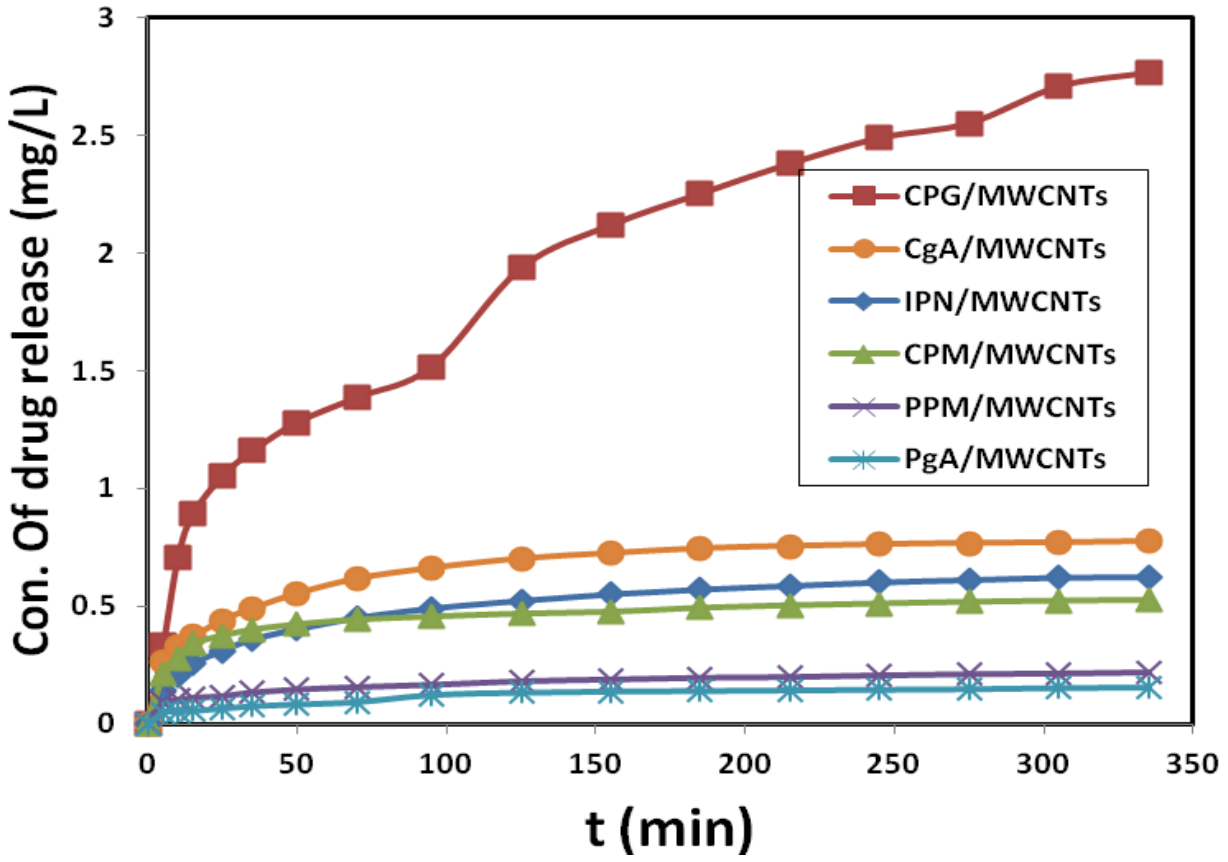

Figure (102): Indigo release from MWCNTs composites at R.T. and Voltage=2

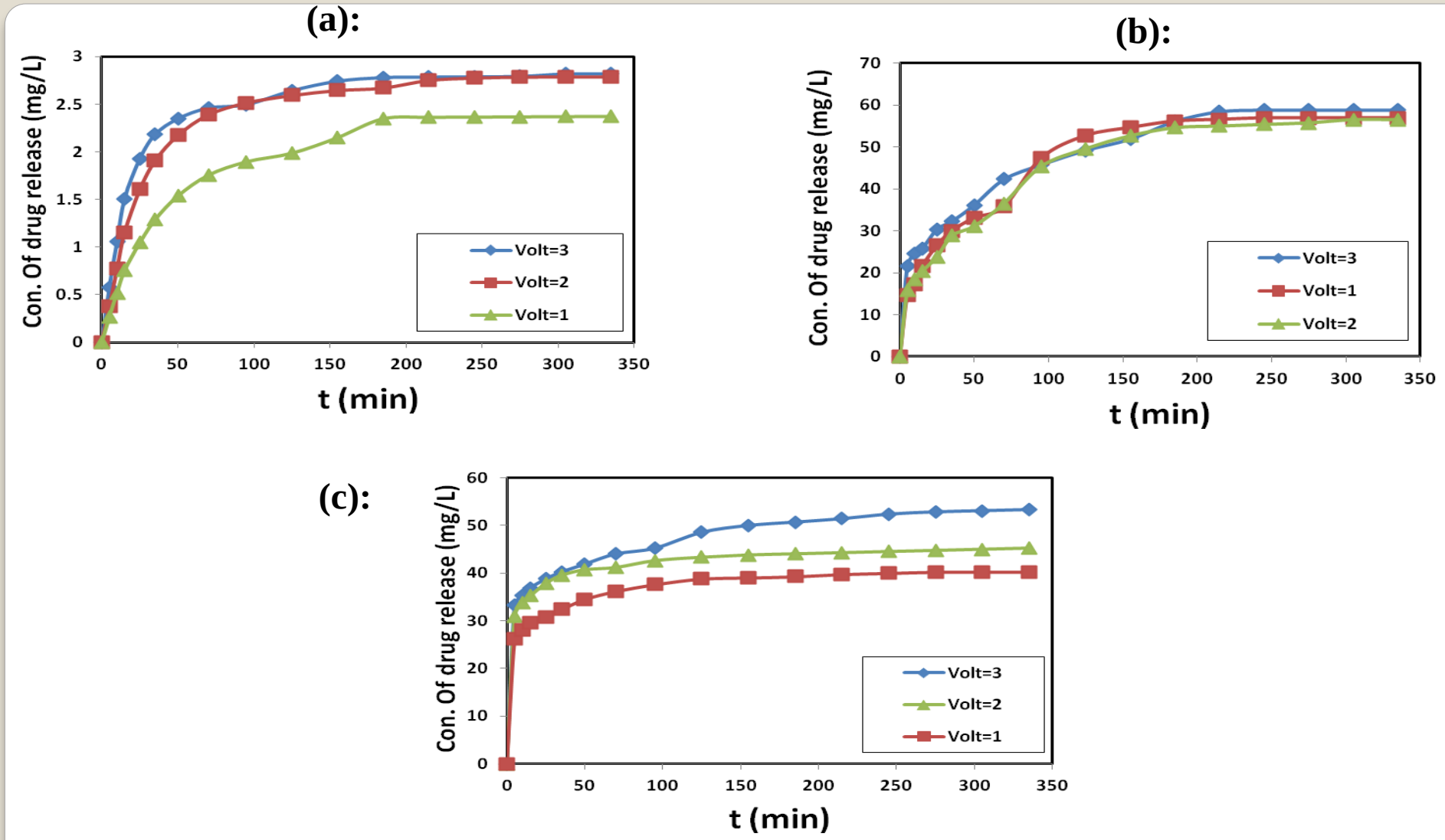

Figure (103): (a): Indigo, (b): Doxorubicin hydrochloride, and (c): Methotrexate release from (CPG/MWCNTs) composite at different Voltages and 37ºC

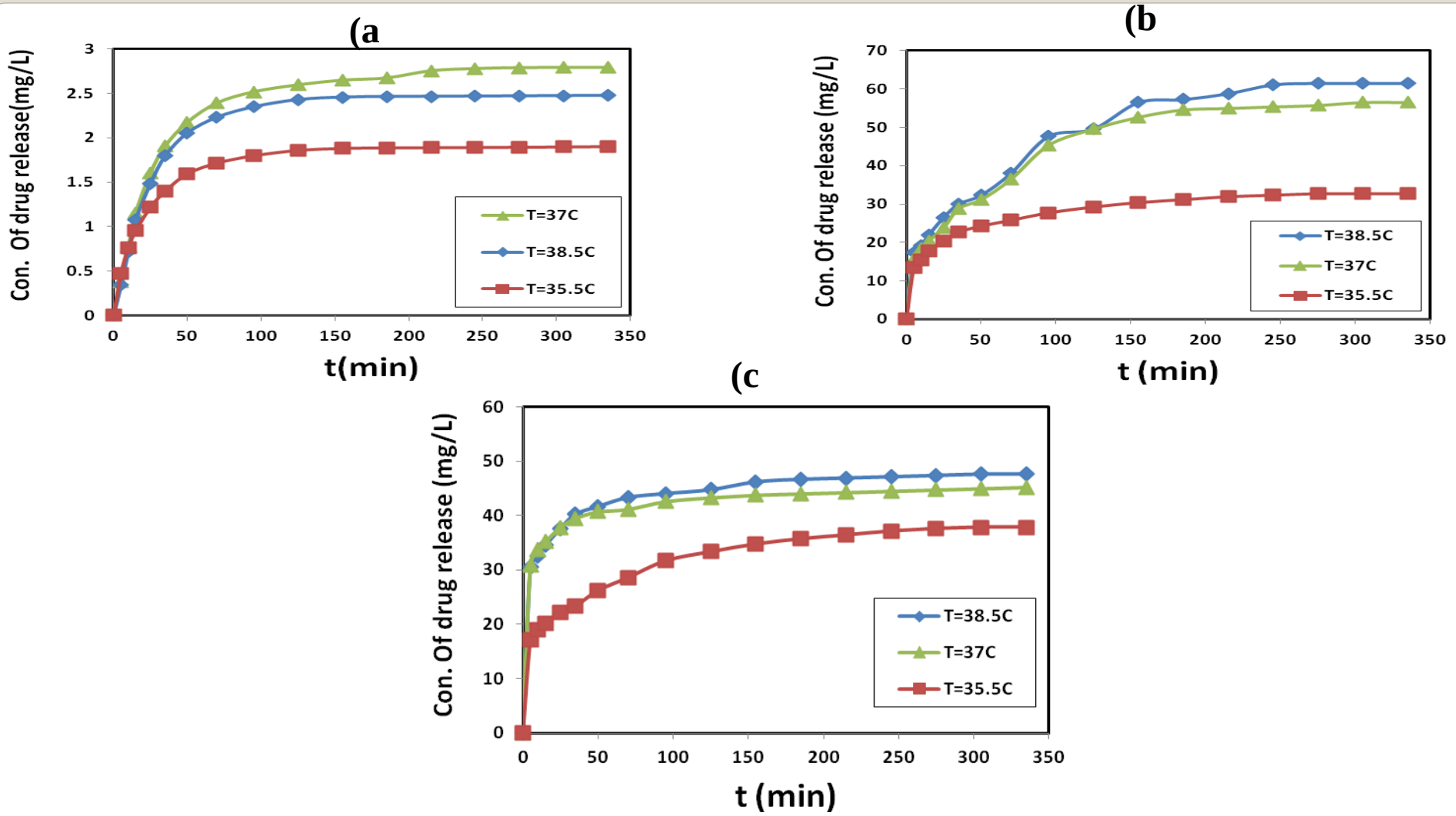

Figure (104): (a) : Indigo , (b): Doxorubicin hydrochloride and (c): Methotrexate release from (CPG/MWCNTs) composite at different temperatures and 2V

Conclusion

❖The swelling of hydrogel and composite were studied in distilled water (pH=6.5) with interval times and after day. The maximum degree of swelling was returned to PgA hydrogel at 305 min and after day equal to S=15.1314, & S=16.4825. The maximum degree of swelling for hydrogel composite was returned to PPM/MWCNTs at 305 min and after day equal to S=11.6776, & S=11.7473.

❖The electrical properties of hydrogel and hydrogel nanocomposite were study with LCR meter with frequencies (100Hz-100 KHz). The real & imaginary permittivity were found increase with decreased of frequency, while electric conductivity was increased with increasing frequency. The maximum electrical conductivity was returned to MWCNTs and its composite form (CPG/MWCNTs), the value is equal to σ=2.5305 S/m & σ=1.9669 S/m, respectively.

❖The highest ratio for drug release was found returned to Doxorubicin hydrochloride loading on CPG/MWCNTs equal to 62.257%.

Thank you for listening to my presentation

شكرا جزيلاً لكم